TWO-DIMENSIONAL ANALYTICAL AND THREE-DIMENSIONAL FINITE-ELEMENT METHOD MODELING OF THE INTERACTIONS BETWEEN WETLANDS AND GROUNDWATER

By

JINHUA ZHONG

A DISSERTATION PRESENTED TO THE GRADUATE SCHOOL
OF THE UNIVERSITY OF FLORIDA IN PARTIAL FULFILLMENT
OF THE REQUIREMENTS FOR THE DEGREE OF
DOCTOR OF PHILOSOPHY

UNIVERSITY OF FLORIDA

2004

TABLE OF CONTENTS

ACKNOWLEDGMENT ii

LIST OF TABLES v

LIST OF FIGURES vi

LIST OF SYMBOLS ix

ABSTRACT xiii

CHAPTER .....

1 INTRODUCTION 1

1.1 Wetland 1

1.2 Wetland Water Budget 2

1.3 Goals and Objectives 4

2 ANALYTICAL GROUNDWATER MODEL RESPONSE TO THE PERIODIC OR NONPERIODIC WATER STAGE FLUCTUATION IN A CIRCULAR LAKE OR WETLAND 7

2.1 Introduction 7

2.2 Problem Formulation: Groundwater Flow Around a Circular Wetland 8

2.3 Analytical Solution for the Periodic Boundary Condition 9

2.4 Analytical Solution for the Non-periodic Boundary Condition 12

2.5 Application 14

2.6 Comparison of Analytical Solution and Numerical Solutions 17

2.7 Summary 18

3 TRANSIENT THREE-DIMENSIONAL DEFORMABLE FINITE-ELEMENT SATURATED GROUNDWATER MODEL 19

3.1 Introduction 19

3.2 Groundwater Flow Models Based on Finite-Difference and Finite-Element Approximation 21
3.3 Three-Dimensional Deformable Finite-Element Saturated Groundwater Model 24
3.3.1 Governing Equation and Boundary Conditions 27
3.3.2 Finite Element Model of Saturated Groundwater Flow 28
3.3.3 Adaptation of the Saturated Finite-Element Model to Describe the Free Surface 36
3.4 Validating the Code of the Three-Dimensional Deformable Finite-Element Groundwater Flow Model 37
3.4.1 Theis Solution 37
3.4.2 Groundwater Flow around a Circular Wetland 41
3.5 A Numerical Model Application to Simulate the Interaction Between a Wetland and an Aquifer 42
3.6 Application of Three-Dimensional Deformable Saturated Groundwater Flow Model to SV5 Wetland 50
3.6.1 Site Description-SV5 50
3.6.2 Field Methods and Wetland Aquifer Interaction Test 52
3.6.3 Stage-Volume Relationships 54
3.6.4 Creation of Finite-Element Model Mesh 56
3.6.5 Solution Procedure 57
3.6.6 Model Calibration and Results 58
3.7 Comparison with Results of Wise and others 69
3.8 Summary 71
4 INVERSE MODEL OF THREE-DIMENSIONAL FINITE-ELEMENT METHOD SATURATED GROUNDWATER MODEL IN SEARCHING FOR THE HYDRAULIC CONDUCTIVITY OF THE PEAT LAYER 69
4.1 Introduction 69
4.2 Adjoint Problem for Three-Dimensional Finite-Element Saturated Groundwater Model 73
4.3 Searching Objective Function 80

4.4 Adjoint State Controlling Equations 80
4.5 Searching Method and Stop Criterion 82
4.6 Field Application on SV5 82
4.8 Summary 85
5 THREE-DIMENSIONAL FINITE-ELEMENT VARIABLY-SATURATED GROUNDWATER MODEL 87
5.1 Introduction 87
5.2 Three-Dimensional Finite-Element Variably-Saturated Groundwater Model 88
5.2.1 Governing Equation 88
5.2.2 Linearizing the Governing Equations 89
5.2.3 Boundary Conditions for the Variably-Saturated Model 91
5.3 Finite-Element Method for Modeling Three-Dimensional Variably-Saturated Flow 94
5.4 Transient, Variably-Saturated Water-Table Recharge Example Test 98
5.5 Application on SV5 Wetland 101
5.5.1 Finite-Element Mesh for Three-Dimensional Variably-Saturated Flow Model 101
5.5.2 Modeling Results and Summary 103
6 SUMMARY AND CONCLUSIONS 111
REFERENCES 113
BIOGRAPHICAL SKETCH 126

LIST OF TABLES

Figure page

2-1 Parameters and their values 17

3-1 Selected early references for the finite-difference method 22

3-2 Selected early references for the finite-element application to model groundwater . 25

3-3 Parameters and their values 42

3-4 Data for calculating the discharge to the wetland from the aquifer at 10 hours 63

3-5 Data for calculating the discharge to the wetland from the aquifer at 20 hours 64

3-6 Data for calculating the discharge to the wetland from the aquifer at 30 hours 64

3-7 Data for calculating the discharge to the wetland from the aquifer at 40 hours 65

3-8 Data for calculating the discharge to the wetland from the aquifer at 50 hours 65

3-9 Sensitivities calculated by saturated groundwater flow model 66

4-1 Error and sensitivities based on the adjoint method model 84

5-1 Data for calculating the discharge to the wetland from the aquifer at 10 hours . . . 107

5-2 Data for calculating the discharge to the wetland from the aquifer at 20 hours . . . 108

5-3 Data for calculating the discharge to the wetland from the aquifer at 30 hours . . . 108

5-4 Data for calculating the discharge to the wetland from the aquifer at 40 hours . . . 109

5-5 Data for calculating the discharge to the wetland from the aquifer at 50 hours . . . 109

5-6 Sensitivities calculated by variably saturated groundwater flow model 110

LIST OF FIGURES

Figure page

2-1 Setup of the groundwater problem around a circular wetland 9

2-2 Transient groundwater level changes at radial distances 1,2,3 and 4 meters away from the wetland shoreline 15

2-3 Groundwater distribution over the distance to the wetland shoreline at 6,7,8,9,10 h 15

2-4 Three-dimensional view of the groundwater table around a circular wetland at t=3hr 16

2-5 Comparison of the analytical solution and numerical solution at 2 and 5 meters from the wetland shore line 18

3-1 Conceptual profile model of a wetland/groundwater system 26

3-2 Comparison of finite element mesh and finite difference mesh 26

3-3 Setup of the saturated groundwater problem around a wetland 27

3-4 Flowchart illustrating the iteration procedure of finding the coupling boundary condition 29

3-5 Unsteady flow to a well in phreatic aquifer at time t 38

3-6 Finite-Element Method mesh of the wedge used to simulate of a well pumping in phreatic aquifer 40

3-7 Comparison of the numerical and analytical head for the example problem of a transient pumping test in a phreatic aquifer 40

3-8 Comparison of the numerical and analytical simulated groundwater table 41

3-9 Three-dimensional finite-element mesh for the simulation of wetland and aquifer . 43

3-10 Relationship between the area of wetland water surface 44

3-11 Relationship between the deepest water depth and the volume of wetland 45

3-12 Illustration of the initial condition where it was assumed a wetland surface-water stage and the phreatic surface elevation were the same 45

3-13 Plan view of the numerical mesh at time zero. 46

3-14 Three-Dimensional Finite-Element mesh and simulated head contour at hour 5 . . 46

3-15 Simulated head contour at hour 5 47

3-16 Simulated iso-surface plot of 10.6 meter head at hour 5 47

3-17 Three-dimensional Finite-Element mesh and head contour on a cross section on a cross section through wetland 48

3-18 Simulated head contour on the vertical cross section through wetland 48

3-19 Modeled iso-surface head plot of 11.1 m,11m and 10.5 m 49

3-20 Mesh and modeled head contour with vertical cross section through the pumping well 49

3-21 Head contour (m) on the vertical cross section through the pumping well 50

3-22 Well location map (Switt et al. 1998) 51

3-23 Top surface of peat layer 54

3-24 Bottom surface of peat layer 55

3-25 Relationship between wetland volume and water stage 55

3-26 Finite-element mesh of wedge of wetland and aquifer for the saturated flow model 57

3-27 Vertical cross-section view of three-dimensional finite-element mesh and head from the saturated flow model 61

3-28 Piezometric head at positions beneath wetland with time 61

3-29 Variation in the inundated area of wetland during simulation 62

3-30 Discharge between wetland and aquifer with respect to time 62

3-31 Comparison between calculated head and observed head 63

3-32 Comparison results using Walser's parameter values 67

3-33 3-D numerical model simulated results over specific storage 67

4-1 Sketch showing setup of the saturated groundwater
inverse problem around a wetland 74

4-2 Relation between error and peat layer hydraulic conductivity 84

4-3 Flowchart illustrating the iteration procedure of inverse problem 85

4-4 Vertical cross-section of the adjoint state distribution at τ = 10 hours 86

5-1 Sketch showing setup of the variably saturated groundwater
flow problem around a wetland 92

5-2 Schematic of relative evapotranspiration (ET/PET),
as affected by soil water potential,ψ 93

5-3 Schematic diagram of the flow domain 99

5-4 Water moisture distribution (x:y=2:1) at 4 hours 100

5-5 Water moisture distribution at 8 hours (x:y=2:1) 101

5-6 Finite-element mesh of the wedge part for
variably saturated flow model (Unite is m) 102

5-7 Calculated piezometric head variation beneath wetland using
the three-dimensional variably saturated groundwater flow model 104

5-8 Model predicted discharge from the aquifer to the overlaying wetland 104

5-9 Inundated area of wetland during simulation 105

5-10 Simulated and observed heads in wetland and in aquifer 105

5-11 Simulated head from the saturated flow model and the variably saturated flow model 106

5-12 Horizontal view of the three-dimensional finite-element mesh and piezometric head distribution from the variably saturated flow model at time of 9 hours . . 106

5-12 Enlarged top and middle part of the mesh and head contour at time of 9 hours . . 107

LIST OF SYMBOLS

C	=	the conductance of the wetland confining unit
C_o	=	coefficient
$d_i(t)$	=	the unknown values of hydraulic head and at time t
ET	=	evapotranspiration [L/T]
$F(\omega)$	=	the Fourier coefficient
G	=	ground-water level [L]
G_i	=	groundwater inflow [L^3/T]
G_o	=	groundwater outflow [L^3/T]
GW_{NS}	=	the net flow or seepage of groundwater to the wetland surface [L^3/T]
h	=	piezometric head [L]
$h^{(e)}$	=	the approximate solution for hydraulic head within element e [L]
H_o	=	initial saturated aquifer thickness [L]
H^l	=	Sobolev space
$H_o(t)$	=	the Hankel function order 0
h_{oo}	=	the regional average water table elevation, [L]
i	=	reference integer spatial interval
J_o	=	the Bessel function of the first kind order 0
k	=	a constant parameter
K	=	the saturated hydraulic conductivity tensor [L/T]
K_h/K_v	=	anisotropic ratio
K_s	=	hydraulic conductivity [L/T]
K_{xx}	=	horizontal hydraulic conductivity in x direction [L/T]

K_{yy}	=	horizontal hydraulic conductivity in y direction [L/T]
K_{zz}	=	vertical hydraulic conductivity [L/T]
$K_{i,j}$	=	the saturated hydraulic conductivity tensor [L/T]
K_{rw}	=	the relative permeability while the degree of water saturation is S_w
L	=	average peat thickness [L]
n	=	current integer time level
$N_i^{(e)}$	=	the interpolation functions for each node within element e
$\underline{n}$	=	a unit outward normal vector to the boundary
N_o	=	the number of observation wells
N_n	=	the total number of nodes used in the numerical solution
p	=	the number of nodes within element e
P_n	=	net precipitation (total precipitation minus intercepted precipitation[L^3/T]
P_c	=	the capillary pressure ($P_c = - \psi$) [M/LT^2]
PET	=	the daily potential evapotranspiration [L/T]
Q	=	pumping discharge [L^3/T]
r	=	the radial coordinate [L] radial distance from the well [L]
r_o	=	the radius of the circular lake [L]
s	=	drawdown [L]
S	=	the specific storage
S_i	=	surface inflows, including flooding stream [L^3/T]
S_o	=	surface outflows [L^3/T]
S_s	=	the specific storativity [L^{-1}]
SA_w	=	wetland wetted surface area [L^2]
SA_{NW}	=	wetland dry surface area [L^2]
SP	=	exchanging flux [L^3/T]
S_w	=	the degree of saturation, equal to θ/θ_s

S_{wr}	=	the residual saturation
S_e	=	effective saturation
t	=	time [T]
t_f	=	the time duration of the simulation [T]
t_j	=	the observation times [T]
T	=	the transmissivity in the aquifer [L^2/T]
T_i	=	tidal inflow (+) or outflow (-) [L^3/T]
u	=	space function
V_w	=	the wetland volume [L^3]
Vp	=	the volume above the bottom of the peat layer [L^3]
W	=	wetland water level [L]
$W_i^{(e)}$	=	the weighting function
x, y, z	=	the axes in the physical domain
X	=	the function of time
Y_o	=	the Bessel function of the second kind order 0
z	=	the vertical coordinate or elevation head (L)
∇	=	the gradient operator
ΔH	=	the average difference in hydraulic head [L]
Δr	=	the radial step [L]
Δt	=	the time step [T]
ΔV	=	change in the volume of water storage in wetland [L^3]
Δx	=	the mesh space step in x-direction [L]
Δz	=	the mesh space step in y-direction [L]
ω	=	the angular frequency
ξ, η	=	the axes in the computational domain
Γ	=	the boundary of volume Ω

Γ_1	=	flux boundary
Γ_2	=	head boundary
γ	=	specific weight of a unit volume of water = ρg [M/L^2T^2]
ψ	=	the pressure [M/LT^2]
Ω_i	=	the exclusive subdomain of node i
δK	=	variation of K [L/T]
δh	=	variation of head h [L]
$\Psi(x,y,t_f - \tau)$	=	the adjoint state of h
τ	=	$t_f - t$ [T]
α and m	=	parameters obtained from a fit of above equations to experimental results
θ	=	the water content, [L^3/L^3]
θ_s	=	the saturated water content, [L^3/L^3]
θ_r	=	residual moisture content, [L^3/L^3]
ψ	=	pressure head; [M/LT^2]
ψ^*	=	the value of ψ when ET = 0.5PET, [M/LT^2]
ψ_{Wmin}	=	the ψ corresponds to PE/PET=0.05, [M/LT^2]
ψ_{Wmax}	=	the value of ψ when PE=0.95 PET [M/LT^2]

Abstract of Dissertation Presented to the Graduate School
of the University of Florida in Partial Fulfillment of the Requirements
for the Degree of Doctor of Philosophy

TWO-DIMENSIONAL ANALYTICAL AND THREE-DIMENSIONAL FINITE ELEMENT METHOD MODELING OF THE INTERACTIONS BETWEEN WETLANDS AND GROUNDWATER

By
Jinhua Zhong
December, 2004
Chairman: Louis H. Motz
Cochair: Kirk Hatfield
Major Department: Civil and Coastal Engineering

Simulating saturated/unsaturated flow between wetlands and the contiguous subsurface is complex, because it involves the modeling of wetland storage changes that in turn cause changes in pertinent hydrologic boundary conditions. Existing groundwater models are incapable of simulating the flow between a wetland and an aquifer, if small changes in wetland storage cause significant vertical and lateral movements of the wetland boundary. In addition to the simulation complexities introduced by a change in wetland geometry and storage, periodic and nonperiodic fluctuations of the wetland stage induce corresponding elevation changes in the phreatic surface of the contiguous aquifer. As these induced waves propagate through an aquifer, friction causes a loss of energy, which is manifested as spatially dampened potentiometric head perturbations along the inland direction. An analytical model was developed that describes subsurface flows around a wetland induced by any nonperiodic fluctuations in surface-water stage, such as a flood wave. Not considered,

however, are any changes in wetland storage, or wetland geometry as a function of surface water stage. The analytical model was validated using a finite-difference numerical groundwater model that is based on the governing equation expressed in radial coordinates. Comparisons of analytical and numerical results show excellent agreement.

Two numerical models were specifically designed to simulate wetland-aquifer interactions. The first model is a saturated groundwater flow model that incorporates adaptive simulation technologies to permit real-time simulation of moving wetland boundaries and their associated local influence on the phreatic surface. This model is numerically efficient and uses deformable hexahedral finite elements to trace phreatic surface changes in real-time. The second model also uses deformable hexahedral finite elements; however, this model simulates variably saturated groundwater flow. For both models, the numerical elements deform as required to characterize the horizontal and vertical extent of the moving wetland boundary (which serves to define a location within the porous system, where the pressure is known). Simulation results from both models were applied to a field site where water was rapidly withdrawn from an isolated wetland to observe system response and evaluate the wetland aquifer hydraulic connection.

CHAPTER 1
INTRODUCTION

1.1 Wetland

Wetlands are transitional lands between terrestrial and aquatic systems where the water table is usually at or near the surface, or the land is covered by shallow water (Cowardin et al. 1979). Wetlands are also called marsh, fen, peatland or water and can be natural or artificial and permanent or temporary. The water can be static or flowing and fresh or brackish, or it can include areas of marine water the depth of which at low tide does not exceed 6 meters (Ramsar Convention 1971, Middleton 1998).

Wetlands perform various environmental functions that include increasing flood mitigation, enhancing storm abatement (i.e., in the case of coastal wetlands), adding groundwater recharge, providing water quality treatment, serving as wildlife habitats, and performing aesthetic functions (Mitsch and Gosselink 1993). These functional attributes can be classified into three basic types: hydrologic, water quality, and life support. Measures of the life-support function must integrate several wetland attributes, including water quality, hydroperiod and hydrodynamics, habitat structure, food chain support, biogeographic setting, nutrient status, corridors for migration, and primary production (Preston and Bedford 1988).

In recent years, increasing interest has focused on the study and protection of wetlands. Development, drainage, population pressure, and pollution have destroyed extensive areas of these sensitive ecosystems. Another increasingly significance to wetlands is municipal well fields supplying water to large urban areas. These well fields affect

wetlands by reducing surficial aquifer levels over large areas that encompass isolated and interconnected wetlands (Sonenshein and Hofstetter 1990). As a result of depressing the water table, historically wet ecosystems have been drained (Switt et al. 1998).

1.2 Wetland Water Budget

Hydrologic conditions are extremely important for the maintenance of a wetland's structure and function. A hydrologic budget is often used to quantify the volume and rate of water flowing into and out of a wetland. The primary hydrologic inflows include precipitation, streams, groundwater, and, in coastal wetlands, tides (Mitsch and Gosselink 1986, Rosenberry 2000). The wetland water budget equation as defined by Mitsch and Gosselink (1993) is:

$$\Delta V/\Delta t = P_n + S_i + G_i - ET - S_o - G_o \pm T \qquad (1\text{-}2)$$

where

ΔV = change in the volume of water storage in wetland [L^3]

Δt = change in time [T]

P_n = net precipitation (total precipitation minus intercepted precipitation (I)) [L^3/T]

S_i = surface inflows, including flooding stream [L^3/T]

G_i = groundwater inflow [L^3/T]

ET = evapotranspiration [L^3/T]

S_o = surface outflows [L^3/T]

G_o = groundwater outflows [L^3/T]

T = tidal inflow (+) or outflow (-) [L^3/T]

Terms in the wetland water budget vary in importance depending on the wetland type, and not all terms are required to characterize a specific type of wetland. In most wetland systems, precipitation and evapotranspiration are major components of the water budget (Winter and Woo 1990). Groundwater can also have a significant influence on some wetland systems, but not always.

Three of the most common relationships that characterize a wetland are groundwater discharge, groundwater inflow and outflow, and groundwater recharge. Groundwater inflow occurs when the contiguous wetland surface water (or groundwater) stage is lower than the phreatic surface of the surrounding aquifer. When the surface water stage or groundwater levels inside a wetland are higher than the phreatic surface in the surrounding contiguous aquifer, groundwater and surface water will flow out of wetland. When a wetland is situated well above the groundwater, the wetland is identified as being perched. This type of hydrologic system, referred to as a surface water depression wetland by Novitzki (1979), loses water only through infiltration into the ground and through evapotranspiration.

The rate of water exchange between a wetland and local aquifer is a function of the hydraulic gradient between the two hydrologic subsystems. The discharge, in accordance with Darcy's law (Truesdell 1995), is proportional to the hydraulic gradient, the hydraulic conductivity, and the cross-sectional area through which the flow occurs. Periodic or nonperiodic fluctuations of the wetland stage in a flow-through wetland will induce fluctuations in the elevation of the phreatic surface in the contiguous aquifer. As these induced waves propagate through an aquifer, friction causes a loss of energy, which is manifested as spatially dampened head perturbations. This damping effect progressively diminishes the amplitude of piezometric head along the inland direction (Carr and Van Der

Kamp 1969). Many studies have examined the problem through one-dimensional analytical solutions (Cooper 1963, Gregg 1966, Nielsen 1990, Serfes 1992, Li, Barry et al. 2000, 2001, Boufadel and Peridier 2002, Seerano 2003, Swamee and Singh 2003). A two-dimensional analytical solution was obtained by considering a shift in phase and a change in amplitude along a straight coastline (Sun 1997). Three-dimensional flow regimes near a shallow circular lake was studied using numerical and analytical mathematical models of aquifer flow (Townley and Trefry 2000).

To further the understanding of the interactions between lakes or wetlands and groundwater, without the restrictive assumptions typically associated with analytical solutions, numerical models are usually used. For example, it is possible to obtain numerical solutions for the case of anisotropic and nonhomogeneous conditions. The accuracy of solutions obtained by numerical methods can be excellent; however, it depends on several factors, including the type of numerical method used, the complexity of boundary and initial conditions, and the computational precision of the computer used to implement the method. Regardless of these advantages, few investigators have chosen to focus on the numerical simulation of interactions between wetlands and groundwater (McDonald and Harbaugh 1988, Schaffranek 1996, Lee 2000).

1.3 Goals and Objectives

Analytical models to simulate the complex groundwater surface water interactions that occur with isolated and flow-through wetlands would be valuable tools for developing hydrologic budgets for wetlands. Given that most surface water fluctuations are nonperiodic, there is a need to develop analytical groundwater models for simulating groundwater table fluctuations induced by both periodic and nonperiodic surface water flood waves. However,

with the exception of the one-dimensional study by Cooper and Rorabaugh (1963), most investigations addressed surface-water fluctuations that were periodic. Thus, the first goal of this dissertation was to develop an analytical method for simulating groundwater table fluctuations induced by both periodic and nonperiodic surface-water flood waves. This goal was achieved by meeting the single objective of developing an analytical model using Fourier transforms.

A limited number of three-dimensional numerical groundwater models have been developed to simulate groundwater wetland interactions; however, these models are generally inadequate tools for simulating the complex interactions between a wetland and a contiguous unconfined aquifer. For example, Walser, Annable and Wise (1998) used FEMWATER (Yeh, 1992), a variably saturated flow model, to simulate the exchange of water between a wetland and an aquifer. McDonald and Harbaugh (1988) used MODFLOW and developed a three-dimensional finite difference groundwater model and studied the dynamic coupling between wetlands and the subsurface. Lee (2000) used the HYDRUS-2D flow model and simulated vertical two-dimensional groundwater flow through Lake Barco in Florida. Neither FEMWATER (1996) nor MODFLOW can simulate or incorporate a moving real-time wetland boundary caused by a change in surface water stage. Furthermore, as a saturated three-dimensional finite-difference model, MODFLOW can not simulate fluctuations of the phreatic surface as a moving transient boundary as required to define fully the three-dimensional flow. Finally, the water stage of a wetland itself is a function of the transient exchange of water between a surface and subsurface systems; which is not fully modeled in any existing groundwater flow codes. Thus, to simulate groundwater surface water interaction without the above identified shortcomings of existing models, a new model is

needed.

The second goal of the dissertation was to develop two numerical models capable of simulating 1) a transient and moving wetland boundary, 2) three-dimensional flow, 3) the movement of the phreatic surface, and 4) the coupling that occurs between the transient surface-water stage and the phreatic surface. To achieve this goal, two objectives were pursued. The first objective was to develop two numerical groundwater models using finite elements. The second objective was to apply both numerical models to simulate groundwater and surface water fluctuations over an isolated wetland in southern Florida. Of the two models developed, the first is a three-dimensional saturated groundwater flow model that employs deformable hexahedral elements. The finite-element mesh deforms in space and time to trace the location of the phreatic surface of an unconfined aquifer and the stage of the contiguous surface water body. Based on the above model and the adjoint state method, an inverse model was developed to estimate the hydraulic conductivity of peat layers which typically exist as a wetland bottom that serves to isolate surface wetlands from subsurface groundwater systems. The second numerical model, a three-dimensional variable saturated flow model, was also developed using deformable mesh. This model was used to investigate prediction differences between the saturated flow code and the variable saturated model. From the groundwater flow pattern given by both models, an improved understanding was obtained for the interactions occurring between surface waters and groundwaters. In addition, an improved understanding was obtained of how short-term pumping from a phreatic aquifer affects wetlands and lake water stages.

CHAPTER 2
ANALYTICAL GROUNDWATER MODEL RESPONSE TO THE PERIODIC OR NON-PERIODIC WATER STAGE FLUCTUATIONS IN A CIRCULAR WETLAND

2.1 Introduction

Periodic or nonperiodic fluctuations of the surface water stage in wetlands or lakes will induce fluctuations in the elevation of the phreatic surface of contiguous unconfined aquifers. As these induced waves propagate through the aquifer, friction causes a loss of energy, which is manifested as spatially dampened head perturbations. This damping effect progressively diminishes the amplitude of fluctuations in the piezometric head along the inland direction (Carr and Van Kamp 1969). Many studies have examined the problem through one-dimensional analytical solutions (e.g.,Cooper and Rorabaugh 1963, Gregg 1966, Nielsen 1990, and Serfes 1992, Li, Barry et al. 2000, 2001, Boufadel and Peridier 2002, Seerano 2003, Swamee and Singh 2003). Cooper and Rorabaugh (1963) obtained the analytical solution for groundwater movement and bank storage due to flood stages in surface streams. Gregg (1966) found a one-dimensional relation between tidal fluctuations and groundwater table perturbations. Nielsen (1990), Serfes (1992) and Carr (1969) also published papers investigating the similar problems. A two-dimensional analytical solution was obtained by considering a phase shift in water-table perturbations and the associated change of amplitude along a straight coastline (Sun 1997). An analytical solution representing vertical two-dimensional groundwater-surface water interaction was obtained by Anderson (2003). Three-dimensional flow regimes near a shallow circular lake was

studied using numerical and analytical mathematical models of aquifer flow (Townley and Trefry 2000, Smith and Townley 2002).

With the exception of Cooper and Rorabaugh (1963), all of the above studies addressed periodic surface-water fluctuations, in spite of the fact that most stage variations are not periodic i.e., consider, for example, the pervasive nonperiodic flooding of rivers, lakes, and wetlands.

Cooper's (1963) nonperiodic analytical model for a river/groundwater system was a one-dimensional solution along an axis perpendicular to the river. However, this analytical model is not suitable for simulating the nonperiodic interactions between a wetland and an aquifer. In this chapter, two analytical groundwater models are developed to describe transient groundwater levels affected by periodic and nonperiodic fluctuations of the surface-water stage in a wetland or a lake.

2.2 Problem Formulation: Groundwater Flow Around a Circular Wetland

Considering a circular wetland that is hydraulically contiguous to a surfacial aquifer and ignoring recharge from rainfall, the governing equation for two-dimensional groundwater flow in a homogeneous isotropic aquifer can be expressed in radial coordinates as:

$$\frac{\partial^2 h}{\partial r^2}+\frac{1}{r}\cdot\frac{\partial h}{\partial r}=\frac{S}{T}\frac{\partial h}{\partial t} \tag{2-1}$$

where h is the piezometric head, r is the radial coordinate, t is time, S is the specific storage and T is the transmissivity in the aquifer. When a thick unconfined aquifer is considered, the gradient and small fluctuations relative to saturated thickness are assumed to be small, T is approximately equal to Kh_{oo} (Figure 2-1) in which K is the hydraulic conductivity and h_{oo} is

the average unconfined aquifer thickness equal to the regional average water-table elevation above an underlying impermeable confining unit.

The boundary condition along the shore line of the wetland is Eq. 2-2, where r_o is the radius of the circular wetland. It is also assumed in Eq. 2-3 that as $r \to \infty$, the groundwater table elevation approaches the regional average water table elevation, h_{oo}.

$$B.C: h(r,t)\big|_{r=ro} = h_{oo} + f(r_o,t) \qquad @\ r = r_o \tag{2-2}$$

$$h(r,t)\big|_{r=\infty} = h_{oo} \qquad @\ r = \infty \tag{2-3}$$

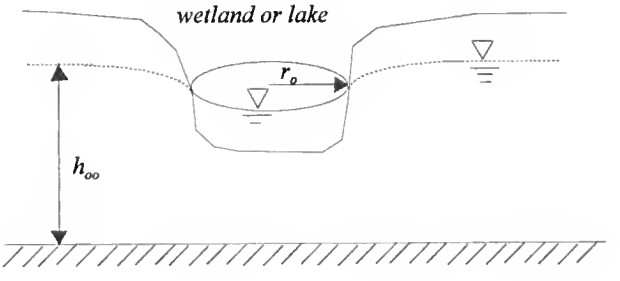

Figure 2-1. Setup of the groundwater problem around a circular wetland

2.3 Analytical Solution for the Periodic Boundary Condition

Since the boundary condition is a periodic function of time, substituting for $f(r_o,t)$, Equation 2-4 is obtained:

$$B.C: h(r,t)\big|_{r=ro} = h_{oo} + h_o\, e^{i\omega t} \qquad @\ r = r_o \tag{2-4}$$

$$h(r,t)\big|_{r=\infty} = h_{oo} \qquad @\ r = \infty \tag{2-5}$$

where h_o is the half height of the periodic constituent and ω is the angular frequency. No initial condition is necessary, since here the steady-state oscillatory solution is sought as $t \to \infty$. Because of the oscillatory boundary condition, a solution is sought in the form

$$h(r,t)=h_{oo}+h_o g(r)e^{\omega ti} \tag{2-6}$$

Substitution of Eq. 2-6 into Eq. 2-1, Eq. 2-2, and Eq. 2-3 yields

$$\frac{\partial^2 g}{\partial r^2}+\frac{1}{r}\cdot\frac{\partial g}{\partial r}-\frac{S\omega}{T}\cdot i\cdot g=0 \tag{2-7}$$

where the boundary conditions are:

$$g(r)=1 \qquad @\ r=r_o \tag{2-8}$$

$$g(r)=0 \qquad @\ r=\infty \tag{2-9}$$

Equation 2-7 can now be rewritten to obtain:

$$v^2\frac{\partial^2 g}{\partial v^2}+v\frac{\partial g}{\partial v}+v^2 g=0 \tag{2-10}$$

$$v=\sqrt{\frac{S\omega}{2T}}\cdot(i-1)\cdot r \tag{2-11}$$

The solution to Equation 2-10 subject to the boundary conditions in Equation 2-8 and 2-9 depends on the value of ω. Considering the boundary condition along the shoreline, groundwater around a circular water body will have the following forms.

When ω is greater than 0:

$$g(r)=C_o(J_o+iY_o)=C_o H_o^{(1)}(v)=\frac{H_o^{(1)}(v)}{H_o^{(1)}(v_o)} \tag{2-12}$$

and when ω is less than 0:

$$g(r)=C_o(J_o-iY_o)=C_oH_o^{(2)}(u)=\frac{H_o^{(2)}(u)}{H_o^{(2)}(u_o)} \tag{2-13}$$

where J_o is the Bessel function of the first kind order 0; Y_o is the Bessel function of the second kind order 0; $H_o(t)$ is the Hankel function order 0; and C_o is a coefficient (Lebedev 1965). Substitution of Eq. 2-12 and Eq. 2-13 into Eq. 2-6 gives the following solution for the groundwater flow around a circular lake affected by periodic function:

$$h_\omega(r,t)=h_{oo}+h_o\frac{H_o^{(1)}(v)}{H_o^{(1)}(v_o)}\cdot e^{\omega ti} \tag{2-14}$$

for ω > 0 and:

$$h_\omega(r,t)=h_{oo}+h_o\frac{H_o^{(2)}(u)}{H_o^{(2)}(u_o)}\cdot e^{\omega ti} \tag{2-15}$$

for ω < 0.

The asymptotic approximations of the functions $H_o^{(1)}(z)$ and $H_o^{(2)}(z)$ are:

$$H_0^{(1)}(z)=\left(\frac{2}{\pi z}\right)^{1/2}e^{i\left(z-\frac{\pi}{4}\right)}\left[\sum_{k=0}^{n}\frac{1\cdot 3^2\cdots(2k-1)^2}{2^{2k}\cdot k!}(2iz)^{-k}+O(|z|^{-n-1})\right] \tag{2-16}$$

$$H_0^{(2)}(z)=\left(\frac{2}{\pi z}\right)^{1/2} e^{(-1)i\left(z-\frac{\pi}{4}\right)}\left[\sum_{k=0}^{n}(-1)^k\frac{1\cdot 3^2\cdots(2k-1)^2}{2^{2k}\cdot k!}(2iz)^{-k}+O(|z|^{-n-1})\right] \tag{2-17}$$

$$u=\sqrt{\frac{S|\omega|}{2T}}\cdot(-1-i)\cdot r \qquad u_o=\sqrt{\frac{S|\omega|}{2T}}\cdot(-1-i)\cdot r_o$$

$$v=\sqrt{\frac{S\omega}{2T}}\cdot(i-1)\cdot r \qquad v_o=\sqrt{\frac{S\omega}{2T}}\cdot(i-1)\cdot r_o$$

2.4 Analytical Solution for the Non-Periodic Boundary Condition

A flood wave will typically induce a nonperiodic variation in the wetland stage. Here, $f(r_o,t)$, which is a nonperiodic function of time, is assumed to describe transient variations in the wetland stage. Using the Fourier transformation, $f(r_o,t)$ can be represented as:

$$f(r_o,t)=\frac{1}{2\pi}\int_{-\infty}^{+\infty}F(\omega)e^{i\omega t}d\omega \tag{2-18}$$

where $F(\omega)$ is the Fourier coefficient, and $F(\omega)d\omega$ is the amplitude of oscillation for the component with a frequency in the range of $(\omega,\omega+d\omega)$. For this $F(\omega)$, the corresponding fluctuations in the groundwater table are described by:

$$h_\omega(r,t)=h_{oo}+F(\omega)\frac{H_o^{(1)}(v)}{H_o^{(1)}(v_o)}\cdot e^{\omega ti} \qquad (\omega>0) \tag{2-19}$$

or

$$h_{\omega}(r,t)=h_{oo}+F(\omega)\frac{H_o^{(2)}(u)}{H_o^{(2)}(u_o)}\cdot e^{\omega ti} \qquad (\omega<0) \qquad (2\text{-}20)$$

as given by Eq. 2-14 and Eq. 2-15. The inverse Fourier transformation of Equation 2-19 and Eq. 2-20 leads to:

$$h(r,t)=h_{oo}+\frac{1}{2\pi}\left(\int_0^{+\infty}F(\omega)\frac{H_o^{(1)}(v)}{H_o^{(1)}(v_o)}\cdot e^{\omega ti}\cdot d\omega+\int_{-\infty}^{0}F(\omega)\frac{H_o^{(2)}(u)}{H_o^{(2)}(u_o)}\cdot e^{\omega ti}\cdot d\omega\right)$$

$$=h_{oo}+\frac{1}{2\pi}\left[\int_0^{+\infty}\left(\int_{-\infty}^{+\infty}f(r_o,\tau)e^{-\omega\tau i}d\tau\right)\frac{H_o^{(1)}(v)}{H_o^{(1)}(v_o)}\cdot e^{\omega ti}\cdot d\omega+\int_{-\infty}^{0}\left(\int_{-\infty}^{+\infty}f(r_o,\tau)e^{-\omega\tau i}d\tau\right)\frac{H_o^{(2)}(u)}{H_o^{(2)}(u_o)}\cdot e^{\omega ti}\cdot d\omega\right.$$

$$=h_{oo}+\frac{1}{2\pi}\int_{-\infty}^{+\infty}f(r_o,\tau)\left(\int_0^{+\infty}\frac{H_o^{(1)}(v)}{H_o^{(1)}(v_o)}\cdot e^{\omega(t-\tau)i}\cdot d\omega+\int_{-\infty}^{0}\frac{H_o^{(2)}(u)}{H_o^{(2)}(u_o)}\cdot e^{\omega(t-\tau)i}\cdot d\omega\right)d\tau \qquad (2\text{-}21)$$

From the above analytical model, it is clear that the unsteady groundwater table around a circular wetland depends not only on the instantaneous values of the wetland water stage but also on the accumulative effect represented by the integration. However, physically it is not possible for the wetland water stage at a later time to affect the groundwater table at an earlier time. Hence, the phreatic surface depends on its current stage and historical stage. The

final analytical solution to the nonperiodic boundary condition 2-2 is then

$$h(r,t)=h_{oo}+\frac{1}{2\pi}\int_{-\infty}^{t} f(r_o,\tau)\left(\int_{-\infty}^{0}\frac{H_o^{(2)}(u)}{H_o^{(2)}(u_o)}\cdot e^{\omega(t-\tau)i}\cdot d\omega+\int_{0}^{+\infty}\frac{H_o^{(1)}(v)}{H_o^{(1)}(v_o)}\cdot e^{\omega(t-\tau)i}\cdot d\omega\right)d\tau \qquad (2\text{-}22)$$

2.5 Application

If it is assumed that wetland stage fluctuations can be described by a nonperiodic Gaussian function of time, then:

$$f(r_o,t)=\frac{1}{\sqrt{2\pi}\sigma}e^{-\frac{(t-t_o)^2}{2\sigma^2}} \qquad (2\text{-}23)$$

The analytical solution obtained when Eq. 2-23 is combined with Eq. 2-21 is:

$$h(r,t)=h_{oo}+\frac{1}{2\pi}\int_{-\infty}^{t}\frac{1}{\sqrt{2\pi}\sigma}e^{-\frac{(\tau-t_o)^2}{2\sigma^2}}\left(\int_{-\infty}^{0}\frac{H_o^{(2)}(u)}{H_o^{(2)}(u_o)}\cdot e^{\omega(t-\tau)i}\cdot d\omega+\int_{0}^{+\infty}\frac{H_o^{(1)}(v)}{H_o^{(1)}(v_o)}\cdot e^{\omega(t-\tau)i}\cdot d\omega\right)d\tau$$

(2-24)

The transient changes of groundwater table described by Eq. 2-24 at four different distances from the wetland are shown in Figure 2-2. The groundwater distributions along the radius at four different times are shown in Figure 2-3. From both figures, it is evident that groundwater fluctuations are greatest near the wetland. From Figure 2-3, it can be seen that the variation of the groundwater table over time is no longer symmetrical although the

variation of the wetland water stage is a Gaussian distribution which is symmetrical over time.

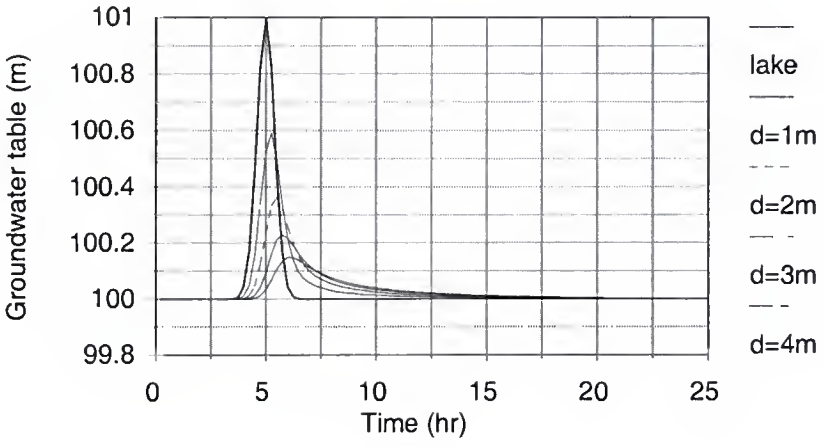

Figure 2-2. Transient groundwater level changes at radial distances 1,2,3, and 4 meters away from the wetland shoreline.

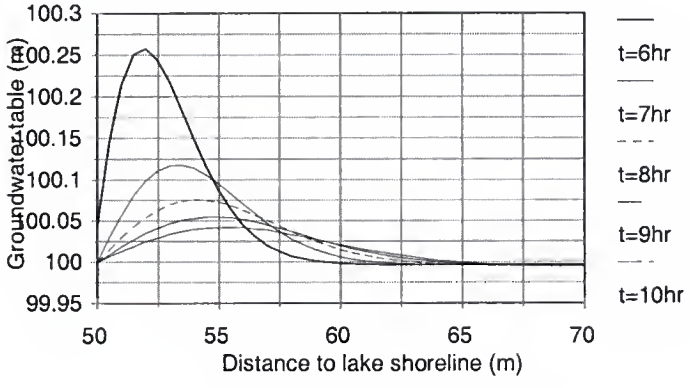

Figure 2-3. Groundwater distribution over the distance to the wetland/lake shoreline at 6,7,8,9, and 10 h.

Figure 2-4 shows the groundwater table elevations around a circular wetland after 3 hours. The radius of the wetland is 50 meters. All other parameters are listed in Table 2-1. Theoretically, when ω is very large, it means that the frequency of the corresponding boundary condition is very large and the period is very short. When the absolute value of ω is very large, its effect on the groundwater around the wetland is very small. This is because the period of the wave component is too small to have any impact on the groundwater around the wetland. That is to say, when the integration of ω is taken, a certain negative number could be used to replace the negative infinite number, and a certain positive number could also be used to replace the positive infinite number. Accurate model results are obtained when ω takes the range of [-5, 5]. Thus, it may be assumed that the boundary condition has no effect on the ground water table if the frequency of the boundary water level is very large.

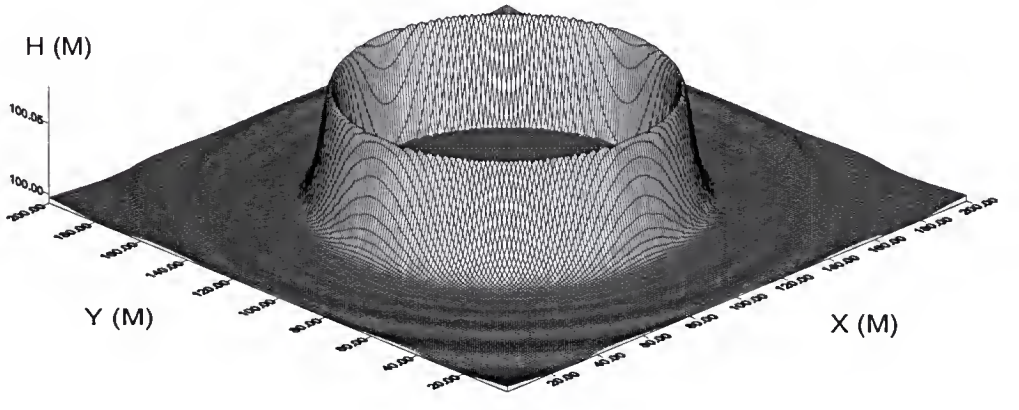

Figure 2-4. Three-dimensional view of the groundwater table around a circular wetland at t=3 h.

2.6 Comparison of Analytical Solution and Numerical Solutions

A comparison was made between the analytical and the numerical solutions to the radial flow problem specified through Eq. 2-1-Eq. 2-3. An implicit finite-difference scheme was used to represent the radial form of the groundwater flow equation Eq. 2-1 as:

$$\frac{h_{i-1}^{n+1}-2h_i^{n+1}+h_{i+1}^{n+1}}{(\Delta r)^2}+\frac{1}{r_i}\frac{h_{i+1}^{n+1}-h_{i-1}^{n+1}}{2\Delta r}=\frac{S}{T}\frac{h_i^{n+1}-h_i^{n}}{\Delta t} \tag{2-25}$$

Here i is the reference integer spatial interval; n is the current integer time level; Δt is the time step; and Δr is the radial step.

A circular wetland which has a radius of 50 meters was assumed. All other system parameters are given in the Table 2-1. By considering the different boundary conditions (Eq. 2-3 and Eq. 2-4), the corresponding numerical results are found [Figure 2-5]. Analytical and numerical results illustrate time variations in groundwater levels. Figure 2-5 shows that the analytical solution and numerical solution compare very well.

Table 2-1. Parameters and their values

Parameter	Value	Parameter	Value
H_{oo} (m)	100.0	T (m^2/h)	0.635
Δr (m)	0.25	S	0.2
Δt (hr)	0.02	t_o (h)	5.0
k (m/hr)	0.00635	σ	0.4

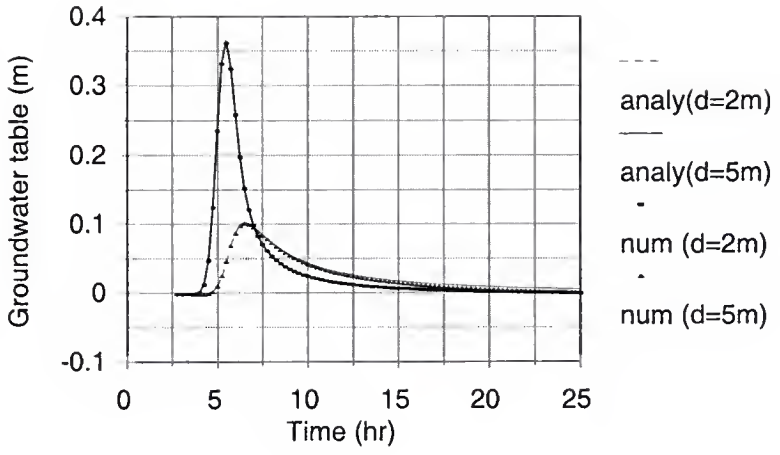

Figure 2-5. Comparison of analytical solution and numerical solution at 2 and 5 meters from the wetland shoreline.

2.7 Summary

The analytical model presented in this chapter can be used to simulate aquifer surface fluctuations caused by the transient wetland stages regardless of the temporal function assumed to describe variations of water stage. In other words, the model can deal with any general transient of the boundary function. The analytical model was validated using a finite-difference numerical groundwater model for a homogenous aquifer. This first numerical method is not recommended for simulations involving heterogenous aquifers. Rather, a new method is presented for simulating wetland/aquifer interactions in such aquifers, which requires a simple transformation of the equations. The excellent agreement between two models shows that the analytical solution presented is valid. This model is also useful in a situation where groundwater and the surface water components are being considered in a system-wide water balance.

CHAPTER 3 TRANSIENT THREE-DIMENSIONAL DEFORMABLE FINITE-ELEMENT SATURATED GROUNDWATER MODEL

3.1 Introduction

Recent research has focused on the details of various wetland functions such as water-quality treatment, flood-wave suppression, and groundwater/surface water interactions (Wise et al. 2000, Krabbenhoft and Webster 1995, Anderson and Cheng 1993, Ruddy and Williams 1991, and Mills and Zwarich 1986). For example, Ruddy and Williams (1991) investigated the hydrologic relation between the South Fork Williams Fork stream in the Colorado River basin and four adjacent subalpine wetlands, and they also evaluated the potential effects on these wetlands when stream flow is diverted. They concluded that stream flow was the primary source of water for two of the four wetlands, whereas precipitation, snowmelt, valley side-slope flow (including overland and small-channel flow), and groundwater inflow served to define the transient hydrological behavior of all wetlands.

The above studies showed that wetland functions (i.e., water quality treatment, floodwave suppression, etc.) are correlated with recharge and discharge areas, ground-water-flow paths and rates, and soil-profile development. The location of recharge and discharge areas can change in response to seasonal or weather-related factors and can affect the groundwater flow direction. As a result, groundwater and surface water quality and the presence of various wetland-plant communities may all vary in response to these changing conditions.

Analytical models such as the one presented in Chapter 2 can be used to simulate deep wetlands or lakes. However, the primary limitation of analytical methods is that solutions can only be obtained by imposing severely restrictive assumptions on aquifer properties and boundary and initial conditions. For example, an assumption commonly made to obtain analytical solutions is that the aquifer is isotropic and homogeneous for hydraulic conductivity. These assumptions, however, are not valid and often not adequate to describe groundwater flow or solute transport in most field situations.

Numerical methods have the primary advantage over analytical approaches in that they do not require such restrictive assumptions. For example, it is possible to obtain numerical solutions for the case of anisotropic and nonhomogeneous conditions. The accuracy of solutions obtained by numerical methods can be excellent. However, this accuracy depends on several factors, including the type of numerical method used, the complexity of boundary and initial conditions, and the computational precision of the computer used to implement the method. Regardless of these advantage, only a few investigators have chosen to focus on the numerical simulation of interactions between wetlands and groundwater (e.g., Schaffranek 1996 and McDonald and Harbaugh 1988, Lee 2000, Rosenberry 2000). In this chapter, a general discussion of the advantages/disadvantages of two numerical methods commonly used to model hydrologic systems is briefly discussed. Next, the mathematical development of a three-dimensional deformable finite-element saturated groundwater model is presented. This model and the associated code are then validated by comparing model predictions with analytical modeling results. A more complicated application of the three-dimensional model is presented to illustrate the type of information provided through the numerical approach taken. Finally, the

model is used to simulate an actual wetland using field data collected when the hydrologic system was responding to induced stress.

3.2 Ground-Water Flow Models Based on Finite-Difference and Finite-Element Approximation

Several types of numerical methods have been used to solve groundwater flow problems, the two principal ones being the finite-difference method and the finite-element method. The finite-difference method was initially applied to the flow of fluids in petroleum reservoirs, and it wasn't until the mid-1960's that problems of groundwater flow and solute transport were examined. The method has a number of advantages that contribute to its continued widespread use and popularity: (1) for simple problems such as one-dimensional, steady-state groundwater flow in an isotropic and homogeneous aquifer, mathematical formulation and computer implementation are easily understood; and (2) the accuracy of solutions to steady-state and transient groundwater flow problems is generally quite good. The finite-difference method also has disadvantages: (1) the method works best for rectangular or prismatic aquifers of uniform composition (for example, it is difficult to incorporate irregular or curved aquifer boundaries, anisotropic and heterogeneous aquifer properties, or sloping soil and rock layers into the numerical model without introducing numerous mathematical and computer programming complexities); and (2) the accuracy of solutions to solute transport problems is less than can be obtained through application of the finite-element method. Table 3.1 lists selected early references where finite-difference methods were applied to model groundwater flow. More recent applications of hydrologic modeling using finite-difference for simulating of surface water /groundwater interactions include studies by Mc Donald and Harbaugh (1998), Winter (1983, 1986, and 1989), Sacks

(1992) and Krabbenhoft and Anderson (1990).

Table 3-1. Selected early references for the finite-difference method.

Topic	Reference
Early Developments in Petroleum Reservoir Modeling	Bruce et al. (1953), Peace and Rachford (1962)
Saturated Groundwater Flow	Remson et al. (1965), Freeze and Whitherspoon (1966), Pinder and Bredehoeft (1968).
Unsaturated Groundwater Flow	Philip (1957), Ashroft et al. (1962), Freeze (1971), Brutsaert (1973), Healy (1990), Kirkland et al. (1992).
Solute Transport	Stone and Brian (1963), Oster et al. (1970), Tanji et al. (1967), Wierenga (1977)
Application to Field Problems	Orlob and Woods (1967), Gambolati et al. (1973), Fleck and McDonald (1978), Jain 1992
Comprehensive Reference	Trescott and Larson (1977), Ames (1977), Mitchell and Griffiths (1980), Lapidus and Pinder (1982)
Computer Program	Trescott et al. (1976), Konikow and Bredehoft (1978), Healy (1990)

Winter (1983, 1986, 1989), Sacks (1992) and Krabbenhoft and Anderson (1990) conducted numerical investigations on the interactions between groundwaters and lakes. Both Winter and Krabbenhoft and Anderson used fixed finite-difference meshes. For lakes, a finite-difference mesh may be suitable; however, because the bed of most wetlands exhibits significant slope, a poorly designed fixed finite-difference mesh may not adequately characterize water fluxes across a bed situated between an overlying body of water and an underlying aquifer. The issue of properly modeling fluxes accross a sloping bed may not be

as important as the fact that accurate simulations of wetland-flow systems require measurements of hydrologic properties at finer scales and frequencies than are commonly made (Hunt 1996, Hunt and others 1996 1997).

Assuming the hydrological model is correct, the accuracy of any computer simulated hydrologic system, such as a wetland, depends on the quality of the data used to calibrate model. Through a well instrumented study-site in the Kankakee River Valley in northwest Indiana, the USGS and the USEPA conducted detailed measurements of many various variables required to characterize a wetland hydrologic system. McDonald and Harbaugh (1998) developed a groundwater model using the available data and conducted the simulations of observed hydrologic process using the computer code commonly known as MODFLOW. The focus of the research effort was to study the effects of various wetland restoration activities on local groundwater levels. Computer simulations were used to predict the effects of wetland restoration on the existing hydrology of the wetlands and adjacent farmlands and to suggest residence times and path ways for surface water and groundwaters.

The finite-element method was first used to solve groundwater flow and solute transport problems in the early 1970s. The method has several advantages: (1) irregular or curved aquifer boundaries, anisotropic and heterogeneous aquifer properties, and sloping soil and rock layers can be incorporated easily into the numerical model; and (2) the accuracy of solution to groundwater flow and solute transport problems is quite good. The main disadvantages of the finite-element method include: (1) for simple problems, the finite element method requires a greater amount of mathematical and computer programming sophistication than does the finite-difference method; and (2) there are fewer well-documented computer programs.

The finite-element method provides approximations of much higher order than does finite-difference methodology. The whole modeling domain can be subdivided into irregular elements as dictated by the physical geometry of the problem. The size of each element can vary. Small elements can be used in areas where rapid change occurs with model parameters and predicted state variables, whereas the large elements can be used where such variations are less severe. Inhomogeneities and anisotropy are easily accommodated with the finite-element method. The advantage of irregular elements and higher-order approximations is certainly important when the "space" domain is complex. However, this advantage is less obvious in problems involving time (evolution) (Gupta 1975). Selected references of early finite-element applications to model groundwater flow are listed in Table 3-2.

3.3 Three-Dimensional Deformable Finite-Element Saturated Groundwater Model

To simulate three-dimensional groundwater flow in phreatic aquifer systems and the exchange of water between a wetland and the contiguous aquifer, a numerical model is needed that is capable of modeling the free groundwater surface. This requires first that the model assume a tentative location of the free surface and then solve for the distribution of the dependent variable, ψ, over a fixed domain. All this requires that the flux boundary condition across the surface be satisfied and that the pressure be atmospheric. To model the exchange of water between a wetland and an aquifer, it is necessary to recognize that significant vertical and lateral movements of the wetland boundary typically occur with changes in wetland storage (see Figure 3-1). This transient boundary suggests that a deformable finite-element mesh may be needed in the model to characterize adequately the moving groundwater/surface-water interface.

Table 3-2. Selected references of early finite-element applications to model groundwater.

Topic	Reference
Early Developments in Petroleum Reservoir Modeling	Price et al. (1968)
Saturated Groundwater Flow	Zienkiewicz et al. (1966), Javandel and Witherspoon (1968), Zienkiewicz and Parekh (1970), Pinder and Frind (1972).
Unsaturated Groundwater Flow	Neuman (1973), Gureghian et al. (1979), Pickens and Gillham (1980) Yeh and Ward (1981),Huyakorn (1984), Yeh (1992).
Solute Transport	Price et al. (1968), Guymon et al. (1970), Neuman (1973), Van Genuchten et al. (1977), Kirkner et al. (1984).
Application to Field Problems	Pinder (1973), Gupta and Tinji (1976), Senger and Fogg (1987).
Comprehensive References	Ziekiewicz (1971), Pinder and Gray (1977), Lapidus and Pinder (1982), Huyakorn and Pinder (1983).
Computer Programs	Neuman and Witherspoon (1970), Reeves and Duguid (1975), Segol et al. (1975), Pickens et al. (1979) Huyakorn (1984), Yeh (1992).

Numerical groundwater modeling that is focused on simulating the interaction between surface-water and groundwater systems, where the groundwater/surface-water interface moves, must use well-defined linking conditions to describe the exchange of water across the interface. These linking conditions are unknown in the beginning of the modeling time step and found through a flux type interaction that then forecasts the linking boundary conditions at the end of each time step. Thus, the model has transient boundary conditions.

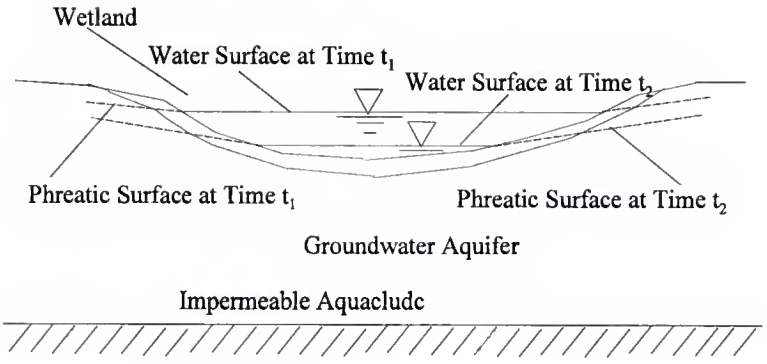

Figure 3-1. Conceptual profile model of a wetland/groundwater system

Finally, typical finite-difference modeling is not able to trace the curvature of the bottom of a wetland (see Figure 3-2). Finite elements, however, are easily configured to fit non-linear spatial geometries. In conclusion, to cope with the above described three technical problems of modeling, i.e., the free surface location, incorporating dynamic changes in the vertical and horizontal extent of the ground/surface-water interface, and tracing the curvature of a wetland bottom, a special three-dimensional finite-element model is needed.

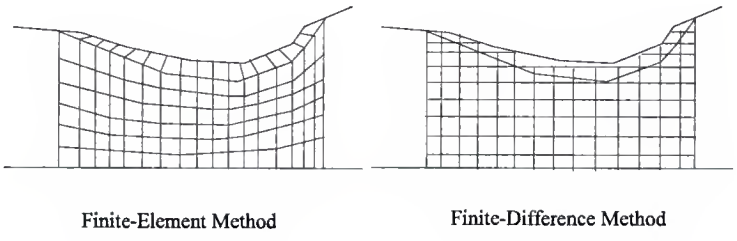

Figure 3-2. Comparison of finite-element mesh and finite-difference mesh

3.3.1 Governing Equation and Boundary Conditions

Eq. 3-1 below can be used to describe incompressible, saturated groundwater flow beneath a wetland and in a phreatic aquifer:

$$\nabla \cdot (K \nabla h) \pm Q = S_s \frac{\partial h}{\partial t} \quad i,j = 1,2,3 \tag{3-1}$$

where K is the saturated hydraulic conductivity tensor (LT^{-1}); h is equal to $z+\psi$ (L); ψ is pressure head (L); z is elevation head (L); and S_s is the specific storativity (L^{-1}). From Figure 3-3, the boundary of volume Ω is characterized through a combination of specified flux boundaries Γ_1 and specified head boundaries Γ_2. Pertinent specific no-flux boundaries include the groundwater phreatic surface (EC and DF) and the bottom impermeable boundary (GH). Relevant specified head boundaries Γ_2 include the wetland head boundary (AB and CD) and lateral boundaries (EG and FH).

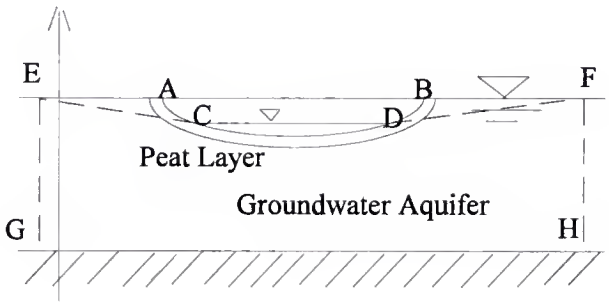

GH, EC, and DF are no-flow boundaries Γ_1

EG, FH, ACDB, and CD are specified head boundaries Γ_2

Figure 3-3. Setup of the saturated groundwater problem around a wetland

As to the boundary condition controlled by the wetland water table, the initial water table of the wetland and the pumping discharge were taken as the only inputs of the coupling model. During pumping, the pumping discharge lowered the wetland water table, and it also triggered an inflow from the aquifer to the wetland through the peat layer. In each simulation time step, the pumping discharge, estimated inflow from the aquifer to the wetland, initial water table of the wetland, and relation between the volume of the wetland and wetland water table were used as inputs in a mass balance equation that was solved to determine the water table at the end of the time step. The estimated water table at the end of the time step was put back into the saturated groundwater model to adjust the inflow from the aquifer to the wetland estimated initially. Therefore, several iterations in each time step were necessary to get an accurate estimated inflow from the aquifer to the wetland and a convergent solution of the water table in the wetland at the end of the time step. When pumping was stopped, the pumping discharge was taken as zero. Figure 3-4 shows the procedure of finding the inflow from the aquifer to the wetland and the coupling boundary.

3.3.2 Finite Element Model of Saturated Groundwater Flow

To obtain a finite element approximation of Eq. 3-1, two spaces, S and V, are defined (Hughes 1987):

$$S = \left\{ u \mid u \in H^1,\ u(x,y,z)|_{\Gamma_2} = q_{\Gamma_2} \right\} \tag{3-2}$$

$$V = \left\{ u \mid u \in H^1,\ u(x,y,z)|_{\Gamma_2} = 0 \right\} \tag{3-3}$$

where H^1 is Sobolev space comprised of functions which are square-integrable generalized

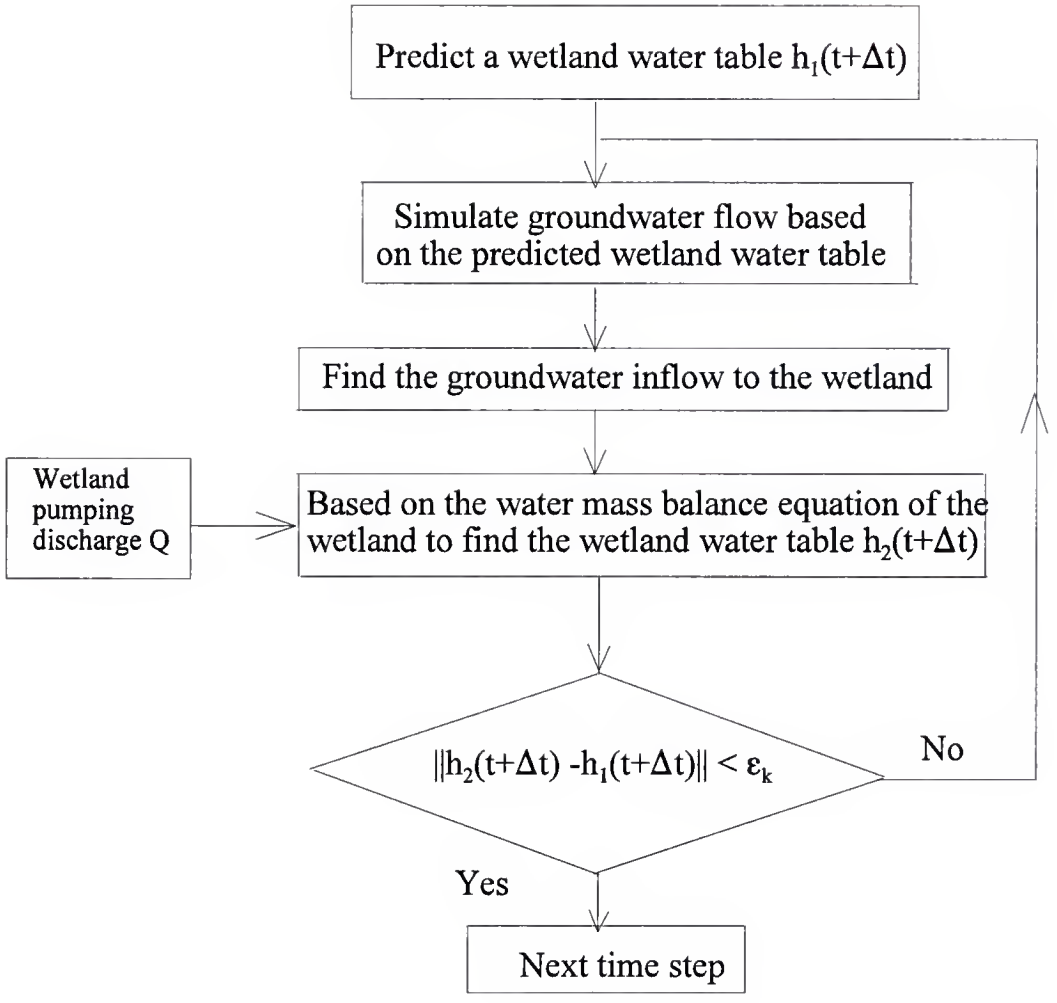

Figure 3-4. Flowchart illustrating the iteration procedure of finding the coupling boundary condition

derivatives through order 1; u is a space function that is member of Sobolev space; $q_{\Gamma 2}$ is the vertical flux along Γ_2, and x, y, z are three spatial coordinates. Any function from *S* space is equal to the flux boundary value along specified head boundary (Γ_2). Also, any function u from *V* space is equal to zero along head boundary (Γ_2). Assuming a basis function *w* is chosen from *V* space, then the following integration of Eq. 3-1 over space domain Ω is always true:

$$\int_{\Omega} w[\nabla\cdot(K\nabla h)]d\Omega \pm \int_{\Omega} w\,Q\,d\Omega = \int_{\Omega} wS_s\frac{\partial h_t}{\partial t}\,d\Omega, \quad i,j = 1,2,3 \tag{3.4}$$

where Eq. 3-4 expresses the governing groundwater flow equation integrated over the modeling domain.

Manipulation of the first term on the left hand side of Eq. 3-4 begins with the application of Green's theorem, which is an expanded form of the divergence theorem. This converts the integral into two terms, one of which is evaluated only on the surface of the region to be simulated. Green's theorem is:

$$\int_{\Omega} \left(\nabla\cdot\underline{P}\right) A\,d\Omega = \int_{\Gamma} \left(\underline{P}\cdot\underline{n}\right) A\,d\Gamma - \int_{\Omega} \left(\underline{P}\cdot\nabla A\right) d\Omega \tag{3-5}$$

where A is a scalar, and $\underline{P}$ is a vector quantity. The boundary of volume Ω is defined by Γ, and $\underline{n}$ is a unit outward normal vector to the boundary. Application of the Galerkin criterion (Hughes 1986) and Green's theorem to Eq. 3-4 leads to:

$$\int_{\Gamma_1} w\left[\left(K\nabla h\right)\cdot\underline{n}\right]d\Gamma + \int_{\Gamma_2} w\left[\left(K\nabla h\right)\cdot\underline{n}\right]d\Gamma - \int_{\Omega} \left(\nabla w\right)\cdot\left(K\nabla h\right)d\Omega$$

$$\pm\int_{\Omega} w\cdot Q\,d\Omega = \int_{\Omega} wS_s\frac{\partial h_t}{\partial t}\,d\Omega \tag{3-6}$$

Because w is a member of V space, it is equal to zero at all specified head boundaries (Γ_2); thus, the second term in Eq. 3-6 equals zero. If it is further assumed that Q equals zero, then Eq. 3-6 reduces to:

$$\int_{\Gamma_1} w\left[(K\nabla h)\cdot \underline{n}\right] d\Gamma - \int_{\Omega} (\nabla w)\cdot(K\nabla h)\, d\Omega = \int_{\Omega} w\, S_s \frac{\partial h_t}{\partial t} d\Omega \tag{3-7}$$

For an approximate solution of h(x, y, z, t), it is assumed that:

$$h^{(e)}(x,y,z,t) = \sum_{i=1}^{p} N_i^{(e)}(x,y,z)\, d_i(t) \;,\; N_i \in V \;,\; h \in S \tag{3-8}$$

$$w^{(e)} = \sum_{i=1}^{p} N_i^{(e)}(x,y,z)\; c_i \quad ,\; N_i \in V \tag{3-9}$$

where $h^{(e)}$ is the approximate solution for hydraulic head within element e, $N_i^{(e)}$ are interpolation functions for each node within element e, p is the number of nodes within element e, and $d_i(t)$ are the unknown values of hydraulic head for each node within element e and at time t. At the specified head boundaries, Γ_2, $d_i(t) = h(x,y,z)|_{\Gamma 2}$. $w_i^{(e)}$ is the weighting function for node i, and the limits of the integration are chosen to represent the volume of the elements. In Galerkin's method, the weighting function for each node in the element is set equal to the interpolation function for the node, $w_i^{(e)} = N_i^{(e)}$.

When the approximate solutions (Eq. 3-8 and Eq. 3-9) are substituted into Eq. 3-7, the resulting equation is not satisfied exactly; consequently, an error or residual occurs at every point in the problem domain. However, if it is also assumed that the aquifer is

isotropic, that is to say, values of saturated hydraulic conductivity in the three coordinate directions are constant within an element (but can vary from one element to the next), the contribution of any element e to the residual at a node i associated with the element can be described through the following system of equations:

$$\begin{bmatrix} R_1^{(e)}(t) \\ \vdots \\ R_p^{(e)}(t) \end{bmatrix} = \left[K^{(e)}\right] \begin{bmatrix} d_1^{(e)}(t) \\ \vdots \\ d_p^{(e)}(t) \end{bmatrix} + \left[C^{(e)}\right] \begin{vmatrix} \dfrac{\partial d_1^{(e)}(t)}{\partial t} \\ \vdots \\ \dfrac{\partial d_p^{(e)}(t)}{\partial t} \end{vmatrix} - \left[F^{(e)}\right] \tag{3-10}$$

where p = the number of nodes in each element (i.e., triangle element: p = 3), and $R_i^{(e)}$ = the residual error at node i in element e:

$$\left[K^{(e)}\right] = \int_{V^{(e)}} \int \int \begin{bmatrix} \dfrac{\partial N_1^{(e)}}{\partial x} & \dfrac{\partial N_1^{(e)}}{\partial y} & \dfrac{\partial N_1^{(e)}}{\partial z} \\ \vdots & \vdots & \vdots \\ \dfrac{\partial N_p^{(e)}}{\partial x} & \dfrac{\partial N_p^{(e)}}{\partial y} & \dfrac{\partial N_p^{(e)}}{\partial z} \end{bmatrix} \begin{bmatrix} K_{xx} & 0 & 0 \\ 0 & K_{yy} & 0 \\ 0 & 0 & K_{zz} \end{bmatrix} \begin{bmatrix} \dfrac{\partial N_1^{(e)}}{\partial x} & \cdots & \dfrac{\partial N_p^{(e)}}{\partial x} \\ \dfrac{\partial N_1^{(e)}}{\partial y} & \cdots & \dfrac{\partial N_p^{(e)}}{\partial y} \\ \dfrac{\partial N_1^{(e)}}{\partial z} & \cdots & \dfrac{\partial N_p^{(e)}}{\partial z} \end{bmatrix} \tag{3-11}$$

and:

$$\left[F^{(e)}\right] = \int_{\Gamma_1^{(e)}} \int \begin{bmatrix} N_1^{(e)} \\ \vdots \\ N_p^{(e)} \end{bmatrix} q_{surface} \tag{3-12}$$

and:

$$\left[C^{(e)}\right] = \iiint_{V^{(e)}} \begin{bmatrix} N_1^{(e)} \\ \vdots \\ N_p^{(e)} \end{bmatrix} \left[S_s\right] \left[N_1^{(e)} \quad \ldots \quad N_p^{(e)}\right] \tag{3-13}$$

where $V^{(e)}$ is the volume of element e. Eq. 3-10 represents a system of equations pertinent to a single element, and there is an equation for every node in the element. When equations for all elements in the mesh are combined, the global equations are obtained for the system:

$$\begin{bmatrix} R_1(t) \\ \vdots \\ R_n(t) \end{bmatrix} = [K] \begin{bmatrix} d_1(t) \\ \vdots \\ d_n(t) \end{bmatrix} + [C] \begin{bmatrix} \dfrac{\partial d_1(t)}{\partial t} \\ \vdots \\ \dfrac{\partial d_n(t)}{\partial t} \end{bmatrix} - [F] \tag{3-14}$$

By setting the residuals equal to zero, we have:

$$[K] \begin{bmatrix} d_1(t) \\ \vdots \\ d_n(t) \end{bmatrix} + [C] \begin{bmatrix} \dfrac{\partial d_1(t)}{\partial t} \\ \vdots \\ \dfrac{\partial d_n(t)}{\partial t} \end{bmatrix} = [F] \tag{3-15}$$

Eq. 3-15 is a system of ordinary differential equations, whose solution provides values of head d and the derivative with respect to time, $\partial d/\partial t$, at each node in the finite-element mesh.

Although several methods are available for solving this system of equations, it has become standard practice to use the finite-difference method:

$$\frac{\partial h}{\partial t}(\varepsilon) = \frac{d(t+\Delta t)-d(t)}{\Delta t} \tag{3-16}$$

If a variable, ω is defined , such that:

$$\omega = \frac{\varepsilon - t}{\Delta t} \tag{3-17}$$

Then:

$$d(\varepsilon) = (1-\omega)d(t)+\omega\, d(t+\Delta t) \tag{3-18}$$

which can be extended to the vector of [d]:

$$[d(\varepsilon)] = (1-\omega)[d(t)]+\omega\,[d(t+\Delta t)] \tag{3-19}$$

If Eq. 3-19 and Eq. 3-18 are substituted into Eq. 3-15, the finite-difference formulation for the transient saturated flow equation is as follows:

$$([C] + \omega\,\Delta t\,[K])[d(t+\Delta t)] = ([C] - (1-\omega)\,\Delta t\,[K])[d(t)] + \Delta t[(1-\omega)[F(t)]+\omega[F(t+\Delta t)]$$

(3-20)

Eq. 3-20 represents a system of linear equations with unknown variables of $d_i(t)$, and where $N_i(x,y,z)$ are the basis functions in a tri-linear hexahedral element domain. $N_i(x,y,z)$ does not change with time. The most common basis functions used are hat functions, which are linear functions of space variables.

The solution of Eq. 3-20 begins by specifying the initial values of [d] (i.e., the values of head at time $t_o = 0$). Next, the system Eq. 3-20 is solved to obtain values of $\{d(t+\Delta t)\}$ at the end of the first time step 1. This solution process is repeated for the next time step, and so on until the specified time duration of simulation is satisfied. Depending on the choice of ω, several different subsets of the finite-difference formulations are defined.

When ω=0, it is the forward-difference method is obtained:

$$([C])[d(t+\Delta t)] = ([C] - \Delta t\,[K])[d(t)] + \Delta t\,[F(t)] \tag{3-21}$$

When ω=1/2, the central-difference, or Crank-Nicholson, method is obtained:

$$\left([C] + \frac{1}{2}\Delta t\,[K]\right)[d(t+\Delta t)] = \left([C] - \left(1 - \frac{1}{2}\right)\Delta t\,[K]\right)[d(t)] + \frac{\Delta t}{2}([F(t)] + [F(t)])$$

(3-22)

When ω=1, it is the backward-difference method is obatined:

$$([C] + \Delta t\,[K])[d(t+\Delta t)] = [C][d(t)] + \Delta t\,[F(t)] \tag{3-23}$$

3.3.3 Adaptation of the Saturated Finite-Element Model to Describe the Free Surface

Several papers have been written on the groundwater free-surface problem (e.g.,Taylor 1967, Neuman 1970, Finn 1976, France 1976, and Huyakorn 1986). Most of these papers discussed the steady-state free-surface problem except for France (1976). This thesis examines the transient problem starting from the basic ideas that Neuman (1970) presented for steady flow. Basically , both France (1976) and Neuman (1970) tried to satisfy the two boundary conditions and are consistent. This chapter is also based on the two conditions and adapts the method they used to locate the free surface.

The primary dependent variable to be used in modeling the free surface presented here is the hydraulic head h defined as:

$$h = z + \frac{\psi}{\gamma} \tag{3-24}$$

where z is the vertical coordinate; γ is specific weight of a unit volume of water ρg and ψ is the pressure. Along the free surface, there are two conditions which must be satisfied. First, $\psi=0$ (pressure atmospheric), and hence for a given position, h is prescribed on it. That is:

$$h = z \tag{3-25}$$

For the steady-state scenario, the second condition is simply that there is a specified flux across the free surface boundary (i.e., a zero flux or a flow imposed equal to net recharge). Thus, in addition to Eq. 3-24 at the free surface, there is:

$$K_x \frac{\partial h}{\partial x} \bar{i} + K_y \frac{\partial h}{\partial y} \bar{j} + K_z \frac{\partial h}{\partial z} \bar{k} = q_o \tag{3-26}$$

If steady state has not been reached and the boundary is moving with a velocity normal to its instantaneous configuration of V_n, then the quantity of liquid entering its unit area is modified, and:

$$K_x \frac{\partial h}{\partial x} \bar{i} + K_y \frac{\partial h}{\partial y} \bar{j} + K_z \frac{\partial h}{\partial z} \bar{k} = q_o + V_n S = q_n \tag{3-27}$$

where i, j, k are unit orthogonal vectors; S is the specific yield coefficient (or the effective porosity) relating the total volume of material to the quantity of liquid which can be drained from it, and q_n equals the net flux across the free surface.

The transient problem is solved by considering the solution to be a number of steady-state problems at small intervals of time Δt. For a given time level, the governing equation is solved to obtain values of nodal heads and velocities of free surface. The components of actual velocities are determined by dividing by the specific yield coefficient. By repeating this process for all modal points on the free surface, a new configuration and a new set of boundary conditions are defined. The actual nodal coordinates of the free surface are found using the Newton-Raphson iterative method. Thus, a new finite-element mesh is generated by modifying the coordinates of the nodes in the new flow domain.

3.4 Validating the Code of Three-Dimensional Deformable Finite-Element Groundwater Flow Model

3.4.1 Theis Solution

To validate the code of the three-dimensional deformable finite-element groundwater flow model, a comparison was made of results generated by the numerical model and those created with an analytical model describing unsteady flow to a well in a phreatic aquifer. Figure 3-5 shows a schematic of unsteady flow to a well in a phreatic aquifer.

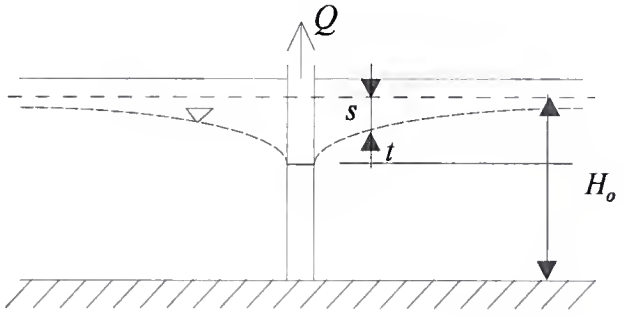

Figure 3-5. Unsteady flow to a well in a phreatic aquifer at time t.

where s = drawdown(L), H_o = initial saturated aquifer thickness (L), Q = pumping discharge (L^3/T), and r = radial distance from the well (L).

As shown in Figure 3-2, the boundary condition along the phreatic surface is nonlinear and the shape and position of the phreatic surface are unknown. As a result, an exact analytical solution that describes groundwater flow is not known. However, by the employing the Dupuit assumptions and assuming recharge is zero, the unsteady flow to a fully penetrating well in a phreatic aquifer can be described in radial coordinates by:

$$\frac{\partial^2 h^2}{\partial r^2} + \frac{1}{r} \cdot \frac{\partial h^2}{\partial r} = \frac{2S}{K} \frac{\partial h}{\partial t} \tag{3-28}$$

Initial condition: $h(t_o) = H_o$

Boundary condition: $h(t)|_{(r=\infty)} = H_o$

Here, S is the phreatic aquifer specific yield (or effective porosity, n_e). If drawdowns are sufficiently small compared to the average depth of flow, (say $0.02H_o$), then the approximate solution to this problem is the Theis solution (Bear 1976):

$$s = \frac{Q}{4\pi T} W(u) \tag{3-29}$$

where $u = r^2S/(4T\,t)$; W(u) is the well function, and $T=KH_o$= initial transmissivity.

The conditions that define the test problem used to validate the numerical groundwater flow model include: a pumping discharge, Q, of 1.5 m^3/hr; an initial saturated phreatic aquifer thickness, H_o, of 20 m; a specific yield S (or n_e), of 0.1; and a hydraulic conductivity, K, of 15 m/day. For the three-dimensional finite-element model, the specific storativity, S_s, is 0.0001 m^{-1}; where $S_s=\rho g(\alpha+n\beta)$; n equals porosity; α equals solid matrix compressibility [$LT^{-2}M^{-1}$]; g is acceleration of gravity [LT^{-2}]; and β is fluid compressibility [LT^2M^{-1}]. Because of problem symetry, modeling was limited to simulating hydraulic head variations over a wedge section of the aquifer using a 21×11×3 mesh (Figure 3-6).

The boundary condition controlled by well water table, the initial water table of well and the pumping discharge were taken as the only input. The pumping pulled water out of the well, on the other hand, the groundwater supplied well. In each simulation time step, based on the known water table in the beginning of time step, and an estimated water table of well, a new discharge supplied from groundwater to well was calculated from the groundwater modeling. Based this new calculated supplying discharge to the well, the pumping discharge, and the circular area of the well, a more accurate well water table could

be estimated again. The groundwater flow model was solved again. After many iterations, a convergent and accurate well water table could be obtained before the modeling of next time step.

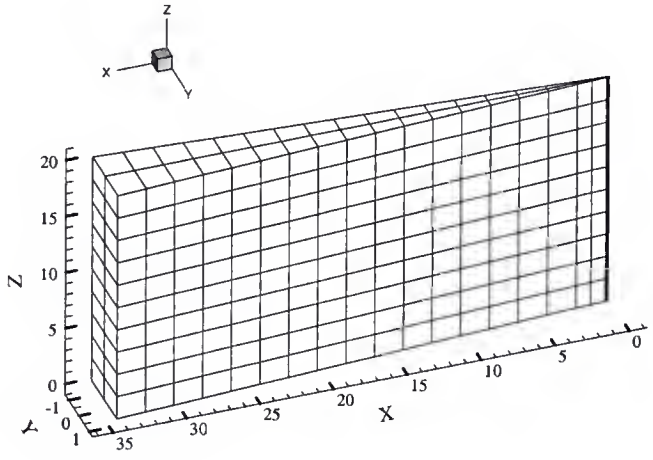

Figure 3-6. Finite-element mesh of the wedge used to simulate of a well pumping in phreatic aquifer

Because the mesh is deformable, the known pressure at the free surface and flux were used to locate the free surface. During calculation, a slice successive over-relaxation (SSOR) method was used as an iterative approach to locate the free surface. The results illustrated in Figure 3-7 validate the coding of the numerical model.

3.4.2 Groundwater Flow around a Circular Wetland

To validate the three-dimensional finite-element saturated groundwater flow model again, the numerical model was used to simulate the groundwater flow around a circular wetland and induced by a flood wave in the wetland. It is assumed that the wetland stage fluctuations can be described by a nonperiodic Gaussian fucntion of time as Eq. 3-30:

$$f(r_o, t) = \frac{1}{\sqrt{2\pi}\sigma} e^{-\frac{(t-t_o)^2}{2\sigma^2}} \tag{3-30}$$

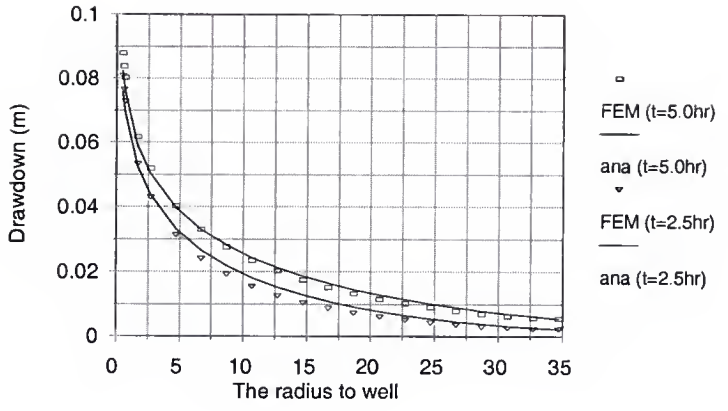

Figure 3-7. Comparison of the numerical and analytically simulated head for the example problem of a transient pump test in a phreatic aquifer

Unlike the coupling boundary condition that was used in the last case, a flood wave boundary condition used in this numerical model here. The solid line and the dash line in Figure 3-8 are the three-dimensional finite-element model simulated results. The triangle points and the diamond points are the groundwater analytical solutions from Eq. 2-24 obtained in Chapter 2. The circular wetland which has a radius of 50 meter was assumed. All other system parameters are given in the Table 3-3. The numerical model and analytical solution matched very well.

3.5 A Numerical Model Application to Simulate the Interaction Between a Wetland and an Aquifer

The finite-element model was applied to simulate the interaction between a wetland and a contiguous phreatic aquifer stressed by an active productive well. A horizontal, irregular quadrilateral mesh was used to define the irregular boundaries of the wetland and the area beyond the wetland. Figure 3-9 illustrates the numerical mesh corresponding to the

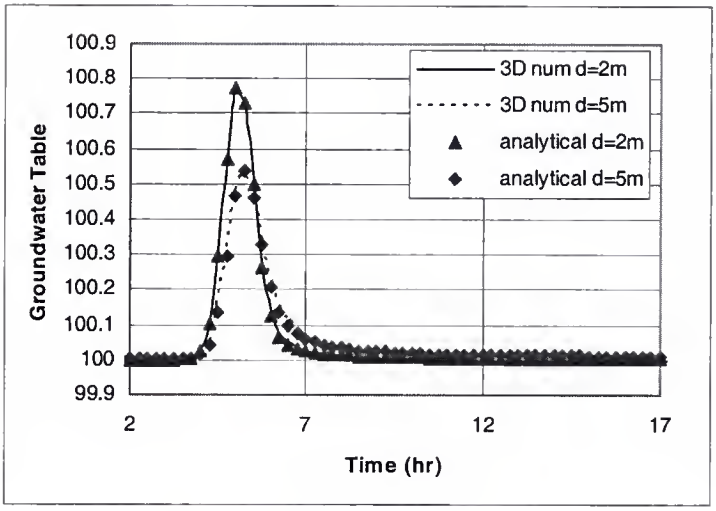

Figure 3-8. Comparison of the numerically and analytically simulated groundwater table.

Table 3-3. Parameters and their values

Parameter	Value	Parameter	Value
H_{oo} (m)	100.0	T (m^2/h)	0.635
Δr (m)	0.25	S	0.01
Δt (hr)	0.02	t_o (h)	5.0
k (m/hr)	0.00635	σ	0.4

horizontal and vertical extent of the phreatic aquifer. Beyond the wetland, the vertical extent of the mesh defines the thickness of the phreatic aquifer. Over the inundated portions of wetland, the thickness of the mesh defines the vertical distance between the wetland bottom and the underlying aquiclude. The wetland is shown in the middle of this area. The model domain is 104×104×10 meters. The four lateral boundaries and bottom boundary are assumed to be impermeable. An active production well is located within the model domain. It was assumed that the initial groundwater table and the water stage of wetland were the same. The deepest water depth in the wetland is 1.0 meter. Model runs were conducted to

simulate the exchange of water between wetland and aquifer. Such interactions between the wetland and the aquifer were examined under transient pumping conditions and precipitation. Since the real-time stage of the wetland is used as a boundary condition over the wetted part of wetland, the horizontal and vertical extent of the mesh must be adjusted to trace the vertical and horizontal movement of the transient wetland water surface.

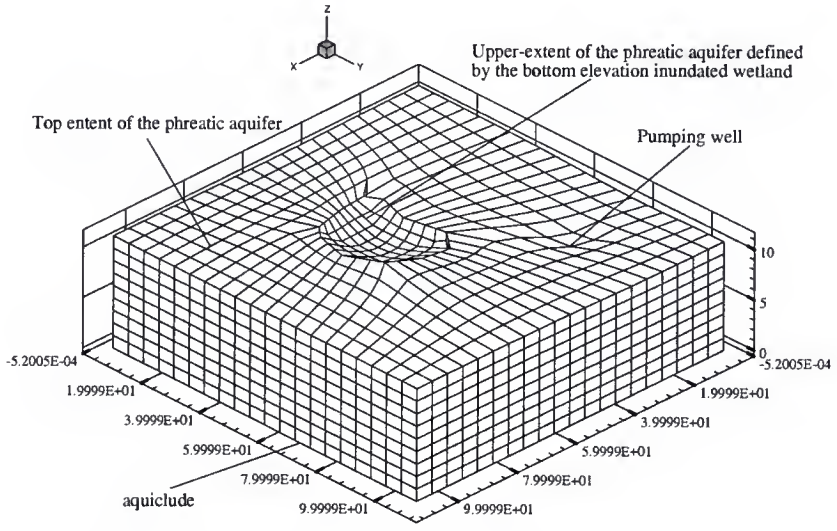

Figure 3-9. Three-dimensional finite-element mesh for the simulation of wetland and aquifer

The modeled area was divided into a 21×21×10 hexahedron mesh. In the middle, a 9×9 quadrilateral mesh was used to represent the wetland area (Figure 3-9). Hydrologic conditions that define the test problem include: a net precipitation rate of 0.02 m/hour; a specific yield, S, of 0.075. a hydraulic conductivity, *K*, of 10 m/day; and a pumping discharge, Q, of 1.554 m^3/hr. Finally, data from Figures 3-10 and Figure 3-11 were used to define the relationship between the wetland water stage, the surface water area of wetland, and the corresponding wetland volume.

Figure 3-12 illustrates the initial condition where it was assumed that the wetland surface-water stage and phreatic surface elevation were the same. Figure 3-13 illustrates a

plan view of the numerical mesh at time zero. Figure 3-14 through Figure 3-21 represent various depictions of head contours and iso-surface plots of head predicted at hour 5 of the simulation. These figures show that water moves laterally into the wetland and pumping well because the same net rainfall forces the water table to increase faster than in the water stage in the wetland. The directions of flow also depend on the active production well. If production is large, more water flows to the well instead of flowing to the wetland. Otherwise, some water flows towards and into the wetland as groundwater inflow. Beneath the wetland, the hydraulic head increases with time and with increasing depth (Figure 3-17 and Figure 3-18), which shows that water flows from the aquifer into the wetland. As to the pumping well, the contours are almost vertical and parallel to each other near the well (Figure 3-20 and Figure 3-21). Groundwater moves towards the well in a horizontal direction because the well fully penetrates the aquifer.

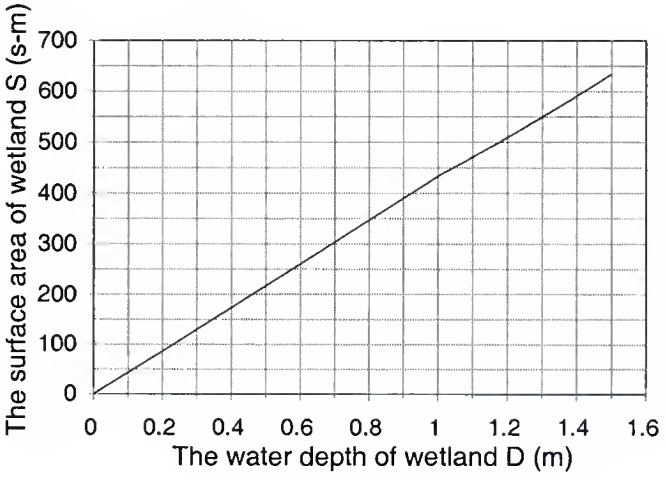

Figure 3-10. Relationship between the area of wetland water surface.

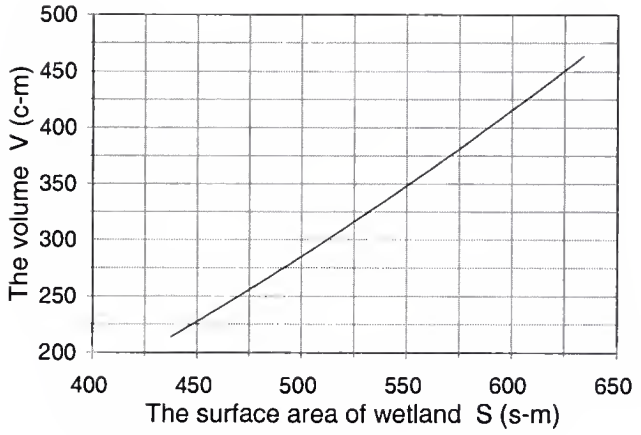

Figure 3-11. Relationship between the deepest water depth and the volume of wetland.

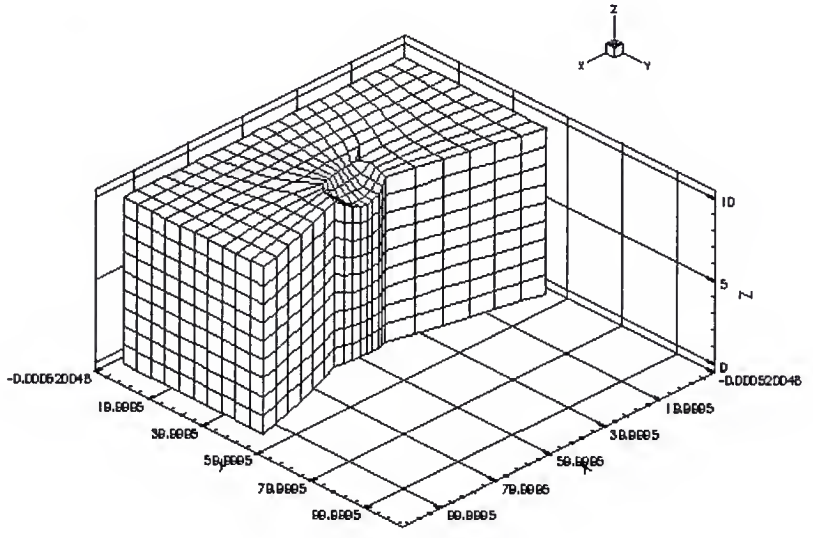

Figure 3-12. Illustration of the initial condition where it was assumed the wetland surface water stage and the phreatic surface elevation were the same

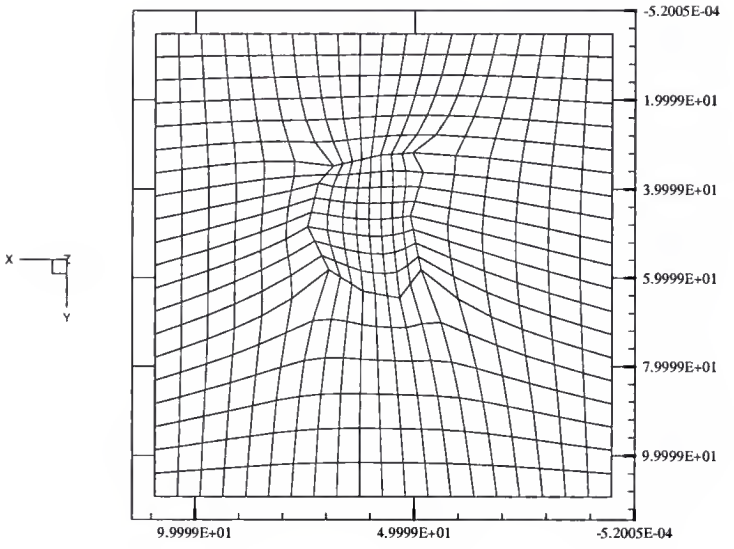

Figure 3-13. Plan view of the numerical mesh at time zero.

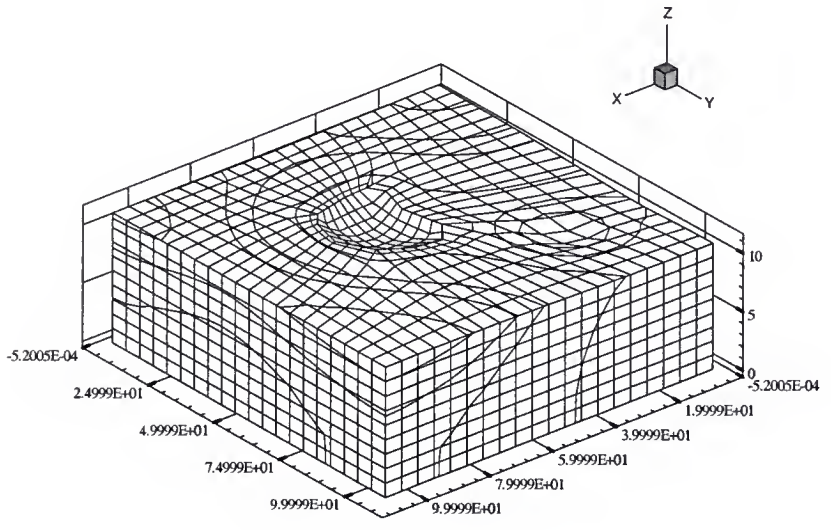

Figure 3-14. Three-dimensional finite-element mesh
and simulated head contours at hour 5.

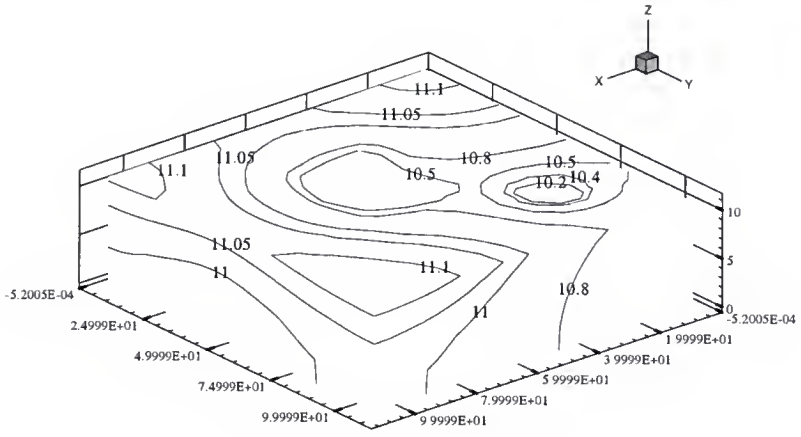

Figure 3-15. simulated head contour at hour 5.

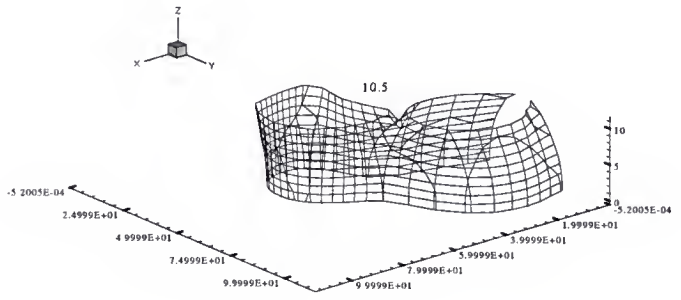

Figure 3-16. Simulated iso-surface plot of 10.6 meter head at hour 5.

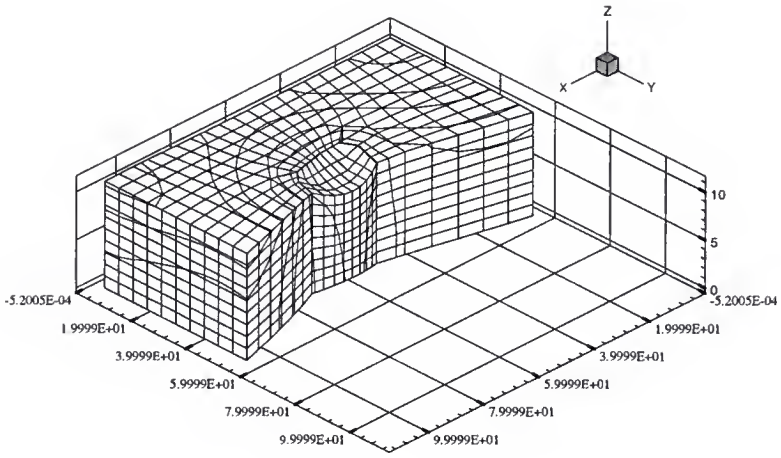

Figure 3-17. Three-dimensional finite-element mesh and head contour on a cross section through wetland

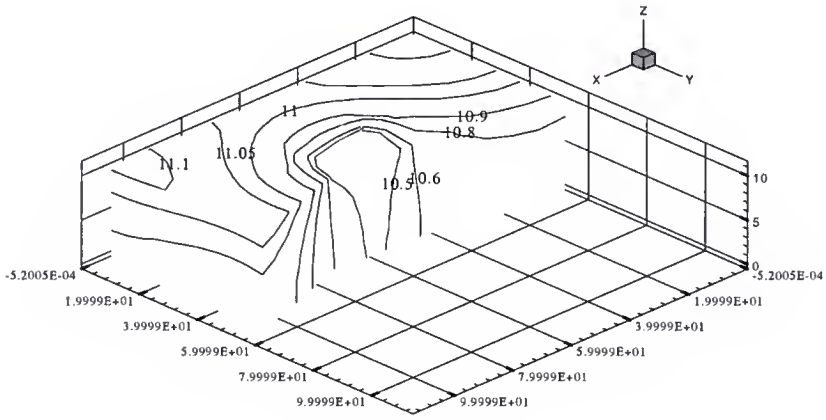

Figure 3-18. Simulated head contour on the vertical cross section through the wetland

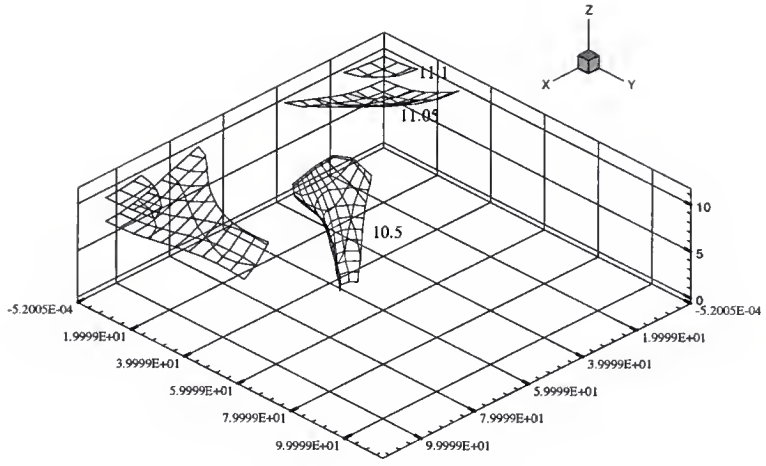

Figure 3-19. Modeled iso-surface plot of head equal to 11.1 m, 11 m and 10.5 m

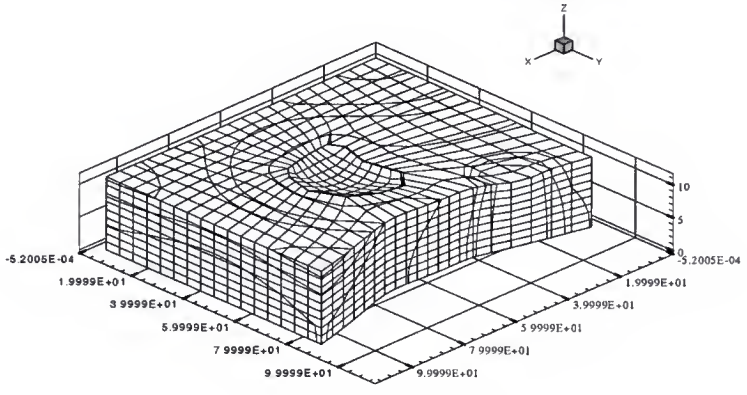

Figure 3-20. Mesh and modeled head contour with vertical cross section through the pumping well

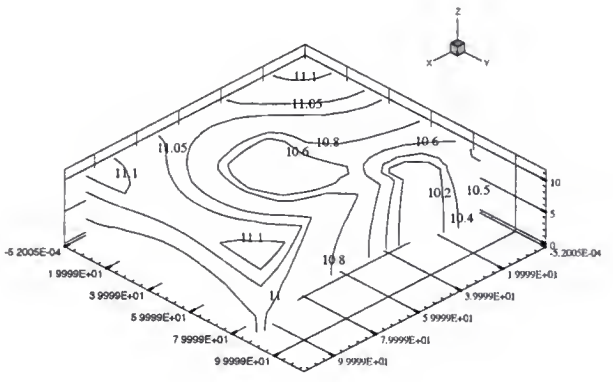

Figure 3-21. Head contour (m) on the vertical cross section through the pumping well

A computer with a Pentium 1.4GHz processor took 4 hours to complete the 5-hour simulation using a time step of 0.1 hours and 3 iterations per time step. To use this model over a real system, a finer mesh would be desirable. Unlike most rectangular finite-difference grids, the finite-element grid used here precludes the use of more efficient solution algorithms that divide simulation domain into three individual directions. In order to use this model to investigate wetland and aquifer interaction on a large scale, it would be desirable to introduce a simplified mesh that would in turn be more amenable to efficient solvers. With computer hardware developing, the simulation speed can be accelerated consequently. To improve the simulation speed of the model from fundamental, a kind of hybrid method which combines finite-element method and finite-difference method could be an effective choice for a large scale practical problem.

3.6 Application of Three-Dimensional Deformable Saturated Groundwater Flow Model to SV5 Wetland

3.6.1 Site Description-SV5

SV5 is an isolated wetland found in pine flatwoods located in southeast Florida. It is part of the Savannas wetland system located south of the city of Jensen Beach in Martin

County. SV5 is located approximately two km west of the Atlantic Ocean and is adjacent to a large municipal well field. The South Florida Water Management District (SFWMD) monitors this wetland system. There are 13 surficial aquifer municipal water-supply wells located from a few hundred meters to four kilometers from SV5 (Figure 3-22). The wetland is roughly circular in shape, with a diameter of approximately 60 meters (Wise et al. 2000, Walser 1998).

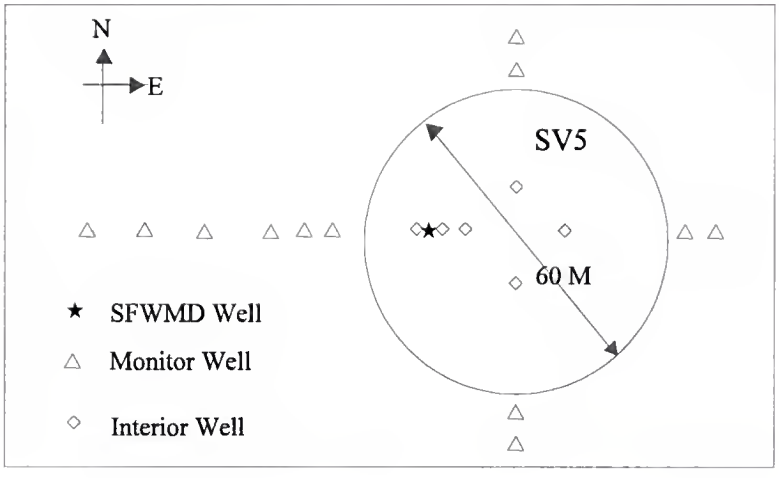

Figure 3-22. Well Locations (Switt et al. 1998)

The surficial aquifer that underlies the wetland is composed of three layers. The first layer, which is located from land surface to 12-18m below the surface, consists of white, gray and brown, largely fine- to coarse-grained quartz sand intermixed with shell beds. It receives recharge directly from precipitation. The second layer, which is 3-6 m thick, is comprised of fine to very fine sand with small amounts of shell and clay. The third layer, which extends to a depth of between 37-43 m, consists of limestone intermixed with sand and shell. The upper confining layer lies beneath the surficial aquifer. This layer consists of low-

permeability rocks that are primarily clastic. The Floridian aquifer system lies under the upper confining layer. The system is quite thick and consists of limestone of variable permeability (Fetter 1994). The climate in the area is considered humid sub-tropical, and the area receives an average of 1.5 m of rainfall per year (Walser 1998).

3.6.2 Field Methods and Wetland Aquifer Interaction Test

The SV5 wetland aquifer interaction test was conducted (Wise et al. 2000). Eighteen monitoring wells were installed. Wells were placed along transects running from east to west and north to south. Six wells were placed outside the wetland on the western transect and two on each of the other three transects. The wells were identified by the transect designation followed by the distance location from the center of the wetland, i.e., well 37 is the well located 37 m from the center of the wetland along the west transect. SFWMD installed two wells and a staff gage at the site. The wells measure groundwater. The groundwater well is screened at a depth of six meters and grouted from the surface to a depth of five meters.

The water and peat depths in the wetland were measured along four transects through the center of the wetland at 45° angles from one another. Peat and water depth measurements were taken at three-meter increments. The peat depth was determined by pushing a piece of 1 cm rebar into the peat at a steady rate until significant resistance was felt. This method is most easily applied to sites such as SV5 that are free of significant tree roots. The depth of the water table was determined by measuring the water level in the exterior monitoring wells. Elevation data for the sites were measured utilizing a Topcon Self-Leveling Rotating laser level. The South Florida Water Management District staff gage on the site was used as a relative reference for the elevation data, and all elevation data were expressed in terms of NGVD of 1929.

The water and peat depth information was entered into Surfer, a three-dimensional graphical interpolation program, to develop three-dimensional contours of the wetland. A stage -volume curve to describe the wetland was developed by utilizing Surfer to determine the wetland volume at varying water levels. A regression curve was fitted to this data to determine the equation that describes the stage-volume curve (Switt et al. 1998, Wise et al. 2000). This curve describes the top of the peat layer. The process was repeated to develop a curve that describes the bottom of the peat layer.

The goal of the test was to stress hydraulically a wetland by pumping the standing water to lower the water level a predetermined amount, which varies from wetland to wetland, and then monitoring the response in wells and subsequent recovery of the water in the wetland. For the wetland test to be effective, the wetland must be a discharge wetland at the end of the pumping phase. The wetland test was conducted utilizing a 10.2 cm centrifugal trash pump to pump the water from the wetland until the water level in the wetland dropped 30.5 cm. The water was pumped into a drainage ditch located approximately 100 m from the wetland. This distance was chosen to ensure that the water pumped from the wetland did not reenter the system. The discharge rate of the pump was approximately 70 m^3/hr. The discharge rate was measured by determining the amount of time it took to fill a five-gallon plastic bucket at the end of the discharge hose. It took nine hours to lower the wetland water level 30.5 cm.

During the testing, water levels in all of wells were manually measured every hour, with the exception of the surface water well, which was measured every 30 minutes, utilizing a Slope Indicator water tape. Once the pump was turned off, water levels in all of the wells were manually measured every hour for 22 hours. Exterior and interior well water levels

were recorded for the wells in the wetland area.

3.6.3 Stage-Volume Relationships

Water and peat depth data were used to produce a three-dimensional contour plot of SV5 (Figure 3-23 and Figure 3-24). The regression equation that describes the volume of water above the peat layer is

$$V_w = 3454S^2 - 148.45s \tag{3-30}$$

where V_w is the wetland volume (m^3) at s, the stage level (m) (Switt et al. 1998, Wise et al. 2000). The bottom of the peat layer is described by the follow regression equation (Figure 3.25):

$$V_p = -116s^4 + 607s^3 + 938s^2 + 108s \tag{3,31}$$

where Vp is the volume above the bottom of the peat layer (m^3); and V_p-V_w ≈volume of saturated peat. The coefficient of determination equals unity for both of these regressions.

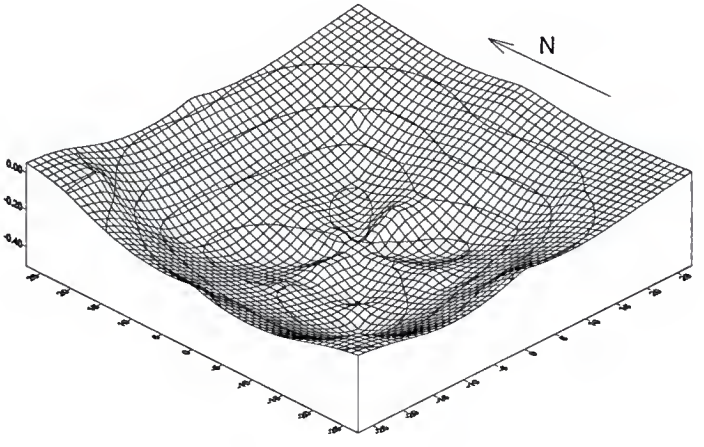

Figure 3-23. Top surface of peat layer of wetland

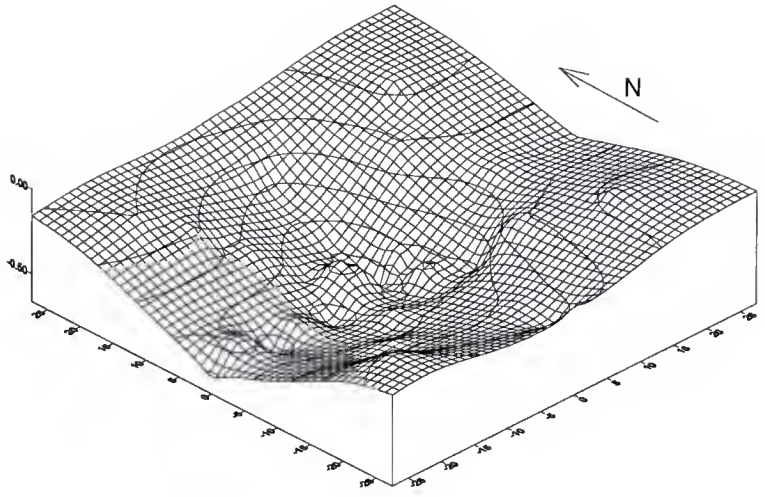

Figure 3-24. Bottom surface of peat layer

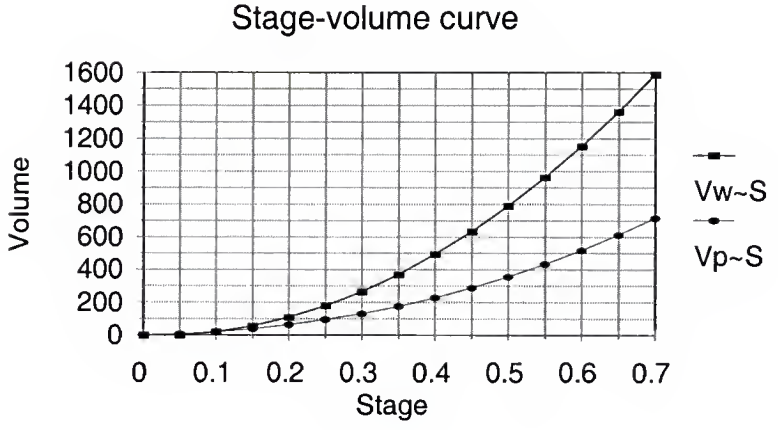

Figure 3-25. Relationship between wetland volume and water stage

Switt et al. (1998) used a similar formula (Eq. 3-32) to calculate the interaction between a wetland and the underlying groundwater:

$$SP = K_s\left(\frac{G-W}{L}\right)SA_W \tag{3-32}$$

where SP= exchanging flux (m^3/day), K_s= hydraulic conductivity (m/day), G = groundwater level (m), W = wetland water level (m), L = average peat thickness (m), and SA_w = wetland wetted surface area (m^2). Over the de-watered area of the wetland, seepage decreases from the above value at the edge of the water to zero at the edge of the wetland. Switt et al. (1998) assumed a standing water head difference equal to 1/3 of the value use in Equation 3-8. Thus, seepage for the de-watered area of the wetland was

$$SP = K_s\left(\frac{G-W}{L}\right)SA_{NW} \tag{3-33}$$

where SA_{NW}= wetland dry surface area (m^2).

The hydraulic conductivity of the organic soil in the peat layer is critical in wetland systems because it controls the amount of groundwater that flows from the aquifer into the wetland or from the wetland into the aquifer (Truesdell 1995). Determining a value of hydraulic conductivity for the soils in wetland system is particularly challenging.

3.6.4 Creation of Finite-Element Mesh

The model domain was approximately three times the size of the wetland. Because the wetland is approximately radically symmetrical it was possible to develop a highly refined 4.0° numerical wedge to represent the wetland aquifer system. The aquifer was

divided into 10 layers to obtain a 11×26×3 mesh (Figure 3-26). The peat layer was divided into three layers producing a 3×11×3 mesh. The mesh was divided and fitted along the shape of peat layer.

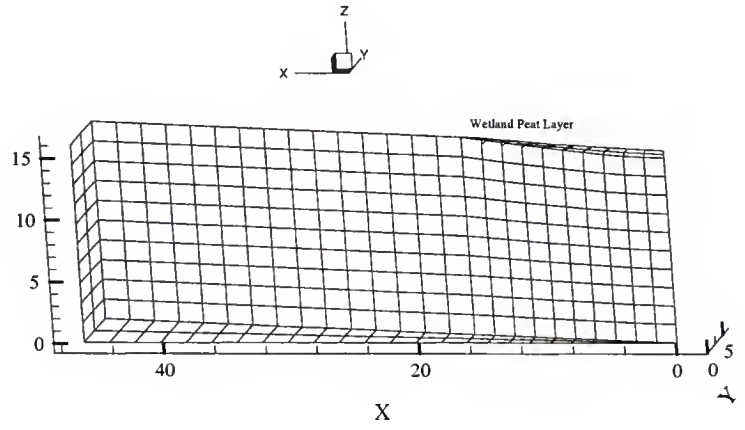

Figure 3-26. Finite-element mesh of wedge of wetland and aquifer for the saturated flow model

3.6.5 Solution Procedure

To simulate the wetland-aquifer interaction observed at SV5, the model must correctly simulate the movement of the free surface as changes occur with the wetland water stage. Two boundary conditions must be satisfied on free surfaces; first, there can be the flux across the surface must be represented, and, second, the pressure must be atmospheric. The initial fixed domain solution usually will not satisfy both boundary conditions simultaneously. Therefore, the trial free surface is adjusted and a solution obtained for the revised fixed domain. This process is repeated until the required adjustment in the free surface is considered negligible. Thus, the solution of the non-linear free surface problem is achieved by a series of solutions to linear problems with prescribed boundaries. Finally, because the wetted part of wetland may change significantly with variations of wetland water stage, the finite-element mesh must be adjusted horizontally and vertically between time

steps.

Before the pumping test began, the SV5 wetland water surface was about 60 meters in diameter. However, after pumping stopped it was less than 30 meters. Thus, the horizontal inundated area changed from 2750 m^2 to 750 m^2. To model the influence of a changing horizontal free surface required that the finite-element mesh be adjusted horizontally. The zone of mesh adjustment would be within the peat layer and include an upper boundary representing the free surface or the surface water stages and a lower boundary corresponding to the vertical limit of the peat layer. Adjusting the mesh horizontally keeps the same number of nodes on the boundary. Thus, the physical domain of the mesh may change horizontally and vertically. However, the calculation domain does not. After each simulation, information defining the location of every node is updated.

Since the wetland boundary was assumed to vary over time, the total head was taken as a boundary condition. Thus, at any time, the wetland boundary can be viewed as an equipotential line. Water moves vertically to and from the equipotential line represented by the free surface boundary. The vertical hydraulic gradient at the wetland boundary times the product of the wetland area and hydraulic conductivity equals the volume of water exchanged between the wetland and the aquifer.

3.6.6 Model Calibration and Results

Because the aquifer underlying SV5 is composed of sand, a specific storativity of $S_s = 10^{-5}$ m^{-1} was used (Bear 1979). The saturated water content and residual water content in the peat layer were $\theta_s = 0.7$ and $\theta_r = 0.6$. In the aquifer, $\theta_s = 0.34$ and $\theta_r = 0.18$, based on Walser (1998). Water stage level observation data and groundwater monitoring data collect during the pump test and many hours after pumping stopped were used to calibrate the

numerical model.

In Krabbenhoft's (1996) interaction model between groundwater and lakes, an anisotropy ratio of 100 was obtained after several trial and error simulations. Also an anisotropy ratio of horizontal to vertical hydraulic conductivity of 10 was obtained by Winter (1978) in his numerical simulation of steady state three-dimensional groundwater flow model near lakes.

In this finite-element model, it was assumed that the hydraulic conductivity of the peat layer was different from the hydraulic conductivity of the underlying aquifer, and the aquifer was also assumed anisotropic. Furthermore, it was assumed that the hydraulic conductivities and anisotropies of both layers were spatially uniform within each layer throughout the aquifer zone. By adjusting the anisotropy ratio (K_h/K_v) and checking for the best agreement between modeled and observed data, it was determined that the best results were obtained when $K_h/K_v = 1.0$, $K_{xx} = K_{yy} = 8.7$ m/day, and $K_{zz} = 8.7$ m/day in the aquifer, while $K_p = 0.2$ m/day in the peat layer. This number is different from the value of 0.03m/day obtained by Switt (1998) and 0.087m/day obtained by Wise (2000). The possible difference may be caused by several reasons. First, the peat layer depth used in the numerical model is not a constant. When the water stage in the wetland is lowered, the peat layer depth in the inundated area is much greater than the average value of 0.25 m used in the analytical model. The variation of groundwater head immediately beneath the peat layer may not be the same value estimated using a groundwater head variation at a depth of 6 meters beneath of the wetland. Thus, the second reason may be that the head distribution beneath the wetland obtained from the numerical model is different from the values used by the analytical model.

Since the aquifer beneath the SV5 wetland is composed of sand, the specific

storativity is extremely small. The heads along the depth are very different. Figure 3-27 shows the head distribution beneath the wetland. Figure 3-28 shows the head variation with time at different depths beneath the wetland. The piezometric head changes relatively quickly in the deep zone, but the head does not change much near the wetland. Figure 3.29 shows the variation of the inundated area of the wetland. The area changes from 2,600 m^2 to 700 m^2just after pumping. Figure 3-30 shows the variation of the interaction discharge. The discharge supplied from the aquifer to the wetland increases quickly and then decreases slowly after pumping was stopped. Figure 3-31 shows excellent agreement between the simulated results given by the saturated flow model and observed groundwater levels. Table 3-4 to Table 3-8 show the modeled data used to calculate the interaction discharges at 5 different times.

Table 3-8 shows the sensitivities of the head relative to changes in the hydraulic conductivities in the pear layer and the aquifer and to changes in the specific storativity. The hydraulic conductivities in both the peat layer and the aquifer play the most important part in the change of head distribution and interaction discharge. The sensitivity of the specific storativity is relatively small.

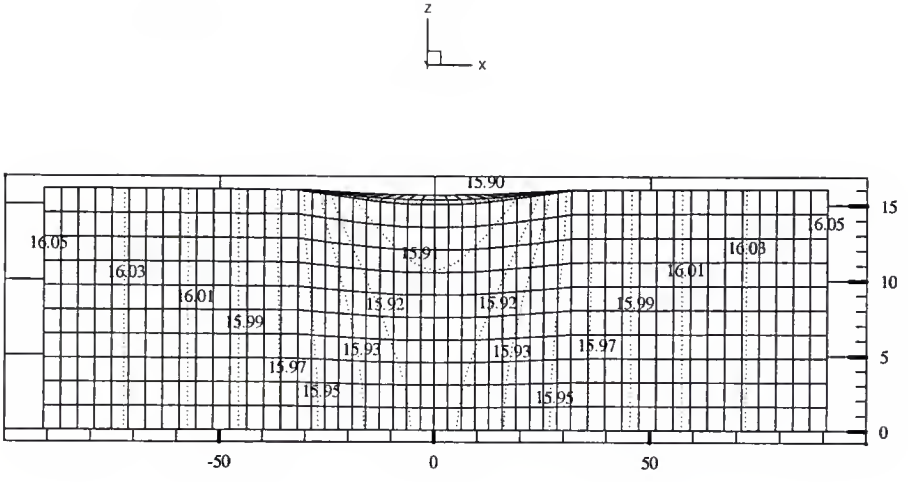

Figure 3-27. Vertical cross-section view of three-dimensional finite-element mesh and head from the saturated flow model at a time of 87 hours.

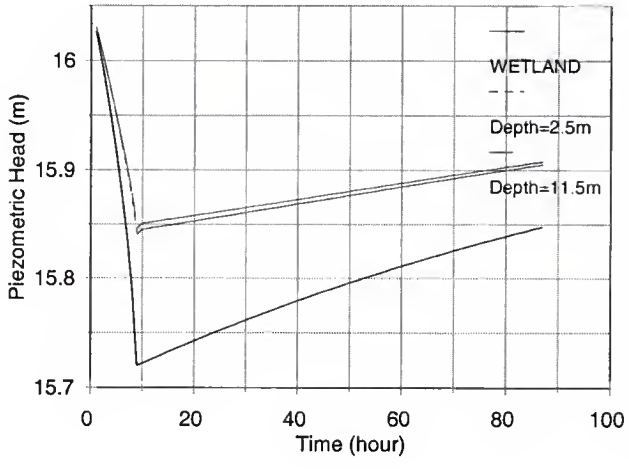

Figure 3-28. Piezometric head at positions beneath the wetland with time

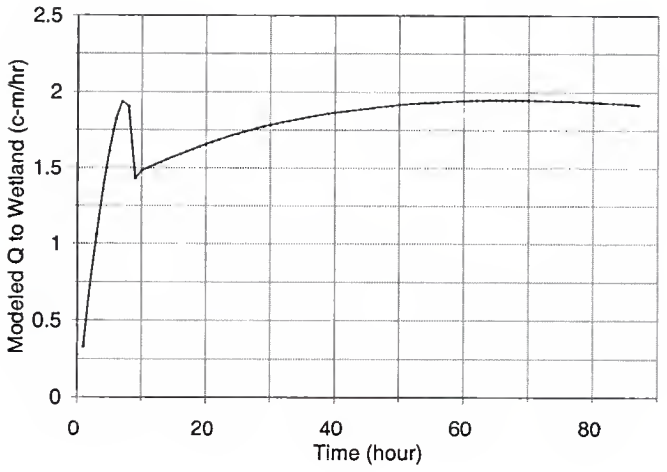

Figure 3-29. Variation in the inundated area of wetland during simulation

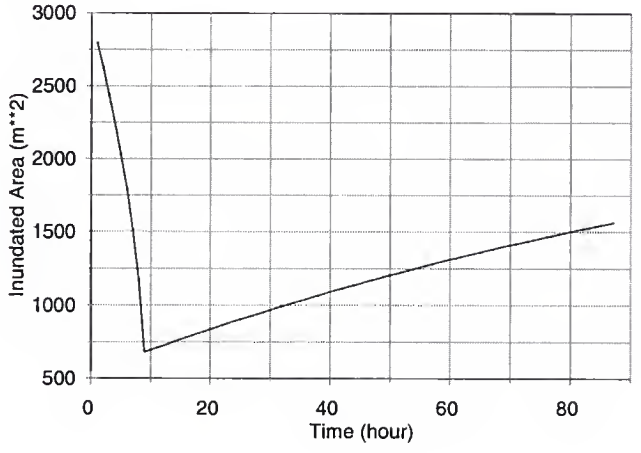

Figure 3-30. Discharge between wetland and aquifer with respect to time

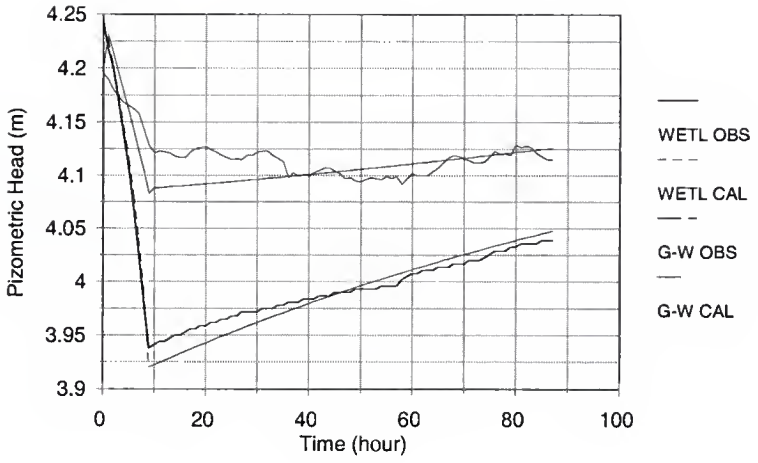

Figure 3-31. Comparison between calculated head and observed head

Table 3-4. Data for calculating the discharge to the wetland from the aquifer at 10 hours

Elements of Peat Layer	Area (m^2)	Head in Peat Layer (m)	Head on Peat Surface (m)	Distance of Two Nodes (m)
1	6.95828	15.7810	15.7223	0.301929
2	20.8748	15.7813	15.7223	0.305786
3	34.7914	15.7819	15.7223	0.306822
4	48.7075	15.7827	15.7223	0.303675
5	62.6240	15.7843	15.7223	0.297326
6	76.5414	15.7868	15.7223	0.289907
7	90.4590	15.7898	15.7223	0.281774
8	104.377	15.7936	15.7223	0.271725
9	118.296	15.7979	15.7223	0.260863
10	132.215	15.8028	15.7223	0.248279
Q to wetland at 10 hr	1.48466 m^3/hr			

Table 3-5. Data for calculating the discharge to the wetland from the aquifer at 20 hours

Elements of Peat Layer	Area (m^2)	Head in Peat Layer (m)	Head on Peat Surface (m)	Distance of Two Nodes (m)
1	8.36449	15.7953	15.7427	0.302115
2	25.0935	15.7956	15.7427	0.306344
3	41.8223	15.7960	15.7427	0.306027
4	58.5508	15.7964	15.7427	0.302183
5	75.2802	15.7982	15.7427	0.294043
6	92.0102	15.8003	15.7427	0.287151
7	108.741	15.8036	15.7427	0.275314
8	125.472	15.8070	15.7427	0.264839
9	142.204	15.8114	15.7427	0.250437
10	158.937	15.8162	15.7427	0.236900
Q to wetland at 20hr	1.65871 m^3/hr			

Table 3-6. Data for calculating the discharge to the wetland from the aquifer at 40 hours

Elements of Peat Layer	Area (m^2)	Head in Peat Layer (m)	Head on Peat Surface (m)	Distance of Two Nodes (m)
1	10.9288	15.8222	15.7797	0.302417
2	32.7864	15.8225	15.7797	0.307252
3	54.6436	15.8225	15.7797	0.304707
4	76.5010	15.8229	15.7797	0.298378
5	98.3597	15.8243	15.7797	0.289097
6	120.219	15.8264	15.7797	0.277635
7	142.080	15.8288	15.7797	0.266032
8	163.941	15.8321	15.7797	0.249581
9	185.804	15.8359	15.7797	0.233460
10	207.669	15.8406	15.7797	0.216548
Q to wetland at 40hr	1.86649 m^3/hr			

Table 3-7. Data for calculating the discharge to the wetland from the aquifer at 60 hours

Elements of Peat Layer	Area (m^2)	Head in Peat Layer (m)	Head on Peat Surface (m)	Distance of Two Nodes (m)
1	13.1219	15.8463	15.8115	0.302649
2	39.3657	15.8466	15.8115	0.307800
3	65.6089	15.8464	15.8115	0.303651
4	91.8530	15.8469	15.8115	0.295196
5	118.098	15.8480	15.8115	0.285844
6	144.345	15.8498	15.8115	0.271268
7	170.593	15.8519	15.8115	0.255422
8	196.843	15.8544	15.8115	0.239015
9	223.095	15.8579	15.8115	0.219572
10	249.349	15.8626	15.8115	0.199788
Q to wetland at 60hr	1.94458 m^3/hr			

Table 3-8. Data for calculating the discharge to the wetland from the aquifer at 80 hours

Elements of Peat Layer	Area (m^2)	Head in Peat Layer (m)	Head on Peat Surface (m)	Distance of Two Nodes (m)
1	15.0334	15.8681	15.8391	0.302835
2	45.1003	15.8683	15.8391	0.307522
3	75.1664	15.8680	15.8391	0.302700
4	105.234	15.8685	15.8391	0.292596
5	135.303	15.8695	15.8391	0.280887
6	165.374	15.8709	15.8391	0.266576
7	195.446	15.8727	15.8391	0.247805
8	225.521	15.8749	15.8391	0.228349
9	255.599	15.8777	15.8391	0.208494
10	285.679	15.8819	15.8391	0.186883
Q to wetland at 80hr	1.93622 m^3/hr			

Table 3-9. Sensitivities calculated by saturated groundwater flow model

Parameter (PR)	Percentage varied	ΔPR	$\|h_1-h_2\|$ (m)	$\|h_1-h_2\|/\Delta PR$
K_a(m/day)	- 0.10	-0.85	0.9924E-02	-1.1675E-02
K_a(m/day)	+0.10	+0.85	0.9055E-02	1.0653E-02
K_p(m/day)	- 0.10	- 0.02	0.6410E-02	-0.3205
K_p(m/day)	+0.10	+0.02	0.5564E-02	0.2782
S_o	-0.50	- 0.000005	0.2068E-04	-4.136
S_o	+0.50	+0.000005	0.1265E-04	2.53

3.7 Comparison with Results of Wise's (2000) and others

Parameter values obtained by Wise (2000), $k_{peat} = 0.087$ (m/day), by Walser (1998), $k_{sand} = 0.75$ (m/day), $k_{peat} = 0.03$ (m/day) for SV5 were put in the three-dimension finite-element model in this dissertation, and the simulated results were plotted on the Figure 3-32. When the specific storage was set on 0.01 (1/m), both the simulated wetland water table and groundwater are pretty close to the observed conditions. The simulated wetland water table and the groundwater table corresponding to the specific storage of 0.001 (1/m) are much different from the observed results.

There are two main differences between Walser's numerical simulation and the models in this dissertation. First, unlike a coupling boundary condition used in this dissertation, the fixed observed water table process over time was used in Walser's numerical simulation. The other difference is that a fixed three-dimension mesh was used in Walser's numerical simulation.

When k_{aqu} at 8m/day and k_{peat} at 0.2m/day were used , and specific storage was varied, the simulated results are plotted on the Figure 3-33. The simulated wetland water tables for both specific storage values are very close to the observed wetland water table results. The

groundwater table for the specific storage of 0.01(1/m), however, is above the observed results.

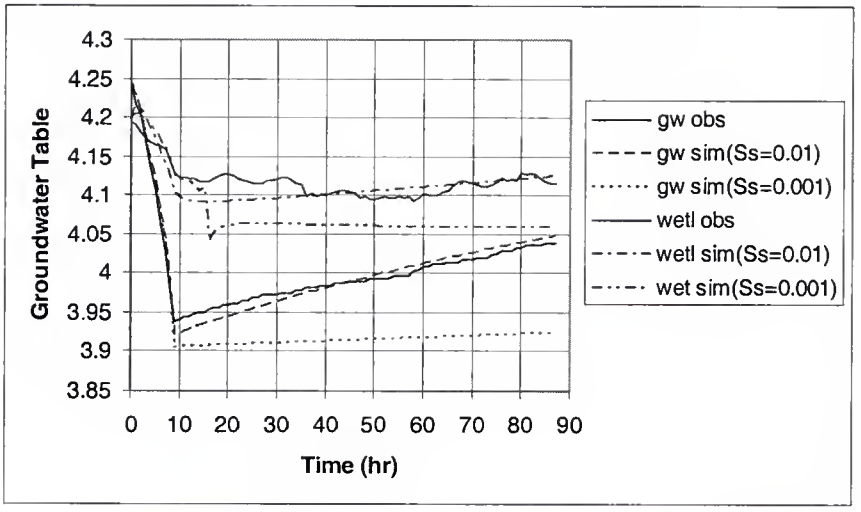

Figure 3-32. Comparison results using Walser's parameter values.

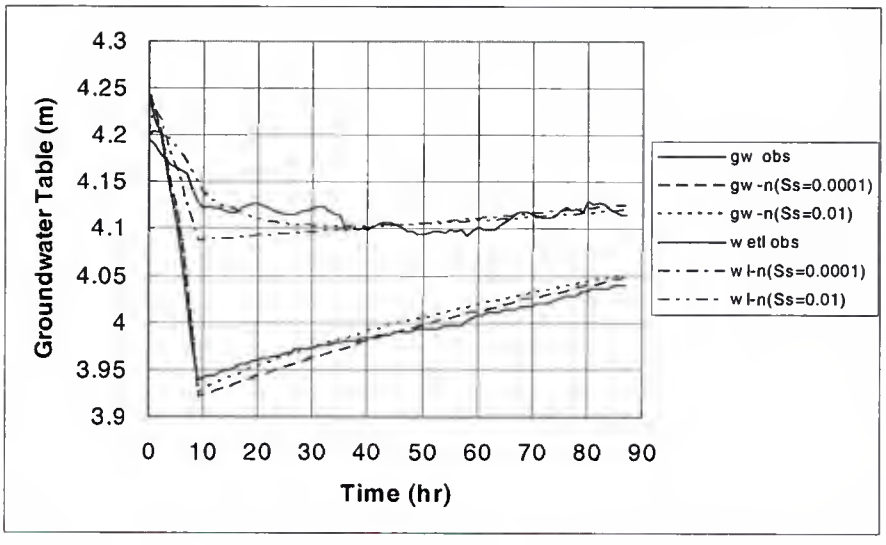

Figure 3-33. 3-D numerical model simulated results over specific storage

Table 3-10 shows the hydraulic conductivities in sand layer and peat layer. The variations are rather large.

Table 3-10. Hydraulic Conductivity values for sand and peat layers

	k in sand layer (m/day)	k in peat layer (m/day)
Switt et al.(1998)	7~12	0.03
Slug test	2	
Rycroft et al. (1975)		10^{-7}-10^{2}
Wise et al. (000)		0.083
Walser Numerical Model (1998)	0.75	0.03/0.3
Models in this dissertation	8	0.2

3.8 Summary

A three-dimensional finite-element numerical saturated groundwater flow model using deformable mesh and real-time wetland-aquifer coupling boundary is developed in this chapter. Considering the area of the water surface changes quickly because most wetlands have a shallow bank slope, the model has the capability of tracking the interaction the interaction boundary between groundwater and a wetland. The model is verified using two analytical solutions, one is Theis solution, the other is the analytical solution found in Chapter 2 of this dissertation, which describes groundwater flow around a circular wetland. The model is further used to simulate the interaction problem of groundwater and the SV5 wetland. The pumping from the SV5 wetland and the recovery of the SV5 wetland surface afterwards are closely simulated by this model, the interaction boundaries are effectively traced by the deformable mesh.

CHAPTER 4
INVERSE MODEL OF THREE-DIMENSIONAL FINITE-ELEMENT METHOD SATURATED GROUNDWATER MODEL IN SEARCHING FOR THE HYDRAULIC CONDUCTIVITY OF THE PEAT LAYER

4.1 Introduction

4.1.1 Inverse Problem

During the past twenty years, mathematical modeling has been extensively used in the study of groundwater problems. However, mathematical models require a number of parameters to characterize the aquifer. Usually, prior knowledge of the values of these parameters is limited, and they must be quantified by calibration which requires observations of hydraulic heads or solute concentrations.

Given a parametric model of the physical system and values of the model parameters, the prediction of system output (response) to any input is referred to as the direct problem, or the forward problem (simulation). The forward problem predicts unknown system states by solving appropriate governing equations.

Conversely, the estimation of model parameters given the parameteric system model and an input-output relationship is known as the inverse problem (calibration). The typical inverse problem involves estimating the values of model parameters, solving the direct problem with this set of parameters to calculate the predicted system response, and then adjusting model parameters until deviations between observed and model predicted responses are in some specified sense minimized (Sun 1994).

Trial and error and graphical matching techniques are the most basic and traditional methods to solve inverse problem. They are widely used because they are simple to implement. Because the number and combinations of parameter adjustments are not bounded, "trial and error" is rather flexible but also time-consuming. Additionally, the solution is strongly dependent on the skill of the practitioner (Keidser 1991).

4.1.2 Parameterization

Most groundwater inverse algorithms adopt either a blocked or a geostatistical (random field) description of spatial variability. The first approach divides the region of interest into a number of discrete blocks or zones that are believed to correspond to distinct geological units (Yeh 1986, Carrera and Neuman 1986a,b,c, and Cooley 1977,1979,1982,1983). Each block is characterized by a set of spatially uniform hydrogeologic properties which are treated as parameters in an appropriate inverse problem. Thus, the unknown distributed paramters can be represented by a number of constants. The weakness of this method is obvious, i.e., although we have some of the geological information is available, it is still difficult to divide the flow region into a limited number of zones. If the zonation pattern is incorrect, the identified paramter values also will be incorrect (Sun and Yeh 1985).

The geostatistical alternative views the properties of interest as stationary random fields that vary relatively smoothly over space (Hoeksma and Kitanidis 1984, Dagan 1985,Yeh 1996, and Zhang 1997, Michalak 2004). In the geostatistical interpolation method of kriging, the unknown parameter is regarded as a stochastic field described by some statistical parameters, such as the mean, variance, and correlation distance. Then the identified parameter vector consists of only a few statistical parameters if the aquifer is

basically homogeneous. The problem of overparameterization may be avoided, and the inverse solution obtained by the maximum likelihood estimate and cokriging is generally stable. The correctness of the inverse solution, however, depends on the correctness of some statistical assumptions and the structure of covariance functions.

Although the two approaches are based on different parameterizations, they both treat hydrogeologic properties as spatial functions. This suggests that it should be possible to formulate a general inverse theory which encompasses both the blocked and geostatistical alternatives, as well as hybird methods which lie between these extremes.

4.1.3 Parameter Identification Methods

Many methods are available for the solution of the common groundwater modeling inverse problem whereby the conductivity or transmissivity of a porous medium are estimated using available observations of head or pressure and other information (Distefano 1975, Chang 1976, Loaiciga 1987, Mishra 1989, Knopman 1989, Keidser 1991, Sun 1995, Yeh 1996, Zhang 1997, Lamorey 1998, Anderman 1999, Michalak 2004). Neuman (1973) classified inverse modeling solution techniques as either "direct" or "indirect".

The direct method or equation error method is used when head variations and derivatives (usually estimated) are known over the entire flow region. If the measurement and model errors are negligible, the original governing equation becomes a linear first-order partial differential equation of the hyperbolic type in terms of the unknown parameters. With the aid of boundary conditions and flow data, a direct solution for the unknown parameters may be possible. In practice, observation wells are sparsely distributed in the flow region and only a limited number of observation wells are available. To formulate the inverse problem by the equation error criterion, missing data have to be estimated by interpolation. The

interpolation data contain errors resulting from the interpolation, and, thus, cause additional errors in the results of parameter identification.

The solution approach of the indirect method to solve inverse problems is to formulate the inverse problem in term of an optimization framework, based on the most common output error criterion, i.e., output error least squares criterion. Using this approach, a set of parameters is identified which best describes observed system states.

With inverse modeling, the structure and parameters of a model are adjusted simultaneously or sequentially so as to obtain a parameter input system and output relations that characterize observed excitation-response functions of the real system. Since the model structure for the wetland/groundwater system is assumed to follow Eq.5-1-5-3, the problem of determining the hydraulic conductivity of the peat layer from the observed water stage and total head in the aquifer may be taken as a typical inverse problem. The investigation of the inverse problem based on the three-dimensional saturated groundwater flow model and the adjoint state method is presented in this chapter.

4.1.4 Computation of Sensitivity Coefficients

Sensitivity coefficients, i.e., the partial derivatives of head with respect to each of the parameters, play an important role in the solution of the inverse problem. In the Gauss-Newton algorithm, elements of the Jacobian matrix are represented by the sensitivity coefficients, $\partial h_i/\partial T_l$, i=1,....,M, l=1,...,L. If h is the head vector, the sensitivity coefficients are $\partial h_i/\partial T_l$, l=1,...,L. There are three methods used in calculation of sensitivity coefficients. There are the influence coefficient method, sensitivity equation method, and variational method. The influence coefficient method determines the sensitivity coefficients by perturbing each parameter once at a time.

In the sensitivity equation method, a set of sensitivity equations is obtained by taking the partial derivatives with respect to each parameter in the governing equation and in the initial and boundary conditions. The sensitivity coefficients are obtained by solving the new governing equations.

The variational method was first used for solving the inverse problem of parameter identification by Jacquard and Jain (1965) and then by Carter et al. (1974, 1982) associated with finite-difference schemes. Sun and Yeh (1985) extended the method to the case of a finite-element scheme. The sensitivity coefficients can be computed using the following equation:

$$\frac{\partial h^{(j)}}{\partial T_I^{(i)}} = \int_0^{t_f} \int_{\Omega_i} \nabla\left(\frac{\partial q(x,y,t-\tau)}{\partial t} \right) \cdot \nabla h(x,y,\tau)\, dx dy d\tau \qquad (4\text{-}1)$$

$$j=1,2,\ldots, N_o \qquad\qquad i=1,2,\ldots,N_n$$

where Ω_i is the exclusive subdomain of node i; ∇ is the gradient operator; h(x,y,t) is the solution of the governing equation; N_o is the number of observation wells; N_n is the total number of nodes used in the numerical solution; and q(x,y,t) is the time derivative of q(x,y,t), which is the solution of the set of adjoint equations.

4.2 Adjoint Problem for Three-Dimensional Finite-Element Saturated Groundwater Model

The focus of this section is the formulation of the adjoint problem which defines sensitivities to be used in determining the hydraulic characteristics of the peat layer and the underlying aquifer. It is assumed that the thickness of the peat and aquifer are known. As

discussed in Chapter 3, three dimensional groundwater flow in an unconfined aquifer is governed by:

$$\nabla \cdot (K \nabla h) \pm Q = S_s \frac{\partial h}{\partial t} \qquad (x,y,z) \in \Omega, \qquad 0 \le t \le t_f \tag{4-2}$$

subject to the initial and boundary conditions:

$$h(x,y,z,0) = f_0 \qquad (x,y,z) \in \Omega \tag{4-3}$$

$$h|_{\Gamma_2} = f_1, \qquad K \nabla h \cdot \bar{n}|_{\Gamma_1} = f_2, \tag{4-4}$$

f_0 is the initial head; f_1 is the specific head condition; f_2 is the specified flux condition; and t_f is the time duration. The boundary of volume Ω shown in Figure 4-1 is denoted by Γ including wetland head boundary (Γ_2), no flow boundary (Γ_1), and lateral head boundary (Γ_2).

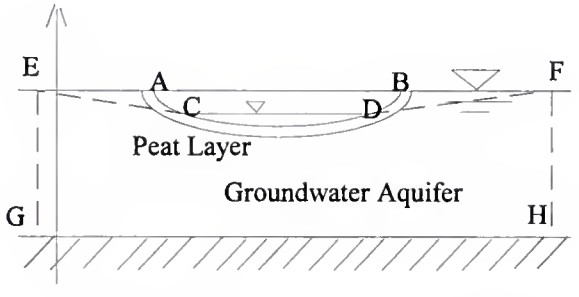

AB, EG, FH or CD are head boundaries Γ_2

GH or EC, DF are no flow boundaries Γ_1

Figure 4-1. Sketch showing setup of the saturated groundwater inverse problem around a wetland

The hydraulic conductivities of the peat layer and the underlying aquifer are the unknown parameters. Any variation δK of K where K=hydraulic conductivity must cause a variation δh of head h, because h is dependent on K through the governing equation and subsidiary conditions. Taking the variation of Eq. 4-2 and subsidiary conditions, the following is obtained:

$$\nabla\cdot(\delta K\nabla h)+\nabla\cdot(K\nabla\delta h)=S_s\frac{\partial(\delta h)}{\partial t}\qquad (x,y,z)\in\Omega,\qquad 0\le t\le t_f \tag{4-5}$$

subject to the conditions:

$$\delta h(x,y,z)|_{t=0}=0\qquad (x,y,z)\in\Omega \tag{4-6}$$

$$\delta h|_{\Gamma_2}=0,\qquad [\delta K\nabla h+K\nabla\delta h]\cdot\bar{n}|_{\Gamma_1}=0, \tag{4-7}$$

Eq. 4-5-Eq. 4-7 represent the variational problem of the primary problem in Eq. 4-2. The variational problem relates the variation δk and δh. Assuming h is an arbitrary function having continuous second-order space derivatives on Ω and first-order derivatives in $[0, t_f]$, then multiplying Eq. 4-5 by Ψ and integrating the result over time-space domains yields:

$$\int_\Omega (S_s\Psi\delta h)|_0^{t_f}d\Omega-\int_0^{t_f}\int_\Omega\left[S_s\delta h\frac{\partial\Psi}{\partial t}+\Psi\nabla\cdot(\delta k\nabla h)+\Psi\nabla\cdot(k\nabla\delta h)\right]d\Omega dt=0 \tag{4-8a}$$

If we define:

$$\Psi(x,y,z,t_f) = 0 \qquad (x,y,z)\in\Omega \tag{4-8b}$$

then the first term of Eq. 4-8a vanishes because of condition 4-7. Thus, Eq. 4-8b reduces to:

$$\int_0^{t_f}\int_\Omega \left[S_s\delta h\frac{\partial\Psi}{\partial t} + \Psi\nabla\cdot(\delta k\nabla h) + \Psi\nabla\cdot(k\nabla\delta h)\right]d\Omega dt = 0 \tag{4-9}$$

where:

$$\int_\Omega \Psi\nabla\cdot(\delta k\nabla h)\,d\Omega = \int_s \Psi(\delta k\nabla h)\cdot\bar{n}ds - \int_\Omega \delta k\nabla h\cdot\nabla\Psi\,d\Omega \tag{4-10}$$

and:

$$\int_\Omega \Psi\nabla\cdot(k\nabla\delta h)\,d\Omega = \int_s \Psi(k\nabla\delta h)\cdot\bar{n}ds - \int_\Omega k\nabla\delta h\cdot\nabla\Psi\,d\Omega \tag{4-11}$$

$$-\int_\Omega k\nabla\delta h\cdot\nabla\Psi\,d\Omega = \int_\Omega \delta h[\nabla\cdot(k\nabla\Psi)]d\Omega - \int_s \delta hk\nabla\Psi\cdot\bar{n}ds \tag{4-12}$$

Using identities of Eq. 4-10, Eq. 4-11 and Eq. 4-12, Eq. 4-9 can be written as:

$$\int_0^{t_f}\left[\int_\Omega\left[S_s\delta h\frac{\partial\Psi}{\partial t}+\delta h[\nabla\cdot(k\nabla\Psi)]-\delta k\nabla h\cdot\nabla\Psi\right]d\Omega\right]dt$$

$$+\int_0^{t_f}\left[\int_s\Psi\delta k\nabla h\cdot\bar{n}ds+\int_s\Psi k\nabla\delta h\cdot\bar{n}ds-\int_s\delta hk\nabla\Psi\cdot\bar{n}ds\right]dt=0 \qquad (4\text{-}13)$$

Using conditions 4-7 and defining:

$$\Psi|_{\Gamma_2}=0,\qquad k\nabla\Psi\cdot\bar{n}|_{\Gamma_1}=0$$

then the second term of Eq. 4-13 is equal to zero. Eq. 4-13 produces:

$$\int_0^{t_f}\int_\Omega\left[S_s\frac{\partial\Psi}{\partial t}+\nabla\cdot(k\nabla\Psi)\right]dh\,d\Omega\,dt-\int_0^{t_f}\int_\Omega(\nabla\Psi\cdot\nabla h)dk\,d\Omega\,dt=0 \qquad (4\text{-}14)$$

In order to identify the hydraulic conductivity k(x,y,z) that would lead to the best prediction of observed heads, a performance criterion must be defined. A general form of the performance function may be written as:

$$E(h,k)=\int_0^{t_f}\int_\Omega f(h,k;x,y,z,t)d\Omega\,dt=0 \qquad (4\text{-}15)$$

Taking the variation of E(h, k) yields:

$$\partial E(h,k) = \int_0^{t_f}\int_\Omega \left(\frac{\partial f}{\partial k}\delta k + \frac{\partial f}{\partial h}\delta h \right) d\Omega\, dt = 0 \tag{4-16}$$

The summation of Eq. 4-16 and Eq. 4-14 gives:

$$\delta E = \int_0^{t_f}\int_\Omega \left[\frac{\partial f}{\partial t} - S_s \frac{\partial \Psi}{\partial t} - \nabla\cdot(k\nabla\Psi) \right] dh\, d\Omega\, dt + \int_0^{t_f}\int_\Omega \left(\frac{\partial f}{\partial k} + \nabla\Psi\cdot\nabla h \right) dk\, d\Omega\, dt \tag{4-17}$$

If Ψ(x,y,z,t) is selected to satisfy the following PDE:

$$S_s \frac{\partial \Psi}{\partial T} + \nabla\cdot(k\,\nabla\Psi) - \frac{\partial f}{\partial h} = 0 \tag{4-18}$$

subject to conditions:

$$\Psi(x,y,z,t_f) = 0,$$

$$\Psi|_{\Gamma_1} = 0, \qquad k\nabla\Psi\cdot\bar{n}|_{\Gamma_2} = 0$$

then, the first integral on the right hand side of Eq. 4-17 related to unknown δh will vanish. Thus:

$$\delta E = \int_0^{t_f} \int_\Omega \left(\frac{\partial f}{\partial k} + \nabla\Psi \cdot \nabla h \right) dk\, d\Omega\, dt \tag{4-19}$$

From Eq. 4-19, the following partial derivative can be defined:

$$\frac{\delta E}{\partial k} = \int_0^{t_f} \int_\Omega \left(\frac{\partial f}{\partial k} + \nabla\Psi \cdot \nabla h \right) d\Omega\, dt \tag{4-20}$$

By introducing the following time transformation:

$$\tau = t_f - t \tag{4-21}$$

the adjoint problem can be expressed as

$$S_s \frac{\partial \Psi}{\partial \tau} - \nabla \cdot (k \nabla \Psi) + \frac{\partial f}{\partial h} = 0 \tag{4-22}$$

subject to:

$$\Psi|_{\tau=0} = 0, \quad (x,y) \in \Omega$$

$$\Psi|_{\Gamma_2=0} = 0 \qquad\qquad k \nabla \Psi \cdot \bar{n}|_{\Gamma_1} = 0 \tag{4-22a}$$

where $\Psi = \Psi(x,y,z,t_f - \tau)$. Solving each equation once, all components of the gradient $\nabla E(k)$ can be obtained.

4.3 Searching Objective Function

To find the best parameter value, the model structure and model parameters are solved simultaneously or sequentially so as to make the input-output relation of the model fit any observed excitation-response relationship of the real system. Since the model structure of the problem in this study is determined, the problem of determining the hydraulic conductivity of the peat layer and the underlying aquifer from the observed water stage and total head in the aquifer may be taken as a typical inverse problem:

$$E(K_{est}) = \min E(K) \tag{4-23}$$

where:

$$E(k) = \sum_{l=1}^{L} \left[h_{cal} - h_{obs}\right]^2 \tag{4-24}$$

The traditional method to solve this kind of problems is using the trial and error method based on the output least squares criterion (Eq. 4-23).

4.4 Adjoint State Controlling Equations

In this study the adjoint state method was used to solve the inverse problem. From the governing equation (Eq. 4-2) and the associated boundary conditions, the adjoint formulation of the primary problem may be found using Green's first and second theorems and other transforms:

$$S_s \frac{\partial \Psi}{\partial \tau} - \nabla \cdot (k \nabla \Psi) + \frac{\partial f}{\partial h} = 0 \tag{4-25}$$

subject to:

$$\Psi|_{\tau=0}=0, \quad (x,y)\in\Omega \tag{4-26}$$

and

$$\Psi|_{\Gamma_2=0}=0 \qquad k\nabla\Psi\cdot\bar{n}|_{\Gamma_1}=0 \tag{4.27}$$

where h is the total head; $\Psi = \Psi(x,y,t_f-\tau)$ is the adjoint state of h; t_f is the time duration of the simulation criterion and f(h,k;x,y,t) expresses the 'goodness' of fit between the predicted head, h, and the observed head, h_{obs} expressed through the ordinary least squares (OLS):

$$f(h,k;x,y,z,t)=\sum_{j=1}^{J}\left\| h(k)-h_{obs}\right\|\delta(x-x_{obs})\delta(y-y_{obs})\delta(z-z_{obs})\delta(t-t_j) \tag{4-28}$$

where (x_{obs}, y_{obs}, z_{obs}) is the location of the observation well; and t_j (j =1,2,$\cdots$,J) are the observation times. Integrating, Eq. 4-28 over time space domains produces:

$$E(h,k)=\int_0^{t_f}\int_{(\Omega)}\sum_{j=1}^{J} f(h,k;x,y,z,t)d\Omega dt \tag{4-29}$$

By solving the governing Equation 4-2 and the adjoint Equation 4-25 once, we may obtain the following functional partial derivative required to solve Equation 4-23 is obatined:

$$\frac{\delta E}{\delta k} = \int_0^{t_f} \int_{(\Omega)} \left[\frac{\partial f}{\partial k} + \nabla \psi \cdot \nabla h \right] d\Omega dt \tag{4-30}$$

4.5 Searching Method and Stopping Criterion

Since the gradient ∇E(k) is known, many searching methods including the gradient method, quasi-Newton method, and the Fletcher-Reeves method could be used to solve the inverse problem 4-23 (Sun 1985). Two stopping criteria used here are:

$$\| K_n - K_{n-1} \| < \varepsilon_1 \tag{4-31}$$

and:

$$\| E(k_n) - E(k_{n-1}) \| < \varepsilon_2 \tag{4-32}$$

Using the adjoint method and the Fletcher-Reeves algorithm to update the search sequence, a highly efficient numerical scheme for solving the inverse problem can be formulated.

4.6 Field Application on SV5

The inverse model was used to estimate the hydraulic conductivity of the peat layer underlying the SV5 wetland (Wise et al. 2000). Since the piezometric head at a depth of 5 meters beneath the wetland was observed, f is defined as:

$$f(h,k;x,y,z,t) = \sum_{j=1}^{J} \| h(k) - h_{obs} \| \delta(x - x_{obs}) \delta(y - y_{obs}) \delta(z - z_{obs}) \delta(t - t_j) \tag{4-33}$$

Water-level data were measured every hour for a total duration, t_f, of 87 hours. An example

of how the hydraulic conductivity, K, is updated between iterations is as follows. Assuming an initial estimate of the vertical hydraulic conductivity K of the peat layer was K_1=1.00m/day, then $\partial E/\partial K$ = -0.0125 by Eq.4-29 and $E(K_1)$= 0.48998. Because it is not possible to match the modeling result with the observed result exactly, the final E(k) is not zero. The sensitivity was used to decide the direction of searching. Assuming E(K) is supposed to be the smallest value, the updated value of $K=K_2$ is assumed to be 0.6 m/day as generated from the formula:

$$E(K_2) = E(K_1) + \frac{\partial E}{\partial K}\Big|_{K_1} (K_2 - K_1) \qquad (4\text{-}34)$$

Based on the new $K = K_2$ = 0.6 m/day, the updated gradient $\partial E/\partial K$ = 0.0188, and $E(K_2)$= 0.41467. Then a new K is assumed until E(K) is minimized. The final K is 0.2 m/day. Figure 4-2 and Table 4-1 are the calculated values from the adjoint method model. In this model, the observed groundwater data were used in the output least squares criterion. The observed water stage in the wetland was not used in the model. This is the major reason that the final result from the inverse model is a little bit different from the result obtained in Chapter 3. The saturated flow model in Chapter 3 uses both the observation of groundwater head beneath the wetland and the surface water stage of wetland to calibrate the model. In the inverse model, however, it is hard to use the surface-water observation result, since it is a boundary of the model.

Because the wetted area of surface water associated with the wetland changes with time, the space location of each finite-element point tied to the location of the water surface must be saved before the adjoint state equations are solved. Thus, for each assumed hydraulic

conductivity in the peat layer, the forward problem, and adjoint state problem must be solved first, and then ∂E/∂k for this assumed value of K could be found. Figure 4-3 shows the procedure for solving an inverse problem using adjoint method.

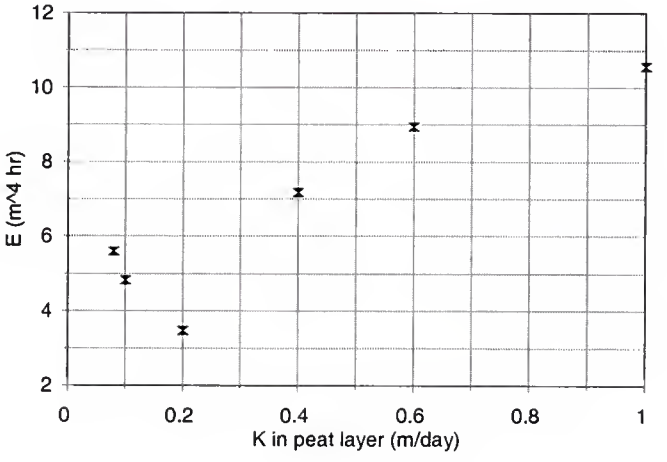

Figure 4-2. Relation between error and peat hydraulic conductivity

Table 4-1. Error and sensitivity based on the adjoint method model

	K (m/day)	E(k)	∂E/∂K
1	1.0	10.5698	0.26965
2	0.6	8.94509	0.40555
3	0.4	7.17941	1.03330
4	0.2	3.47742	0.31495
5	0.1	4.82392	3.72980
6	0.08	5.59932	3.14520

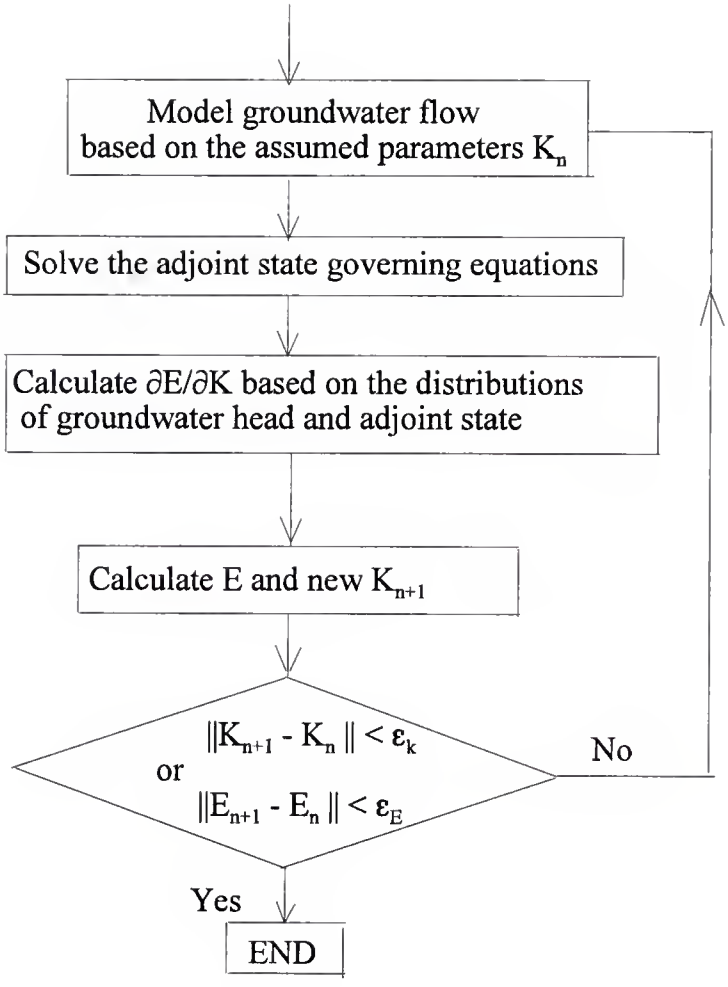

Figure 4-3. Flowchart illustrating the iteration procedure of inverse problem

4.8 Summary

The inverse problem for three-dimensional transient groundwater flow in a phreatic aquifer is more complicated, because the free surface changes with time such that the simulation zone is not stationary. In order to solve the adjoint state governing equations, the position of each node must be saved at all time steps. In other words, for a deformable mesh, it is not suitable to use the adjoint method to solve the inverse problem. The second problem is that the observed information related with interaction discharge, such as the surface water stage in the wetland in the SV5 case, is difficult to be used.

As shown in Figure 4-4, to finish each iteration of searching parameters, four steps including solving the forward problem and the adjoint state equations must be executed. For one parameter in the case here, the above method seems excessive. The "trial and error" method is clearer and faster.

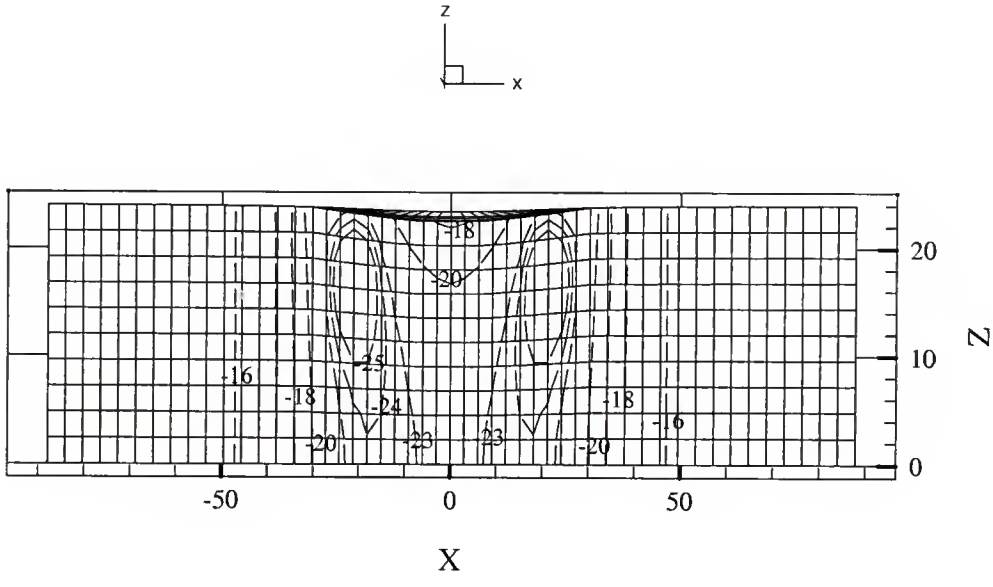

Figure 4-4. Vertical cross-section of the adjoint state distribution at τ=10 hours

CHAPTER 5
THREE-DIMENSIONAL VARIABLY-SATURATED GROUNDWATER MODEL

5.1 Introduction

The limitations associated with saturated subsurface flow models have inspired hydrologists to develop variably saturated groundwater models that consider both saturated and unsaturated flow (e.g. Voss 1984, van Genuchten 1980, Kirkland et al. 1992, Cox et al. 1994, and Boufadel et al. 1996). Flow in variably-saturated media has been investigated by a number of investigators over the past several decades. Rubin (1968) used the finite-difference and alternating-direction-implicit (ADI) methods to solve the two-dimensional Richards' equation. Freeze (1971) used the finite-difference and line successive over-relaxation methods to simulate three-dimensional variably saturated flow. Neuman (1973) initiated the use of the finite-element method to model two-dimensional variably saturated flow in 1973. Huyakorn el al.(1984, 1986) developed the SATURN two-dimensional and three-dimensional variably-saturated flow models using finite elements. Yeh (1992) used the finite-element method and Gauss elimination (or point iteration) methods to solve the three-dimensional Richards' equation. His model is the well known three-dimensional FEMWATER model. Other significant contributions to the area of variably-saturated flow can be found in Brutsaert (1971), Narasimhan (1978), Cooley (1983), Kirkland et al.(1992), Clement et al.(1994) and Bates et al. (2000), Zhang (2000), Thorenz, 2002, and Russo (2003).

The general modeling approach has consisted of extending Darcy's law to unsaturated media and combining it with the continuity equation to obtain Richard's equation. Empirical relations are then used to relate unsaturated hydraulic conductivity to the soil moisture content and pressure head [Brooks and Corey 1966; and Van Genuchten 1980]. Although there are many papers on variably-saturated flow modeling, few have investigated variably-saturated flow using deformable finite elements.

This chapter describes an efficient three-dimensional finite-element variably-saturated groundwater model that is suitable for characterizing wetland/aquifer interactions using a deformable mesh and real-time boundary conditions. The model was tested using experimental data from Vauclin (1979) and then applied to simulate surface stage and groundwater level variations measured in an isolated wetland in South Florida. A comparison was made between the simulation results predicted by the variably saturated flow model and that of the saturated flow model (described in Chapter 3) for the isolated wetland field study.

5.2 Three-Dimensional Finite-Element Variably-Saturated Groundwater Model

5.2.1 Governing Equation

Eq. 5-1 describes variably-saturated groundwater flow, assuming that the fluid is incompressible, the system is isothermal, and the air phase is infinitely mobile:

$$\frac{\partial}{\partial x_i}\left(K_{ij} K_{rw} \frac{\partial(\psi + z)}{x_j} \right) \pm Q = \frac{\partial}{\partial t}(\theta_s S_w), \quad i,j = 1,2,3 \tag{5-1}$$

where S_w is the degree of saturation, equal to θ/θ_s; θ is the water content; θ_s is the saturated water content; $K_{i,j}$ is the saturated hydraulic conductivity tensor [L/T]; $K_{rw}=K_{rw}(S_w)$ represents the relative permeability of the medium, which is a function of the degree of water

saturation S_w; ψ is pressure head [L]; and z is elevation head [L]. In order to solve this nonlinear flow equation, constitutive relations must be established that relate the primary unknowns ψ and S_w. Such relations are often given by a prescribed functional relationship that is determined experimentally. The following functional relation given by Van Genuchten (1980) was used in this development:

$$S_e = \left[\frac{1}{1+(\alpha P_c)^n}\right]^m \quad , \quad m = 1 - \frac{1}{n} \; ; \quad 0<m<1 \tag{5-2}$$

where: α and m are parameters obtained from a fit of above equations to experimental results; P_c is the capillary pressure (P_c = - ψ); and:

$$S_e = \frac{S_w - S_{wr}}{1 - S_{wr}} = \frac{\theta - \theta_r}{\theta_s - \theta_r} \tag{5-3}$$

where S_{wr} is the residual saturation; S_e is effective saturation; and θ_r is residual moisture content.

The relative permeability is obtained from the effective saturation using the following relationship from Van Genuchten (1980):

$$k_{rw} = S_e^{1/2}\left|1-(1-S_e^{1/m})^m\right|^2 \tag{5-4}$$

In using Eq. 5-4, hysteresis was not considered.

5.2.2 Linearizing the Governing Equations

To solve the governing equations, the nonlinear Eq. 5-1 was linearized. Substituting Eq. 5-3 into the right-hand-side of Eq. 5-1 yields:

$$\frac{\partial(\theta_s S_w)}{\partial t} = \frac{\partial \theta}{\partial t} = \frac{\partial[(\theta_s - \theta_r)S_e + \theta_r]}{\partial t} \tag{5-5}$$

Combining Eq. 5-5 and Eq. 5-2 produces:

$$\frac{\partial(\theta_s S_w)}{\partial t} = (\theta_s - \theta_r)\, m \left[\frac{1}{1+\alpha^n P_c^{\,n}}\right]^{m-1} \frac{(-1)}{(1+\alpha^n P_c^{\,n})^2} \alpha^n n P_c^{\,n-1} \frac{\partial P_c}{\partial t} + S_e S_s \frac{\partial \psi}{\partial t} \tag{5-6}$$

where:

$$\frac{\partial P_c}{\partial t} = -\frac{\partial \psi}{\partial t} = -\frac{\partial(\psi + z)}{\partial t} \tag{5-7}$$

Thus, Eq. 5-5, Eq. 5-6 and Eq. 5-7 yield:

$$\frac{\partial(\theta_s S_w)}{\partial t} = f_t(\theta_s, \theta_r, m, \alpha, P_c, n, S_s, s_e) \frac{\partial(\psi + z)}{\partial t} \tag{5-8}$$

By substituting Eq. 5-6 into the left hand side of Eq. 5-1, the following linearized equation was obtained:

$$\frac{\partial}{\partial x_i}\left(K_{ij} K_{rw} \frac{\partial(\psi + z)}{\partial x_j} \right) \pm Q =$$

$$\left[(\theta_s - \theta_r)\, m \left(\frac{1}{1+\alpha^n P_c^{\,n}} \right)^{m-1} \frac{1}{(1+\alpha^n P_c^{\,n})^2} \alpha^n n P_c^{\,n-1} + S_e S_s \right] \frac{\partial(\psi + z)}{\partial t} \qquad i,j = 1,2,3 \tag{5-9}$$

The governing Eq. 5-9 was solved using the finite-element method.

5.2.3 Boundary Conditions for Variably-Saturated Model

Figure 5-1 shows a hypothetical wetland consisting of a surface-water body lined with a peat layer, and beneath the wetland is an aquifer. The lower boundary of the aquifer is assumed to be an impermeable unit. As to the top boundary condition (IA, BJ), constant moisture or a moisture flux can be specified. In the case of rainfall, the net rainfall would be a specified flux as long as $P_{precipitation} < K_s$. For the case of no precipitation, the moisture flux is equal to actual evapotranspiration.

As to the coupling boundary condition controlled by wetland water level, the same way used in saturated flow model was used in this model. The initial water table of the wetland and pumping discharge were taken as the only inputs. During pumping, the pumping discharge lowered the wetland water level, and it also triggered the discharge from aquifer supplying to wetland through the peat layer. In each simulation time step, the pumping discharge, the estimated discharge from aquifer to wetland, the initial water table of wetland, and the relation between the volume of wetland and wetland water level were put together, and the water table at the end of the time step was estimated. The estimated water table at the end of the time step was again put back to the model of the variably-saturated groundwater in the aquifer and peat layer; it corrected the discharge from aquifer to wetland estimated before. Therefore, several iterations in each time step were necessary to get the accurate estimated discharge from aquifer to wetland and the convergent solution of water table in wetland at the end of the time step. While the pumping was stopped, the pumping discharge was taken as zero. Thus, the boundary condition at any time unknown in the beginning depended on the modeling results of the coupling problem itself before this time.

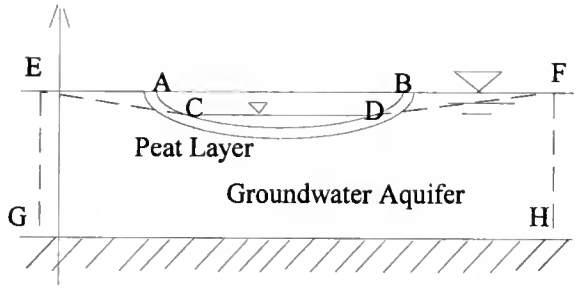

AB, EG, FH or CD are head boundaries Γ_2

GH or EC, DF are no flow boundaries Γ_1

EA, BF are head, flow boundaries Γ_1

Figure 5-1. Sketch showing setup of the variably saturated groundwater flow problem around a wetland

The determination of evapotranspiration (ET) is a two-step process in the model based on Fraisse and Campbell (1997). First, the daily potential evapotranspiration (PET) is calculated in terms of atmospheric data. Maximum evaporation depends on climatological factors which include net radiation, temperature, humidity, and wind velocity. The PET represents the maximum amount of water that will leave the soil system by evaporation when there is a sufficient supply of soil water. After PET is calculated, checks are made to determine if ET is limited by soil water conditions. If soil water conditions are not limiting, ET is set equal to PET. When PET is higher than the amount of water that can be supplied from the soil system, ET is set equal to the smaller amount. Maximum evaporation is equal to potential evaporation. The following relationship between ET and PET developed by Norero (1969) was used in the groundwater flow model:

$$ET = \frac{PET}{\left[1 + \left(\frac{\psi}{\psi^*}\right)^k\right]} \tag{5-10}$$

and

$$k = \frac{2.56}{\log\left(\frac{\psi_{Wmin}}{\psi_{Wmax}}\right)} \tag{5-11}$$

where k is a constant, ψ is the soil water potential or metric pressure in the root zone, ψ^* is the value of ψ when ET= 0.5PET, ψ_{Wmin} is the value of ψ that corresponds to PE/PET=0.05, and ψ_{Wmax} is the value of ψ that corresponds to PE/PET=0.95. Norero (1969) used ψ_{Wmin} =-1350 joules/kg and ψ_{Wmax}=-200 joules/kg. Figure 5-2 illustrates the relative evapotranspiration as a function of soil water potential.

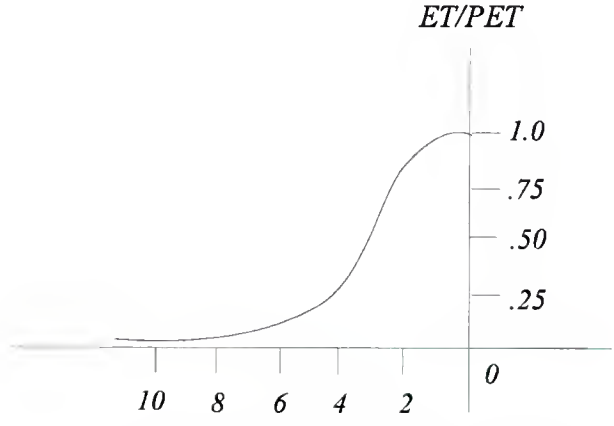

Figure 5-2. Schematic of relative evapotranspiration (ET/PET), as affected by soil water potential, ψ [Norero 1969].

5.3 Finite-Element Method for Modeling Three-Dimensional Variably-Saturated Flow

Given the complexity of the unsaturated flow Eq. 5-9, it is not readily seen that it has the same form as the governing equation for satuarted flow (Eq. 3-1). However, if $f(\theta_s, \theta_r, m, \alpha, p_c, n)$ from Eq. 5-8 is used in lieu of specific storativity S_s in the saturated groundwater equation, the form of both the saturated and unsaturated flow equations becomes the same. As a result, the strategy taken to develop an finite-element model for saturated flow (Chapter 3) was applied again to develop an appropriate equation for an finite-element model for variably saturated flow. Similar to what was done in Chapter 3, assuming that the basis function w is chosen from V space, the follow equation is always true:

$$\int_{\Omega} w\left[\nabla\cdot\left(KK_{rw}\nabla h\right)\right]d\Omega \pm \int_{\Omega} w\,Q\,d\Omega$$

$$= \int_{\Omega} w f_t(\theta_s,\theta_r,m,\alpha,P_c,n)\frac{\partial h_t}{\partial t}\,d\Omega, \quad i,j = 1,2,3 \tag{5-12}$$

Manipulation of the first term in the left hand side of Eq. 5-12 begins with the application of Green's theorem, which is an expanded form of the divergence theorem. This converts the integral into two terms, one of which is evaluated only at the surface of the region to be simulated. Application of the Galerkin criterion and Green's theorem to Eq. 5-12 leads to

$$\int_{\Gamma_1} w\left[\left(KK_{rw}\nabla h\right)\cdot \underline{n}\right]d\Gamma + \int_{\Gamma_2} w\left[\left(KK_{rw}\nabla h\right)\cdot \underline{n}\right]d\Gamma - \int_{\Omega} (\nabla w)\cdot\left(KK_{rw}\nabla h\right)d\Omega$$

$$\pm\int_{\Omega} w\,Q\,d\Omega = \int_{\Omega} w f_t(\theta_s,\theta_r,m,\alpha,P_c,n)\frac{\partial h_t}{\partial t}\,d\Omega \qquad (5\text{-}13)$$

The first term, which depends on the moisture flux on the surface, is no longer zero as it is in the saturated model. For head boundaries that are used along Γ_2, w is equal to zero, because it belongs to V space, Thus, with the second term set equal to zero, Eq. 5-13 can be rewritten as:

$$\int_{\Gamma_1} w\left[\left(KK_{rw}\nabla h\right)\cdot \underline{n}\right]d\Gamma - \int_{\Omega} (\nabla w)\cdot\left(KK_{rw}\nabla h\right)d\Omega \pm \int_{\Omega} wQd\Omega$$

$$= \int_{\Omega} w f_t(\theta_s,\theta_r,m,\alpha,P_c,n)\frac{\partial h_t}{\partial t}\,d\Omega \qquad (5\text{-}14)$$

An approximate solution for h(x, y, z, t) can be assumed to have the following form:

$$w^{(e)} = \sum_{i=1}^{p} N_i^{(e)}(x,y,z)\,c_i \quad , \quad N_i \in V \qquad (5\text{-}15)$$

and:

$$\overline{h^{(e)}}(x,y,z,t) = \sum_{i=1}^{p} N_i^{(e)}(x,y,z)\, d_i(t) \;,\; N_i \in V \;,\; h \in S \tag{5-16}$$

where $h^{(e)}$ is the approximate solution for hydraulic head within element e, $N_i^{(e)}$ are interpolation functions for each node within element e, p is the number of nodes within element e, and $d_i(t)$ are the unknown values of hydraulic head for each node within element e and at time t. At the head boundaries, Γ_2, $d_i(t) = h(x,y,z)|_{\Gamma 2}$. $w_i^{(e)}$ is the weighting function for node i and the limits of integration are chosen to represent the volume of the elements. In Galerkin's method, the weighting function for each node in the element is set equal to the interpolation function for the node, $w_i^{(e)} = N_i^{(e)}$.

When the approximate solutions for Eq. 5-15 and Eq. 5-16 are substituted into Eq. 5-14, Eq. 5-17 is obtained which is not satisfied exactly, and an error or residual occurs at every point in the problem domain. If it is also assumed that the aquifer is isotropic, that is to say, values of saturated hydraulic conductivity in the three coordinate directions are constant within an element (but can vary from one element to the next), the contribution of any element e to the residual at a node i associated with the element can be described through the flow system of Eq. 5-17:

$$\begin{bmatrix} R_1^{(e)}(t) \\ \vdots \\ R_p^{(e)}(t) \end{bmatrix} = \left[K^{(e)} K_{rw}\right] \begin{bmatrix} d_1^{(e)}(t) \\ \vdots \\ d_p^{(e)}(t) \end{bmatrix} + \left[C^{(e)}\right] \begin{vmatrix} \dfrac{\partial d_1^{(e)}(t)}{\partial t} \\ \vdots \\ \dfrac{\partial d_p^{(e)}(t)}{\partial t} \end{vmatrix} - \left[F^{(e)}\right] \tag{5-17}$$

where:

$$\left[K^{(e)}K_{rw}\right] = \int\int\int_{V^{(e)}} \begin{bmatrix} \frac{\partial N_1^{(e)}}{\partial x} & \frac{\partial N_1^{(e)}}{\partial y} & \frac{\partial N_1^{(e)}}{\partial z} \\ \vdots & \vdots & \vdots \\ \frac{\partial N_p^{(e)}}{\partial x} & \frac{\partial N_p^{(e)}}{\partial y} & \frac{\partial N_p^{(e)}}{\partial z} \end{bmatrix} \begin{bmatrix} k_{xx}k_{rw} & 0 & 0 \\ 0 & k_{yy}k_{rw} & 0 \\ 0 & 0 & k_{zz}k_{rw} \end{bmatrix} \begin{bmatrix} \frac{\partial N_1^{(e)}}{\partial x} & \cdots & \frac{\partial N_p^{(e)}}{\partial x} \\ \frac{\partial N_1^{(e)}}{\partial y} & \cdots & \frac{\partial N_p^{(e)}}{\partial y} \\ \frac{\partial N_1^{(e)}}{\partial z} & \cdots & \frac{\partial N_p^{(e)}}{\partial z} \end{bmatrix} \tag{5-18}$$

and:

$$\left[C^{(e)}\right] = \int\int\int_{V^{(e)}} \begin{bmatrix} N_1^{(e)} \\ \vdots \\ N_p^{(e)} \end{bmatrix} \left[f_t(\theta_s,\theta_r,m,\alpha,p,n)\right] \begin{bmatrix} N_1^{(e)} & \cdots & N_p^{(e)} \end{bmatrix} \tag{5-19}$$

and:

$$\left[F^{(e)}\right] = \int\int_{\Gamma_1^{(e)}} \begin{bmatrix} N_1^{(e)} \\ \vdots \\ N_p^{(e)} \end{bmatrix} q_{surface} \tag{5-20}$$

Combining Eq. 5-17-Eq. 5-20 from each element together, global equations are obtained:

$$\left[KK_{rw}\right]\begin{bmatrix} d_1(t) \\ \vdots \\ d_p(t) \end{bmatrix} + \left[C\right]\begin{bmatrix} \dfrac{\partial d_1(t)}{\partial t} \\ \vdots \\ \dfrac{\partial d_p(t)}{\partial t} \end{bmatrix} - \left[F\right] = \begin{bmatrix} R_1(t) \\ \vdots \\ R_p(t) \end{bmatrix} \tag{5-21}$$

By setting the residuals equal to zero, the final system of ordinary differential equations is obtained:

$$\left[KK_{rw}\right]\begin{bmatrix} d_1(t) \\ \vdots \\ d_p(t) \end{bmatrix} + \left[C\right]\begin{bmatrix} \dfrac{\partial d_1(t)}{\partial t} \\ \vdots \\ \dfrac{\partial d_p(t)}{\partial t} \end{bmatrix} - \left[F\right] = \begin{bmatrix} 0 \\ 0 \\ 0 \end{bmatrix} \tag{5-22}$$

The system of Eq. 5-22 representing the variably saturated flow system was solved using finite differences.

5.4 Transient, Variably-Saturated Water-Table Recharge Example Test

An example problem was formulated using laboratory data to verify the performance of the model. Details concerning the following laboratory data and the experiment were presented by Vauclin et al. (1979). The flow domain consisted of a rectangular soil slab, 6.00 m by 2.00 m (Figure 5-3), with an initial horizontal water table located at a height of 0.65 m. At the soil surface, a constant flux of q = 3.55 m/day was applied over an infinite zone 1 m wide. The remaining soil surface was covered to prevent evaporation losses. Because of symmetry, it was necessary to model only one side (for this test the right side) of the flow domain. No-flow boundaries were set on the bottom and along the axis of symmetry

(Figure 5-3). At the soil surface, the constant flux of 3.55 m/day was applied over the left 0.50 m of the top of the modeled domain. The remaining soil surface represented a no-flow boundary condition. A no-flow boundary was used above the water table on the right side of the domain (Figure 5-3).

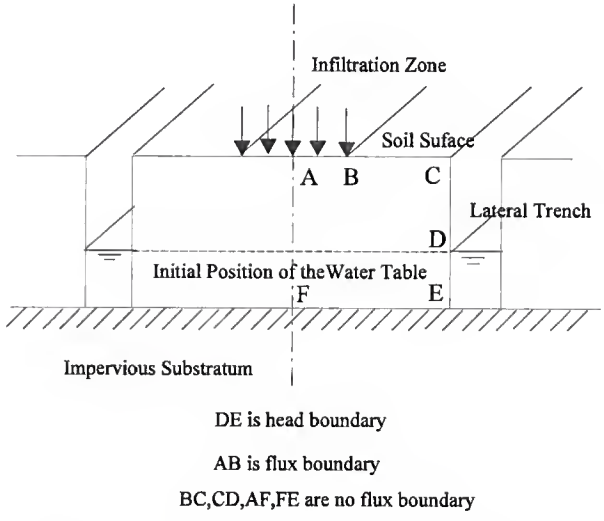

Figure 5-3. Schematic diagram of the flow domain

From Vauclin et al. (1979), the characteristics of the experimental soil properties included a saturated hydraulic conductivity of 8.40 m/day, a porosity of $\eta = \theta_s = 0.30$, and a residual saturation of $\theta_r = 0.01$. When Eq. 5-2 was fitted to the water retention and the relative hydraulic conductivity data given by Vauclin et al. (1979), estimated values for model parameters α and n were $\alpha = 3.3\ m^{-1}$ and $n = 4.1$. Specific storage was neglected for this problem because changes in storage are facilitated by the filling of pores, which overshadows the effects of compressibility for the vertical extent of this flow domain. Hence, the specific storage coefficient was set to zero.

The mesh spacing used in the test problem in the horizontal x- and vertical z-directions was $\Delta x = 0.10$ m and $\Delta z = 0.05$m, respectively. The soil system was assumed

to be initially at hydrostatic equilibrium with respect to the water table throughout the flow domain. Transient simulations were performed using time steps that varied from $\Delta t = 180$ secondes to $\Delta t = 360$ secondes.

Transient positions of the water table are compared with the experimental results presented by Vauclin et al. (1979) in Figure 5-4 and Figure 5-5. These figures show excellent agreement between the transient water-table positions predicted by the variably saturated model and those obtained from Vauclin et al. (1979).

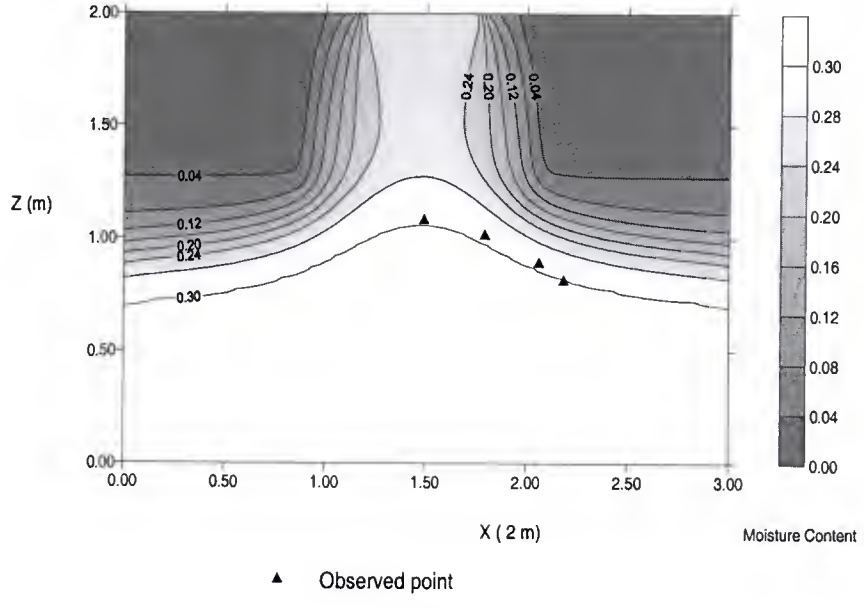

Figure 5-4. Water moisture distribution (x : y = 2 :1) at 4 hours
(Observed points are from Vauclin et al.1979)

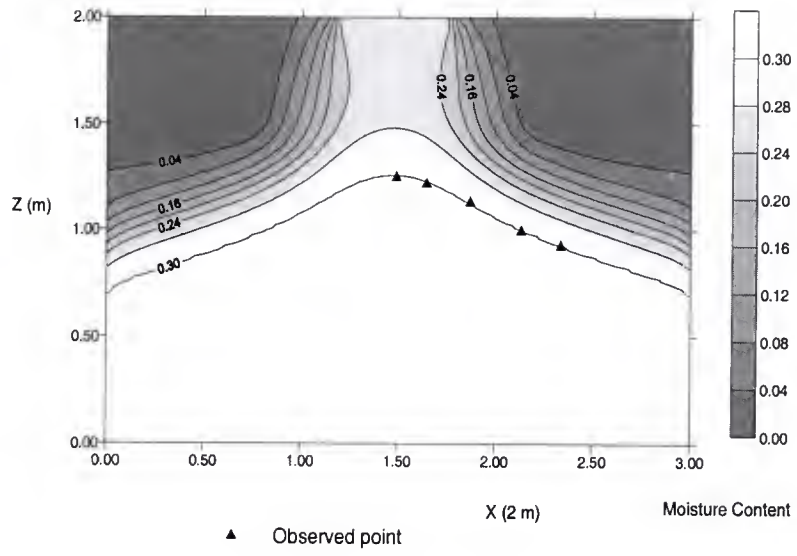

Figure 5-5. Water moisture distribution at 8 hours (x : y = 2:1)
(Observed points are from Vauclin et al.1979)

5.5 Application on SV5 Wetland

5.5.1 Finite-Element Mesh for Three-Dimensional Variably-Saturated Flow Model

Unlike the saturated groundwater flow model (Chapter 3), matric pressure and water content may vary rapidly in time and space in the variably-saturated model, which produces rapid spatial and temporal variation in the variably-saturated flow hydraulic conductivity. In order to simulate the moisture or pressure variation accurately, a fine numerical mesh must be used over zones of rapid change to determine flow parameter variations accurately. Like the saturated flow model, the SV5 (Wise et al. 2000) simulation domain was divided into two main areas. One area was the aquifer; the other area was the wetland peat layer. Two parameters, $k_{aquifer}$ and k_{peat}, were used to represent their hydraulic conductivities. The numerical mesh was 26×21×3. The top 10 layers of mesh represent about top 1.55 m of the

aquifer. Among the top10 layers, the upper 4-5 layers were given a finer descretization, and the remaining layers of the top 10 were given a coarse descretization. The bottom 10 layers represented about 15 meters of saturated aquifer. The mesh in the saturated portion of the flow field was considerably coarser.

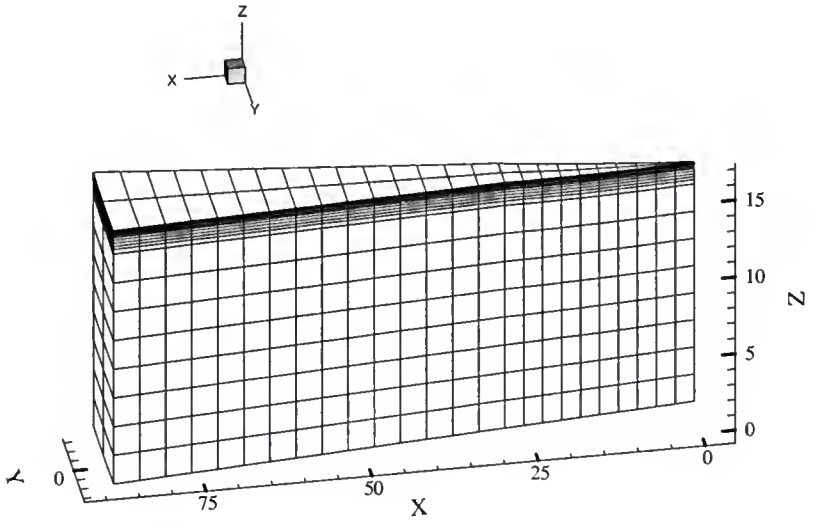

Figure 5-6. Finite-element mesh of the wedge part for variably saturated flow model (Unit is m)

Unlike the model for saturated flow, certain of the boundaries surrounding the simulation area are fixed. The top boundaries are the aquifer surface or the wetland bottom. The mesh deforms during a simulation because the elevation of the surface water changes. The model seeks to locate the same elevation as the surface-water stage and at a location where a horizontal line defines where the surface-water surface intersects with the bottom of the wetland. As the mesh deforms during a simulation, a subroutine program is used to determine whether a cell is in the peat layer or the underlying aquifer and then the corresponding hydraulic conductivity and other parameters of the element are assigned. As the mesh deforms, some elements are enlarged and some of them are compressed, but the

total area of the model domain does not change.

5.5.2 Modeling Results and Summary

For the SV5 wetland simulation, the same hydraulic conductivity values used in the saturated model were used in the variably saturated flow model. Thus, $K_{xx}=K_{yy}=8.5$ m/day; $K_{zz}=8.5$ m/day; the anisotropy ratio $K_h/K_v = 1.0$ in aquifer; and $K_p = 0.2$ m/day in the peat layer were used throughout the model domain. The specific storativity of $S_s =0.00001$ (1/m) and the saturated water content and residual water content in the peat layer $\theta_s = 0.7$; $\theta_r = 0.6$; n=5.0; m=0.8; $\alpha = 0.001$ (1/cm) = 0.1 (1/m); and in the aquifer $\theta_s = 0.34$; $\theta_r = 0.18$; n=9.1; m=0.89; $\alpha = 0.01$(1/cm) = 1 (1/m) were also used, based on Walser et al. (1998) and Wise et al. (2000). Figure 5-7 shows the simulated piezometric head variation at selected depths beneath the wetland.

When surface water was pumped from the wetland, the water stage decreased, and the associated piezometric head changes were greatest immediately beneath the wetland. The time needed for the wetland to recover from the stress was much longer. Figure 5-8 shows that the aquifer discharge to the wetland increased as the surface-water component of the wetland was drained and that the aquifer discharge decreased a little after the pumping stopped. Figure 5-9 shows the transient variation of the inundated wetland area. During pumping, the inundated area decreased from 2,800 m^2 to 700 m^2. During the recovery period, the inundated area increased slowly. Figure 5-10 shows that the model was able to fit the observed aquifer well, which is the SFWMD well screened at a depth of six meters and grouted from the surface to a depth of five meters. In a comparison prediction, results from both the saturated model and the variably saturated flow model are consistent (Figure 5-11). The piezometric head distribution beneath the wetland is shown in Figure 5-12 and Figure

5-13. Tables 5-1 through 5-5 show the simulated heads, the corresponding areas, and the distances which were used to calculate the exchange discharge.

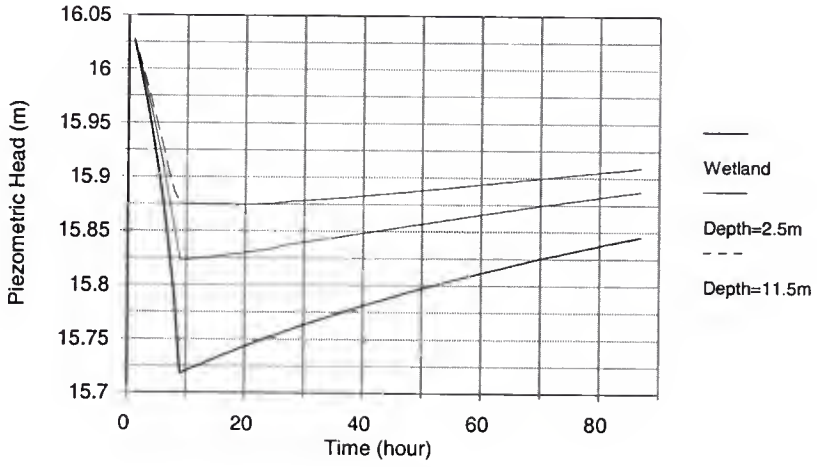

Figure 5-7. Calculated piezometric head beneath the wetland using the three-dimensional variably saturated groundwater flow model

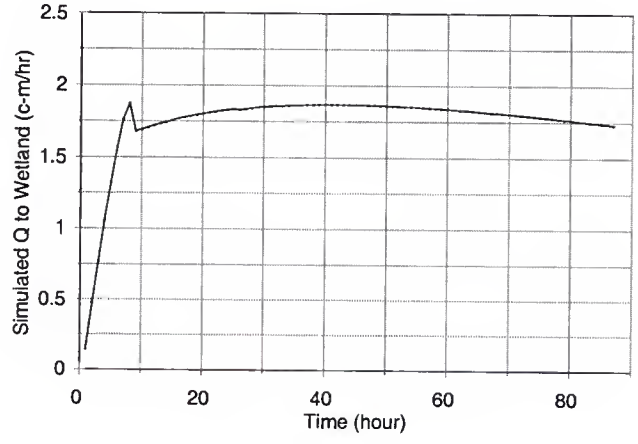

Figure 5-8. Model predicted discharge from the aquifer to the overlying wetland

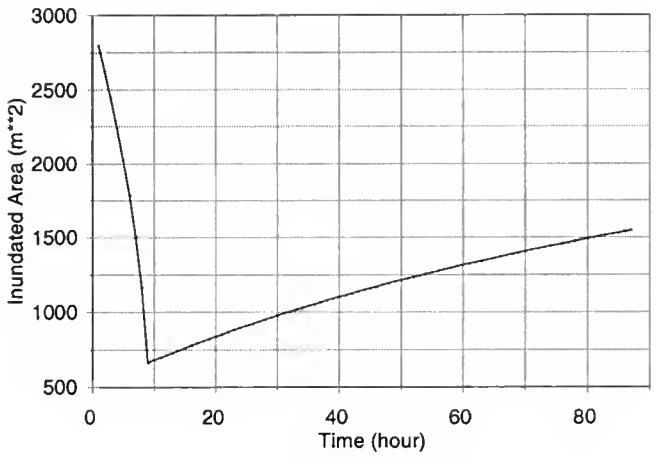

Figure 5-9. Inundated area of wetland during simulation

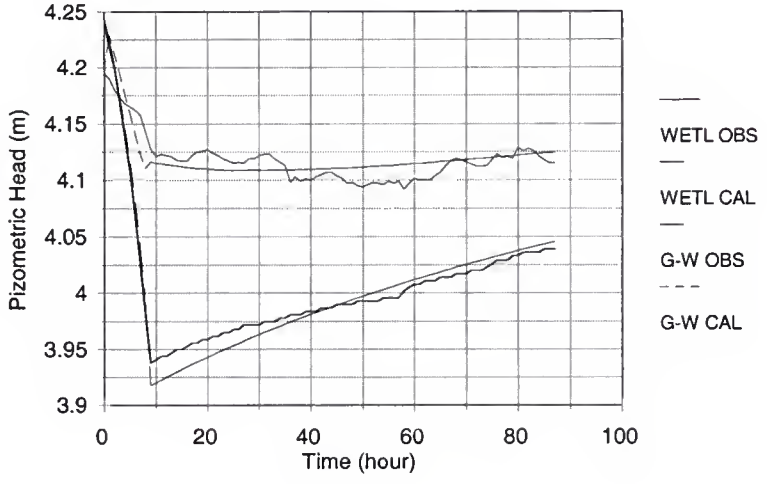

Figure 5-10. Simulated and observed heads in the wetland and in aquifer

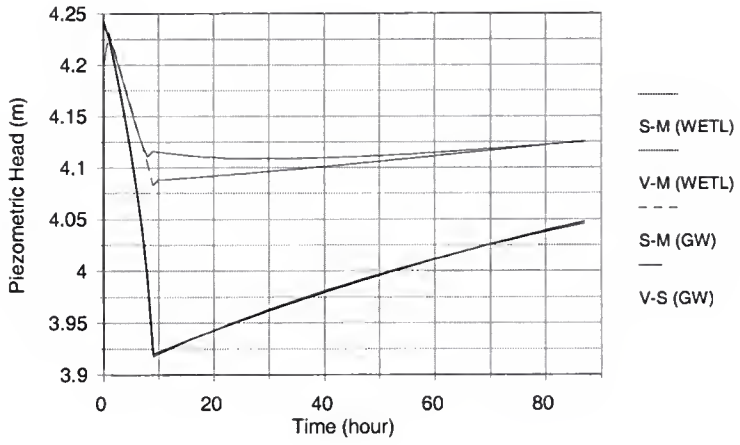

Figure 5-11. Simulated heads from the saturated flow model and the variably saturated flow model

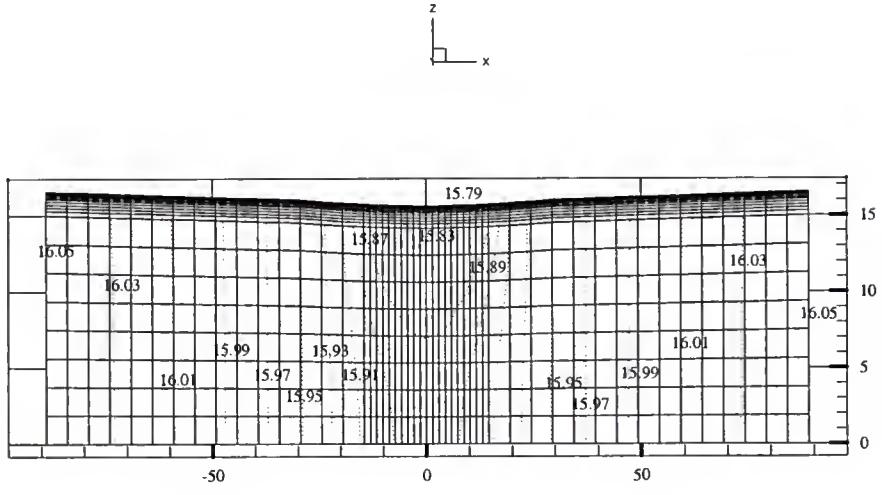

Figure 5-12. Horizontal view of the three-dimensional finite-element mesh and piezometric head distribution from the variably saturated flow model at a time of 9 hours.

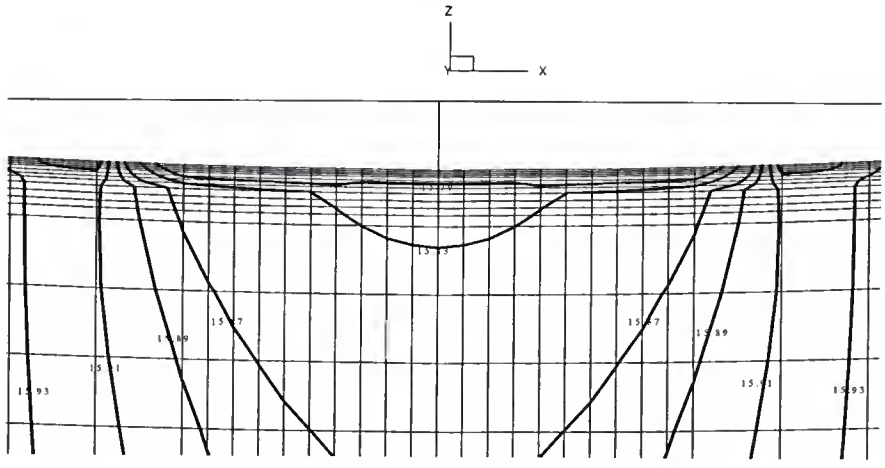

Figure 5-13. Enlarged top and middle part of the mesh
and head contour at a time of 9 hours.

Table 5-1. Data for calculating the discharge to the wetland from the aquifer at 10 hours

Elements of Peat Layer	Area (m^2)	Head in Peat Layer (m)	Head on Peat Surface (m)	Distance of Two Nodes (m)
1	6.82502	15.7300	15.7203	0.04715
2	20.4751	15.7301	15.7203	0.04718
3	34.1251	15.7301	15.7203	0.04721
4	47.7747	15.7291	15.7203	0.04723
5	61.4246	15.7285	15.7203	0.04726
6	75.0755	15.7289	15.7203	0.04729
7	88.7265	15.7292	15.7203	0.04732
8	102.378	15.7296	15.7203	0.04736
9	116.030	15.7301	15.7203	0.04741
10	129.683	15.7308	15.7203	0.04747
Q to wetland at 10 hr	1.6954 m^3/hr			

Table 5-2. Data for calculating the discharge to the wetland from the aquifer at 20 hours

Elements of Peat Layer	Area (m^2)	Head in Peat Layer (m)	Head on Peat Surface (m)	Distance of Two Nodes (m)
1	8.39429	15.7513	15.7431	0.04715
2	25.1829	15.7514	15.7431	0.04718
3	41.9713	15.7515	15.7431	0.04721
4	58.7594	15.7506	15.7431	0.04724
5	75.5484	15.7501	15.7431	0.04727
6	92.3379	15.7505	15.7431	0.04731
7	109.128	15.7508	15.7431	0.04735
8	125.919	15.7512	15.7431	0.04740
9	142.711	15.7517	15.7431	0.04746
10	159.504	15.7524	15.7431	0.04753
Q to wetland at 20hr	1.8041 m^3/hr			

Table 5-3. Data for calculating the discharge to the wetland from the aquifer at 40 hours

Elements of Peat Layer	Area (m^2)	Head in Peat Layer (m)	Head on Peat Surface (m)	Distance of Two Nodes (m)
1	11.0360	15.7876	15.7813	0.04715
2	33.1081	15.7876	15.7813	0.04719
3	55.1798	15.7870	15.7813	0.04722
4	77.2516	15.7866	15.7813	0.04726
5	99.3248	15.7869	15.7813	0.04729
6	121.399	15.7871	15.7813	0.04734
7	143.474	15.7874	15.7813	0.04740
8	165.550	15.7877	15.7813	0.04747
9	187.628	15.7882	15.7813	0.04754
10	209.707	15.7889	15.7813	0.04763
Q to wetland at 40hr	1.8693 m^3/hr			

Table 5-4. Data for calculating the discharge to the wetland from the aquifer at 60 hours

Elements of Peat Layer	Area (m^2)	Head in Peat Layer (m)	Head on Peat Surface (m)	Distance of Two Nodes (m)
1	13.1576	15.8171	15.8120	0.04715
2	39.4727	15.8171	15.8120	0.04719
3	65.7872	15.8166	15.8120	0.04723
4	92.1052	15.8163	15.8120	0.04723
5	118.419	15.8165	15.8120	0.04727
6	144.737	15.8167	15.8120	0.04731
7	171.057	15.8170	15.8120	0.04737
8	197.378	15.8173	15.8120	0.04744
9	223.701	15.8177	15.8120	0.04752
10	250.027	15.8184	15.8120	0.04772
Q to wetland at 60hr	1.8396 m^3/hr			

Table 5-5. Data for calculating the discharge to the wetland from the aquifer at 80 hours

Elements of Peat Layer	Area (m^2)	Head in Peat Layer (m)	Head on Peat Surface (m)	Distance of Two Nodes (m)
1	14.9321	15.8419	15.8377	0.04715
2	44.7963	15.8419	15.8377	0.04720
3	74.6597	15.8415	15.8377	0.04724
4	104.525	15.8412	15.8377	0.04728
5	134.391	15.8415	15.8377	0.04733
6	164.259	15.8417	15.8377	0.04739
7	194.129	15.8419	15.8377	0.04747
8	224.001	15.8422	15.8377	0.04756
9	253.875	15.8426	15.8377	0.04767
10	283.753	15.8432	15.8377	0.04779
Q to wetland at 80hr	1.7653 m^3/hr			

The saturated model and the variably saturated model are different in several aspects. First of all, the variably saturated flow model requires that the moisture flux be specified on the soil surface as the boundary condition. This moisture flux on the soil surface induces the head distribution in the vadose zone that is not described in the saturated flow model. Second, the empirical formula used to characterize the matric pressure as a function of the degree of saturation may not be accurate, and, as a result, it displaces the phreatic surface (where pressure head is zero) to a location not consistent with observations.

Table 5-6 shows the sensitivities of the heads related to charges in its hydraulic conductivities in the peat layer and aquifer and to changes in the specific storativity. The hydraulic conductivities in both the peat layer and in the aquifer are important in the change of head distribution. Changes in the specific storativity do not affect the head very much relatively .

Table 5-6 Sensitivity calculated by variably saturated groundwater flow model

Parameter (PR)	Percentage varied	ΔPR	$\|h_1-h_2\|$ (m)	$\|h_1-h_2\|/\Delta PR$
K_a(m/day)	-0.1	-0.85	0.5700E-02	-0.6706E-02
K_a(m/day)	+0.1	+0.85	0.5090E-02	0.5988E-02
K_p(m/day)	-0.1	- 0.02	0.5155E-02	-0.2578
K_p(m/day)	+0.1	+0.02	0.4665E-02	0.2333
S_o	-0.5	-0.000005	0.2990E-04	-5.980
S_o	+0.5	+0.000005	0.1998E-04	3.996

CHAPTER 6
SUMMARY AND CONCLUSIONS

This dissertation describes an analytical formula for groundwater variation affected by a flood wave in a wetland and also describes the development of two three-dimensional finite-element method numerical models, one of which is a saturated groundwater flow model and the other a variably saturated groundwater flow model. Both models use a deformable mesh and real-time coupling for the wetland-aquifer boundary along the interface between the surface water and groundwater. In the saturated groundwater flow model, a predictor-corrector method is used to find the real-time boundary condition that satisfies both the head condition and flux condition at the same time. The saturated groundwater flow model was verified using two analytical solutions; one is the Theis solution, and the other is the analytical solution found in Chapter 2 of the dissertation, which describes groundwater flow around a circular wetland. The saturated groundwater flow model was further used to simulate the interaction problem of groundwater and the SV5 wetland in south Florida.

The three-dimensional finite-element variably-saturated flow model was developed based on the linearized Richard equation. This model is different from previous variably-saturated flow models in the deformable three-dimension finite-element mesh and dynamically interacting boundary conditions applied in this model. The predictor-corrector method is also used in the variably-saturated groundwater flow model to find the real-time boundary conditions that satisfies both the head condition and flux condition at the same

time. The variably-saturated groundwater flow model was verified based on the field and laboratory work described by Vauclin et al. (1979).

The following specific conclusions can be drawn from this dissertation:

1. The analytical model describing the interaction between a flood wave in a lake and surrounding groundwater is an original development that can be used to simulate the groundwater fluctuations caused by a transient wetland surface water stage regardless of the function used to characterize the transient variation of the wetland stage.
2. Considering that the area of the water surface changes quickly because most wetlands have a shallow bank slope, the saturated groundwater flow model has the capability of successfully tracking the interaction boundary between groundwater and a wetland. The pumping from the SV5 wetland and the recovery of the wetland water surface afterwards were closely simulated by this model, and thus the interacting boundaries were effectively traced by the deformable mesh.
3. The variably saturated groundwater flow model also successfully simulated the groundwater flow affected by the pumping from the SV5 wetland and the water level recovery in the wetland after pumping. The rapidly moving boundary, i.e., the special phenomenon that occurs in the groundwater and wetland interaction problem, is effectively dealt with by this model also using a deformable mesh.

REFERENCES

Allen, M. B. And Murphy, C. L., 1986. A finite element collocation method for variably saturated flow in two space dimensions. Water Resour. Res., 22(11): 1537-1547.

Ames, W. F. 1977. Numerical methods for partial differential equations, 2nd ed. Academic Press. New York.

Anderman, Evan R., and Hill, Mary C. 1999. A new multistage groundwater transport inverse method: Presentation, evaluation, and implications, Water Resour. Res., 35(4):1053-1063.

Anderson, E. I., 2004. An analytical solution representing groundwater-surface water interaction. Water Resour. Res. 39(3), 1071, doi:10.1029/2002WR001536.

Anderson, M. P., and Cheng, Xiangxue. 1993. Long-term and short-term transience in a groundwater/lake system in Wisconsin, USA. Journal of Hydrology, 145: 1-18.

Asherson, M. P. 1979. Using models to simulate the movement of contaminants through groundwater flow system. Critical Reviews in Environmental Control, 9(2):97-156.

Barry, D. A. Li, L., and Jeng, D.-S., 2001. Tidal fluctuations in a leaky confined aquifer: Dynamic effects of an overlying phreatic aquifer. Water Resour. Res., 37(4): 1095-1098.

Barry, D. A., Li, L., Stagnitti, F., and Parlange, J.-Y., 2000. Groundwater waves in a coastal aquifer: A new governing equation including vertical effects and capillarity. Water Resour. Res., 36(2): 411-420.

Bates, P. D., Stewart, M. D., Desitter, A., Anderson, M. G., Ronaud, J.-P., and Smith, J. A., 2000. Numerical simulation floodplain hydrology. Water Resour. Res. 36(9): 2517-2529.

Bear, Jacob. 1979. Hydraulics of groundwater, McGraw-Hill, Inc., New York

Boufadel, Michel C., and Peridier, Vallorie, 2002. Exact analytical expressions for the piezometric profile and water exchange between stream and groundwater during and after a uniform rise of the stream level. Water Resour. Res., 38(7).

Boufadel, Michel C., and Suidan, Makram 1998. 2-D variably-saturated flow: physical scaling and Bayesian estimation. Journal of Hydrologic Engineering, Vol.3 No. 4.

Boufadel, Michel C., Suidan, Makram T., and Venosa, Albert D. 1997a. Density-dependent flow in one-dimensional variably-saturated media. Journal of Hydrology, 202: 280-301.

Boufadel, Michel C., Suidan, Makram T. and Venosa, Albert D. 1999, A numerical model for density-and-viscosity-dependent flows in two-dimensional variably saturated porous media. Journal of Contaminant Hydrology, 37:1-20

Boufadel, Michel C., Suidan, Makram T., Venosa, Albert D. and Bowers, Mark T.1997b. Steady seepage in trenches and dams: effect of capillary flow, Journal of Hydrologic Engineering, 125 (3):302-323.

Bruce, G. H., D. W. Peaceman, and H. H. Rachford, Jr. 1953, Calculation of unsteady -state gas flow through porous media. Petrol. Trans. AIME 198. Pp74-92.

Bruch, John C. 1975. Finite element solutions for unsteady and unsaturated flow in porous media. California Water Resources Center, Davis.

Brutsaert, W. F., 1971. A functional iteration technique for solving the Richards' equation applied to two-dimensional infiltration problems. Water Resour. Res., 7(6): 1538-1596.

Brutsaert, W. 1973. Numerical solution of multiphase well flow. Journal of the Hydraulic Division, American Society of Civil Engineers, 99(HY1):1981-2001.

Carr, P. A., and Van Der Kamp, G. S. 1969. Determining aquifer characteristics by tidal method, Water Resour. Res., 5, 1023-1031.

Carrera, J., and Neuman, S. P. 1986a. Estimation of aquifer parameters under transient and steady state conditions, 2, Uniqueness, stability, and solution algorithms, Water Resour. Res., 22(2):211-227.

Carrers, J. and Neuman, S. P. 1986b. Estimation of aquifer parameters under transient and steady state conditions, 3, Application to synthetic and field data, Water Resour. Res., 22(2):228-242.

Chang, Shin and Yeh, William W-G. 1976. A proposed algorithm for the solution of the large-scale inverse problem in groundwater, Water Resour. Res., 12(3):368-371.

Clement, T. P., Wise, William R. and Molz, Fred J. 1994. A physical based, two-dimensional, finite-difference algorithm for modeling variably saturated flow, Journal of Hydrology, 161: 71-90

Cooley, R. L. 1971. A finite difference method for unsteady flow in variably saturated porous media: application to a single pumping well. Water Resour. Res., 7: 1607-1625.

Cooley, R. L., 1977. A method to estimating parameters and assuming reliability for models of steady state groundwater flow, 1, Theory and numerical properties, Water Resour. Res., 13(2):1977.

Cooley, R. L., 1979. A method of estimating parameters and assuming reliability for models of steady state groundwater flow, 2, Application of statistical analysis, Water Resour. Res., 15(3):603-617.

Cooley, R. L., 1982. Incorporation of prior information on parameters into nonlinear regression groundwater flow models, 1, Theory, Water Resour. Res., 18(4):965-976.

Cooley, R. L., 1983a Incorporation of prior information on paramters into nonlinear regression groundwater flow models, 2, Application, Water Resour. Res., 19(3):662-676.

Cooley, R. L. 1983b Some new procedures for numerical solution of variably saturated flow problems. Water Resour. Res., 19: 1271-1285.

Cooper, H. H. And M. I. Rorabaugh. 1963. Groundwater movements and bank storage due to flood stages in surface streams. U.S. Geol. Surv. Water Supply Paper 1536-J.

Cowardin, L. M., Virginia, Golet, Francis C. and LaRoe, Edward T. 1979. Classification of wetlands and deepwater habitat of the United States. U.S. Fish and Wildlife Service, Washington, DC.

Cox, C. L., Jones, W. F., Quisenberry, V. L., Yo, F., 1994. One dimensional infiltration with moving finite elements and improved soil diffusivity, Water Resour. Res., 30:1431-1438.

Czarnecki, John B., and Waddell, Richard K. 1984. Finite-Element Simulation of Ground-Water Flow in the Vicinity of Yucca Mountain, Nevada-California, U.S. Department of Energy, Washington, DC.

Dagan, G. 1985. Stochastic modeling of groundwater flow by unconditional and conditional probabilities: The inverse problem, Water Resour. Res., 21(1):65-72.

Dean, Robert G., and Dalrymple, Robert A. 1991. Water wave mechanics for engineers and scientists, World Scientific, Singapore.

Distefano, N., and Rath A. 1975. An identification approach to subsurface hydrological systems, Water Resour. Res., 11(6):1005-1012.

Doughty, Christine, 2000. Numerical model of water flow in a fractured basalt vadose zone: Box Canyon site, Idaho. Water Resour. Res. 36(12): 3521-3534.

Erskine, A. D. 1991. The effect of tidal fluctuation on a coastal aquifer in the U.K. Ground Water, 29(4): 556-65.

Finn, W. D. Liam, and Varoglu, Erol. 1976. Variable domain finite element analysis of free surface flow problems. The first International Conference on Finite Elements in Water Resources, Princeton University, NJ.

Fleck, W. B., and McDonald, M. G. 1978. Three-dimensional finite-difference model of groundwter system underlying the Muskegon County wastewater disposal system, Michigan. U. S. Geological Survey Journal of Research, 6(3): 307-318.

Fraisse, Clyde W., and Campell, Kenneth L. 1997. FHANTM (field hydrologic and nutrient transport model), Version 2.0 User's Manual. University of Florida, Gainesville.

France, P. W. 1976. Finite element analysis of two and three dimensional unconfined seepage problems, Proceedings of the First International Conference on Finite Elements in Water Resources, Princeton University, NJ.

Freeze, R. A. 1971a. Three dimensional transient, saturated-unsaturated flow in a groundwater basin. Water Resour. Res., 7: 347-366.

Freeze, R. A.1971b. Influence of the unsaturated flow domain on seepage through earth dams. Water Resour. Res., 7: 929-941.

Freeze, R. A., and Witherspoon, P. A. 1966, Theoretical analysis of regional groundwater flow; 1. Analytical and numerical solutions to the mathematical model. Water Resources Research, 2: 641-656.

Fretwell, J. D., Williams, J. S., and Redman, P. J. (Compliers). 1996. National water summary on wetland resources. U.S. Geological Survey Water Supply Paper 2425. 431 p.

Gambolati, G. , Gatto, P. and Freeze, R. A. 1973, Mathematical simulation of the subsidence of Venice, 2 results. Water Resources Research, 9: 721-733.

Gleason, P. J. 1989. Northern Martin County wellfield wetlands impact study-aquifer performance test. James M. Montgomery Consulting Engineers, Lake Worth, FL.

Gonthier, Gerard J., Kleiss, And Barbara A. 1996. Groundwater flow patterns and water budget of a bottomland forested wetland, Black swamp, eastern Arkansas, U.S. Geological Survey Water-Resources Investigations Report 95-4192.

Gregg, D. O. 1966. An analysis of groundwater fluctuation caused by ocean tides in Glynn County. Georgia, Ground Water, 4: 211-232.

Groundwater Modeling System. 1996. Brigham Young University. Provo, UT.

Gupta, Sumant K., Tanji, Kenneth K. and Luthin, James N. 1975. A three-Dimensional finite element ground water model, California Water Resources Center, Davis.

Gureghian, A. B., Ward, D. S. and Cleary, R. W. 1979. Simultaneous transport of water and reacting solutes through multilayered soils under transient unsaturated flow conditions. Journal of Hydrology, 41: 253-278.

Guymon, G. L., Scott, V. H. and Hermann, L. R. 1970. A general numerical solution of the two-dimensional diffusion-convection equation by finite element method. Water Resources Research, 6(6): 1611-1617.

Hoeksema, R. J., and Kitanidis, 1984. An application of the geostatistical approach to the inverse problem in two-dimensional groundwater modeling, Water Resour. Res., 20(7):1003-1020.

Hughes, T. J. R. 1987. The Finite Element Method, Prentice Hall, Englewood Cliffs, NJ.

Hunt, R. J. 1996. Do created wetlands replace the wetlands that are destroyed? U.S. Geological Survey Fact Sheet FS-96-246, 4 p.

Hunt, R. J., Bullen, T. D., Krabbenhoft, D. P., and Kendall, C. 1998. Using isotropes of water and strontium to investigate the hydrology of a natural and a constructed wetland: Ground Water, 36(3): 434-443.

Hunt, R. J., Krabbenhoft, D. P., and Anderson, M. P. 1996. Groundwater inflow measurements in wetland systems: Water Resources Research, 32(3): 495-507.

Hunt, R. J., Krabbenhoft, D. P., and Anderson, M.P., Assessing hydrogeochemical heterogeneity in natural and constructed wetlands. Biogeochemistry, 39: 271-293.

Huyakorn, P. S., Guvanasen, V. and Wadsworth, T. D. 1986. Three-Dimensional finite techniques for simulating unconfined flow with seepage faces. Proceeding of the 6th International Conference, Lisbon, Portugal.

Huyakorn, P. S., and Pinder, G. F. 1983. Computational Methods in Subsurface Flow, Academic Press, New York.

Huyakorn, P. S., and Thomas, S. D. 1984. Techniques for making finite elements competitive in modeling flow in variably saturated porous media, Water Resources Research, 20(8).

Istok, Jonathan. 1989. Groundwater Modeling by the finite element method, American Geophysical Union, Washington, DC.

Jain, S. K., Storm, B., Bathurst, J. C., Refsgaard, J. C., and Singh, R. D., 1992. Application of the SHE to catchments in India-Part 2: Field experiments and simulation studies on the Kolar Subcatchment of the Narmada River. Journal of Hydrology, vol. 140, p. 25-47.

Javandel, I., and Witherspoon, P. A. 1968. Applciation of the finite element method to transient flow in porous media. Society of Petroleum Engineers Journal, 8(3): 241-252.

Keidser, A., and Rosbjerg, D. 1991. A comparison of four inverse approaches to groundwater flow and transport parameter identification, Water Resour. Res., 27(9): 2219-2232.

Kirkland, M. R., Hills, R. G. and Wierenga, P. J. 1992. Algorithms for solving Richards' equation for variably saturated soils. Water Resour. Res., 12(1): 57-64.

Kirkner, D. J., Theis, T. L. and Jennings, A. A. 1984. Multicomponent solute transport with sorption and soluble complexation. Advances in Water Resources, 7:120-125.

Knopman, Debra S. and Voss, Clifford I. 1989. Multiobjective sampling design for paramter estimation and model discrimination in groundwater solute transport, Water Resour. Res., 25(10):2245-2258.

Konikow, L. F. and Bredehoeft, J. D. 1978. Computer model of two-dimensional solute transport and dispersion in groudnwater. U.S. Geological Investigation, Book 7.

Krabbenhoft, D. P., Anderson, Mary P. and Bowser, Carl J. 1990a. Estimating groundwater exchange with lakes 2. Calibration of a three-dimensional, solute transport model to a stable isotope plume. Water Resources Research, 26(10): 2455-2462.

Krabbenhoft, D. P., Bowser, Carl J., Anderson, Mary P. and Valley, John W. 1990b, Estimating groundwater exchange with lakes 1. The stable isotope mass balance method. Water Resources Research, 26(10): 2445-2453.

Krabbenhoft, D. P., and Webster, A.W. 1995. Transient hydrogeological controls on the chemistry of a seepage lake: Water Resources Research, 31(9): 2295-2305.

Lal, A. M. Wasantha, 2000. Numerical errors in groundwater and overland flow models. Water Resour. Res. 36(5): 1237-1247.

Lamorey, Gregg and Jacobson, Elizabeth 1998. Incorporation of constraints on hydraulic head gradients near no-flow boundary conditions in the determination of spatial drift and their use in an inverse groundwater flow model, Water Resour. Res. 34(11):2889-2910.

Lal, A. M. Wasantha, 2000. Numerical errors in groundwater and overland flow models. Water Resour. Res. 36(5): 1237-1247.

Lapidus, L. and Pinder, G. F. 1982. Numerical solution of partial differential equations in science and engineering, John Wiley & Sons, New York.

Lebedev, N. N. 1965. Special functions and their applications, Prentice-hall, Inc. Englewood Cliffs, NJ.

Lee, Terrie M., 2000. Effects of nearshore recharge on groundwater interactions with a lake in mantled karst terrain. Water Resour. Res., 36(8): 2167-2182.

Loaiciga, Hugo and Marino, Miguel A. 1987. The inverse problem for confined aquifer flow identification and estimation with extensions, 23(1):92-104.

Mayer, A. S. and Miller, C. T. 1988. A Three-Dimensional Finite Element-Finite Difference Model for Simulating Confined and Unconfined Groundwater Flow, Proceedings of the VII International Conference, MIT, Cambridge, MA.

McDonald, M.G., and Harbaugh, A. W. 1988. A modular three-dimensional finite-difference groundwater flow model: US. Geological Survey Techniques of Water-Resources Investigations of the U.S. Geological Survey, book 6, Chap A1, not sequentially paginated.

Michalak, Ann M., and Kitanidis, Peter K., 2004. Estimation of historical groundwater contaminant distribution using the adjoint state method applied to geostatistical inverse modeling. Water Resour. Res. Vol.40, W08302.

Middleton, Beth. 1998. Wetland restoration, flood pulsing, and disturbance dynamics. John Wiley & Sons, Inc., New York.

Mills, J. G., and Zwarich, M.A. 1986, Transient groundwater flow surrounding a recharge slough in a till plain: Canadian Journal of Soil Science, 66(1):121-134.

Mishra, S. and Parker, J. C. 1989. Parameter estimation for coupled unsaturated flow and transport, Water Resour. Res., 25(3):385-396.

Mitchell, A. R. and Griffiths, D. F. 1980. The finite difference method in partial difference equations. Wiley, New York.

Mitsch, W. J. and Gosselink, J. G. 1986. Wetlands. Van Nostrand Reinhold, New York.

Mitsch, W. J. and Gosselink, J. G. 1993. Wetlands-2nd ed. Van Nostrand Reinhold, New York.

Narasimhan, T. N. and Witherspoon, P. A. 1976. An integrated finite difference method for analyzing fluid flow in porous media. Water Resour. Res., 12(1): 57-64.

Narasimhan, T. N., Witherspoon, P. A., and Edwards, A. L. 1978. Numerical model for saturated-unsaturated flow in deformable porous media, 2. The algorithm. Water Resour. Res., 14:225-261.

Neuman, S. P., 1973a Calibration of distributed parameter groundwater flow models viewd as a multiple-objective decision process under uncertainty, Water Resour. Res., 9(4):1006-1021.

Neuman, S. P. 1973b Saturated-unsaturated seepage by finite elements. Proceedings American Society of Civil Engineers, 99(HY12): 2233-2250.

Neuman, S. P., and Witherspoon, P. A. 1970. Finite-element method of analyzing steady seepage with free surface. Water Resources Research, 6(3): 889-897.

Nielsen, P. 1990. Tidal dynamics of the water table in Beaches, Water Resour. Res., 26: 2127-2134.

Norero, A. L. 1969. A formula to express evapotranspiration as a function of soil moisture and evaporative demands of the atmosphere. PhD Diss. Utah State University, Logan.

Novitzki, R. P. 1979. Hydrologic characteristics of Wisconsin's wetlands and their influence on floods, stream flows, and sediment. In wetland functions and values: The state of our understanding, P. E. Greeson, J. R. Clark, J. E. Clark, eds. American Water Resources Association, Minneapolis, pp. 377-388.

Orlob, G. T., and Woods, P. C. 1967, Water-quality management in irrigation systems. Journal of the Irrigation and Drainage Division, American society of Civil Engineers, 93: 49-66.

Oster, C. A., Sonnichsen, J. C. and Jaske, P. T. 1970. Numerical calculation of the convective diffusion equation. Water Resources Research, 6: 1746-1752.

Peaceman, D. W. and Rachford, H. H. 1962, Numerical calculation of multidimensional miscible displacement. Society of Petroleum Engineers Journal, 2: 327-339.

Philip, J. R. 1957. The theory of infiltration: 1. The infiltration equation and its solution. Soil Science, 83: 345-357.

Pickens, J. F., Gillham, R. W. and Cameron, D. R. 1979. Finite-element analysis of the transport of water and solutes in tile-drained soils. Journal of Hydrology, 40: 243-264.

Pinder, G. F. 1973. A Galerkin finite element simulation of groundwater contamination in Long Island, New York. Water Resources Research, 9(6): 1657-1669.

Pinder, G. F., and Bredehoeft, J. D. 1968. Application of the digital computer for aquifer analysis. Water Resources Research, 8(1):108-120.

Pinder, G. F., and Frind, E. O. 1972. Application of Galerkin's procedure to aquifer analysis. Water Resources Research, 8(1):108-120.

Pinder, George F., and Gray, William G. 1977. Finite element simulation in surface and subsurface hydrology, Academic Press, New York.

Price, H. S., Cavendish, J. C. and Varga, R. W. 1968. Numerical methods of higher order accuracy for diffusion convection equations. Society of Petroleum Engineers Journal, 1: 293-303.

Pricket, T. A. 1975. ModeLing techniques for groundwater evaluation. In: Advances in Hydro-science, Vol. 10. Academic Press, New York, pp. 1-143.

Reeves, M. and Duguid, J. O. 1975. Water movement through saturated- unsaturated porous media: A finite-element Galerkin model. ORNL-4927, Oak Ridge National Laboratory, Oak Ridge, TN.

Remson, I., Appel, C. A. and Webster, R. A. 1965. Groundwater models solved by digital computer. Journal of the Hydraulics Division, American Society of Civil Engineers, 91(HY3): 133-147.

Rubin, J. 1968. Theoretical analysis of two-dimensional, transient flow of water in unsaturated and partly saturated soils. Soil Sci. Soc. Am. Proc., 32: 607-615.

Ruddy, Barbara C. and Williams, Robert S. Jr., 1991. Hydrologic relations between streamflow and subalpine wetlands in grand county, Colorado. Water-Resources Investigations Report 90-4129, U.S. Geological Survey, Washington, DC.

Rushton, B. 1996. Hydrologic budget for a freshwater marsh in Florida. Water Resources Bulletin, 32(1), 13-21.

Russo, D., 2003. Simulation of transport in three-dimensional heterogeneous unsaturated soils with upscaled dispersion coefficients. Water Resour. Res. 39(12), 1358.

Sacks, L. A., Herman, J. S., Konikow, L. F., and Vela, A. L. 1992. Seasonal dynamics of groundwater-lake interactions at Donana National Park, Spain. J. Hydrol., 136: 123-154.

Segol, G., Pinder, G. F. and Gray, W. G. 1975. A Galerkin-finite element technique for calculating the transition position of the salt-water front. Water Resources Research, 11(2): 343-347.

Senger, R. K., and Fogg, G. E. 1987. Regional under pressuring in deep brine aquifers, Palo Dura Basin, Texas I, Effects of hydrostratigraphy and topography. Water Resources Research, 23(8): 1481-1493.

Serfes, M. E. 1992. Determining the mean hydraulic gradient of ground water affected by tidal fluctuations. Ground Water, 29:549-555.

Serrano, Sergio E., 2003. Modeling Groundwater flow under transient nonlinear free surface. Journal of Hydrologic Engineering, Vol. 8, No. 3.

Shaffranek, Raymond W. 1996. Coupling models for canel and wetland interactions in the south Florida ecosystem. U.S. Dept. of the Interior, U.S. Geological Survey.

Smith, A. J., and Townley, L. R., 2002. The influence of regional setting on the interaction between shallow lakes and aquifers, 38(9), 1170, doi:10.1029/2001wr000781.

Sonenshein, Roy S., and Hofstetter, Ronald H. 1990. Hydrologic effects of well-field operations in a wetland Dade County, Florida. U.S Geological Survey, Water Resources Investigations Report 90-4143.

Stone, H. L., and Brain, P. T. L. 1963. Numerical solution of convective transport problems, AICHE J., 9: 5205-5213.

Sun, Hongbing. 1997. A two-dimensional analytical solution of groundwater response to tidal loading in an estuary, Water Resour. Res., 33(6):1429-1435.

Sun, Ne-Zheng, 1994, Inverse problems in groundwater modeling, Kluwer Academic Publishers, Boston.

Sun, Ne-Zheng, Jeng, Ming-Chin, and Yeh, William W. G. 1995. A proposed geological parameterization method for parameter identification in three-dimensional groundwater modeling, Water Resour. Res. 31(1):89-102.

Sun, Ne-Zheng, Yeh, W. W-G. 1985. Identification of parameter structure in groundwater inverse problem, Water Resour. Res., 21(6):869-883.

Swamee, Prabhata K. and Singh, Sushil K., 2003. Estimation of aquifer diffusivity from stream stage variation. Journal of Hydrologic Engineering, Vol. 8, No. 1.

Switt, R. S., Annable, M. D., Wise, W. R., and Walser, J. A. E. 1998. Hydrologic impacts of groundwater fluctuations on wetlands system, Proceeding of the 1998 International Water Resources Engineering Conference and Mini-Symposia, Memphis, TN.

Tanji, K. K., Dutt, G. R., Paul, J. L., and Doneen, L. D. 1867. A computer method for predicting salt concentrations in soils at variable moisture contents. Hilgardia, 38: 307-318.

Tannehill, John C., Anderson, Dale A. and Pletcher, Richard H. 1997. Computational fluid mechanics and heat transfer. Taylor & Francis, Washington, DC.

Therrien, R. and Sudicky, E. A. 1996. Three-dimensional analysis of variably-saturated flow and solute transport in discretely-fractured porous media, Journal of Contaminant Hydrology, 23: .

Throrenz, Carsten, Kosakowski, Georg, Kolditz, Olaf, and Berkowitz, Brian, 2002. An experimental and numerical investigation of saltwater movement in coupled saturated-partially saturated systems. Water Resour. Res. 38(6).

Townley, Lloyd R., and Trefry, Michael G., 2000. Surface water-groundwater interaction near shallow circular lakes: Flow geometry in three dimensions. Water Resour. Res., 36(4): 935-949.

Trescott, P. C. and Larson, S. P. 1977. Comparison of iterative methods for solving two-dimensional groundwater flow equations. Water Resources Research, 13(1):125-136.

Trescott, P. C., Pinder, G. F. and Larson, S. P. 1976. Finite difference model for aquifer simulation in two dimensions with results of numerical experiments. U. S. Geological Survey, Techniques of Water Resources Investigation, Book 7, Automated Data Processing and Computations, 116pp.

Tritscher, Peter, and Read, W. Wayne, and Broadbridge, Philip, 2000. Specific yield for a two-dimensional flow. Water Resour. Res. 36(6): 1393-1402.

Truesdell, B. P. 1995. The use of a wetland-groundwater interaction test to investigate the hydrologic connection between isolated wetland and the surrounding groundwater. Master's Project, University of Florida, Gainesville.

U.S. Geological Survey. 1996. Ground-water flow pattern and water buget of a bottomland forested wetland, Black Swamp, eastern Arkansas.

Van Genuchten, M. Th., 1980. A closed-form equation for predicting the hydraulic conductivity of unsaturated soil. Soil Sci. Soc. Am. J., 44: 892-898

Van Genuchten, M.Th., Pinder, G. F. and Frind, E. O. 1977. Simulation of two-dimesional contaminant transport with isoparametric-Hermitain finite elements. Water Resources Research, 13(2): 451-458.

Vauclin, M., Khanhi, D., and Vachaud, G., 1979. Experimental and numerical study of a transient, two-dimensional unsaturated-saturated water table recharge problem. Water Resour. Res., 15(5): 1089-1101.

Volker, Ray E. and Zhang, Qi, 2001. Comment on "Analytical solution of groundwater response to tidal fluctuation in a leaky confined aquifer" by Jiu Jimmy Jiao and Zhonghua Tang. Water Resour. Res., 37(1): 185-186.

Voss, Clifford I. 1984. A finite-element simulation model for saturated-unsaturated, fluid-density-dependent groundwater flow with energy transport or chemically reactive single-species solute transort. U.S. Geological Survey and U.S. Air Force Engineering and Services Center, Tyndall A. F. B., FL.

Walser, J. E., Annable, M. D., Wise, W. R., and Switt, R. S. 1998. Investigating Isolated Wetlands-Aquifer Interaction Through Modeling, Proceeding of the 1998 International Water Resources Engineering Conference and Mini-Symposia, Memphis, TN.

Wierenga, P. J. 1977. Solute distribution profiles computed with steady state and transient water movement models. Soil Science Society of America Journal, 41: 1050-1055.

Winter, T. C. 1978. Numerical simulation of steady-state, three-dimensional groundwater flow near lakes. Water Resour. Res., 14: 245-254.

Winter, T. C. 1983. The interaction of lakes with variably saturated porous media. Water Resour. Res., 19: 1203-1218.

Winter, T. C., 1986. Effect of groundwater recharge on configuration of the water table beneath sand dunes and on seepage in lakes in the Sandhills of Nebraska, U.S.A.. J. Hydrology, 1986.

Winter, T. C. and Woo, M. K. Eds. 1990. Hydrology of Lakes and Wetlands. In Surface water hydrology, Geological Society of American, Bounder, CO.

Wise, W. R., Annable, M. D., Walser, J. A. E., Switt, R. S., and Shaw, D. T. A Wetland-aquifer interaction test, 2000, Journal of Hydrology, 227 (2000) 257-272.

Yeh, G. T., 1992. Users' Manual: A finite element model of water flow through saturated-unsaturated porous media. Department of Civil Engineering, The Pennsylvania State University.

Ye, S., Xue, Y., and Xie, C., 2004. Application of the mutltiscale finite element method to flow in heterogeneous porous media. Water Resour. Res. Vol. 40, W09202.

Yeh, William W-G. 1986. Review of parameter identification procedure in groundwater hydrology: The inverse problem, Water Resour. Res., 22(2):95-108.

Zhang, Jinqi and Yeh, T.-C. Jim 1997. An iterative geostatistical inverse method for steady flow in the vadose zone, Water Resour. Res., 33(1):63-71.

Zhang, Xiaoxian, and Ewen, John, 2000. Efficient method for simulating gravity-dominated water flow in unsaturated soils. 36(9): 2777-2780.

Zienkiewicz, O. C. 1971. The finite element method in engineering science, McGraw-Hill, London.

Zienkiewicz, O. C., Meyer, P. and Cheung, Y. K. 1966. Solution of anisotropic seepage problems by finite elements. Proceedings American Society of Civil Engineers, 92 EMI: 111-120.

Zienkiewicz, O. C., and Parekh, C. J. 1970. Transient field problems: Two-dimensional and three dimensional analysis by isoparametric finite elements. International Journal of Numerical Methods in Engineering, 2: 61-71.

BIOGRAPHICAL SKETCH

Jinhua (Jay) Zhong was born on August 1, 1966, in a small village of Jiangsu Province, China. He received his Bachelor of Science degree in civil engineering, with special emphasis in hydrology and water resources engineering; in 1988; and the Master of Science degree in 1991 from the Department of Hydrology and Water Resources Engineering at Hohai University Nanjing, P. R. China. Soon after earning his master's degree, he began to work as an engineer in the Institute of Environmental Hydraulics at Hohai University. In 1995, he came to the United States and entered the Graduate School of the University of Florida. In 2001, he obtained his MS degree from Electrical and Computer Engineering Department of the University of Florida. He earned the Doctor of Philosophy degree from the Civil and Coastal Engineering Department of the University of Florida in 2004.

I certify that I have read this study and that in my opinion it conforms to acceptable standards of scholarly presentation and is fully adequate; in scope and quality as a dissertation for the degree of Doctor of Philosophy.

Louis H. Motz, Chairman
Associate Professor of Civil and
Coastal Engineering

I certify that I have read this study and that in my opinion it conforms to acceptable standards of scholarly presentation and is fully adequate; in scope and quality as a dissertation for the degree of Doctor of Philosophy.

Kirk Hatfield, Cochair
Associate Professor of Civil and
Coastal Engineering

I certify that I have read this study and that in my opinion it conforms to acceptable standards of scholarly presentation and is fully adequate; in scope and quality as a dissertation for the degree of Doctor of Philosophy.

Wendy D. Graham
Professor of Agricultural and
Biological Engineering

I certify that I have read this study and that in my opinion it conforms to acceptable standards of scholarly presentation and is fully adequate; in scope and quality as a dissertation for the degree of Doctor of Philosophy.

Robert J. Thieke
Assistant Professor of Civil and
Coastal Engineering

I certify that I have read this study and that in my opinion it conforms to acceptable standards of scholarly presentation and is fully adequate; in scope and quality as a dissertation for the degree of Doctor of Philosophy.

Michael D. Annable
Professor of Environmental
Engineering Sciences

This dissertation was submitted to the Graduate Faculty of the College of Engineering and to the Graduate School and was accepted as partial fulfillment of the requirements for the degree of Doctor of Philosophy.

December, 2004

Pramod Khargonekar
Dean, College of Engineering

Kenneth J. Gerhardt
Interim Dean, Graduate School

LD
1780
2004
.Z63

UNIVERSITY OF FLORIDA
3 1262 08554 5712